US ARMY MATERIEL COMMAND

CONTRACT REPORT BRL-CR-543

THEORETICAL MODELING OF LASER INDUCED OPTICAL DEGRADATION

Physical Sciences, Inc
P.O. Box 3100, Research Park
Andover, MA 01810

May 1985

US ARMY BALLISTIC RESEARCH LABORATORY
ABERDEEN PROVING GROUND, MARYLAND

SECURITY CLASSIFICATION OF THIS PAGE *(When Data Entered)*

REPORT DOCUMENTATION PAGE		READ INSTRUCTIONS BEFORE COMPLETING FORM
1. REPORT NUMBER Contract Report BRL-CR-543	2. GOVT ACCESSION NO.	3. RECIPIENT'S CATALOG NUMBER
4. TITLE *(and Subtitle)* THEORETICAL MODELING OF LASER INDUCED OPTICAL DEGRADATION		5. TYPE OF REPORT & PERIOD COVERED FINAL REPORT 3/19/82 - 3/18/83
		6. PERFORMING ORG. REPORT NUMBER
7. AUTHOR(s) R.G. Root, G. Weyl, M.G. Miller, L.A. Popper		8. CONTRACT OR GRANT NUMBER(s) F29601-82-C-0050
9. PERFORMING ORGANIZATION NAME AND ADDRESS PHYSICAL SCIENCES INC. P.O. Box 3100, RESEARCH PARK ANDOVER, MA 01810		10. PROGRAM ELEMENT, PROJECT, TASK AREA & WORK UNIT NUMBERS 1S263749D462
11. CONTROLLING OFFICE NAME AND ADDRESS US ARMY BALLISTIC RESEARCH LABORATORY ATTN: AMXBR-OD-ST ABERDEEN PROVING GROUND, MD 21005-5066		12. REPORT DATE May 1985
		13. NUMBER OF PAGES 125
14. MONITORING AGENCY NAME & ADDRESS(*if different from Controlling Office*)		15. SECURITY CLASS. (*of this report*) UNCLASSIFIED
		15a. DECLASSIFICATION/DOWNGRADING SCHEDULE

16. DISTRIBUTION STATEMENT (*of this Report*)

Approved for public release; distribution is unlimited.

17. DISTRIBUTION STATEMENT (*of the abstract entered in Block 20, if different from Report*)

18. SUPPLEMENTARY NOTES

19. KEY WORDS (*Continue on reverse side if necessary and identify by block number*)

Laser Glass Damage
Optical Aberrations
Optical Systems Performance

20. ABSTRACT (*Continue on reverse side if necessary and identify by block number*)

Laser irradiation of optical elements can degrade the performance of an optical system. In this report methodology has been established for predicting the system performance of an irradiated optical system. Models required to implement the methodology have been developed and improved; the models predict (1) the physical damage caused by laser irradiation, (2) the optical aberrations corresponding to the physical damage, and (3) the point spread function (or

(Continued)

DD 1 JAN 73 FORM 1473   EDITION OF 1 NOV 65 IS OBSOLETE   UNCLASSIFIED

SECURITY CLASSIFICATION OF THIS PAGE (*When Data Entered*)

optical transfer function) for the optical system which includes the aberrations induced by laser irradiation.

The glass damage models have been upgraded to include improved material properties and to predict the fraction of the surface damaged by the various mechanisms. Simple models have been used to relate the damage to the reduction in contrast ratio. In general, the models predicted the trends in contrast ratio; however, for some types of damage, the expected reduction cannot be accurately quantified unless details of the optical system used in measurements are specified.

The optical aberrations caused by three types of physical damage have been modelled. The aberrations are represented as a local change in amplitude and phase of the light. Surface cracks effectively reduce the local transmission to zero. Exfoliation reduces the transmission slightly (≈ 0.08) but its main effect is to introduce a random phase difference between different flakes. Vaporization does not affect transmission, but it introduces potentially large phase differences over distances associated with variations in the vaporization dynamics.

The point spread function has been calculated for a simple optical system which has optical aberrations produced by laser irradiation. The main features of the point spread function are (1) a central spike whose proportional to the square of the area which is not damaged, and (2) a damage halo whose width is determined by the characteristic size of the individual damage elements and whose total height is proportional to the incoherent sum of the square of the area of each damaged element. This description of the damage halo assumes that the phase difference between any two damage elements is large (greater than 2π) and random. Severe optical degradation requires that the central spike have only a small fraction of the total energy, therefore the damage must completely cover the surface of the damaged optical element and the phase difference between adjacent damage elements must be large.

TABLE OF CONTENTS

3

TABLE OF CONTENTS (continued)

LIST OF ILLUSTRATIONS

1. INTRODUCTION

Optical glasses which have been exposed to laser irradiation may suffer physical damage that degrades their performance in an optical system. Models have previously been developed that predict the threshold laser parameters required to produce nine types of physical damage.[1] In this report, the physical damage predictions are further quantified, a methodology is established for predicting degradation of system performance, and models that are essential components in the system performance analysis are developed.

The elements of a system performance model are most easily identified by first reviewing how the performance of undamaged optics is evaluated. The main features are summarized for a simple optical system in Fig. 1.1. The dimensions, location, illumination and other relevant features of the object are specified when the scenario is detailed. The object is imaged onto a detector system by the optical system. The imaging characteristics of an optical system for incoherent radiation can be succinctly described by the point spread function or its Fourier transform, the optical transfer function. The point spread function is defined as the image that is produced in the focal plane by a point source. The image of the object can then be determined by convoluting the object with the point spread function. Finally, the ability of the system to detect or resolve the image is controlled by the detector response characteristics.

For an optical system that has been damaged by laser irradiation, the elements of the system performance analysis are summarized in Fig. 1.2. First, the physical damage inflicted by the laser irradiation must be predicted as a function of laser irradiation parameters (Fig. 1.2a). The next step is to determine the effect of the physical damage on the propagation of electromagnetic radiation (Fig. 1.2b); the effects may include reflection, attenuation, scattering or phase distortion. These effects are conveniently described as optical aberrations in the damaged element. After having detailed the optical qualities of the damaged element, it is straightforward, in theory, to calculate the point spread function for the damaged optical system; in practice, it will be necessary to simplify the calculation, but the salient

9
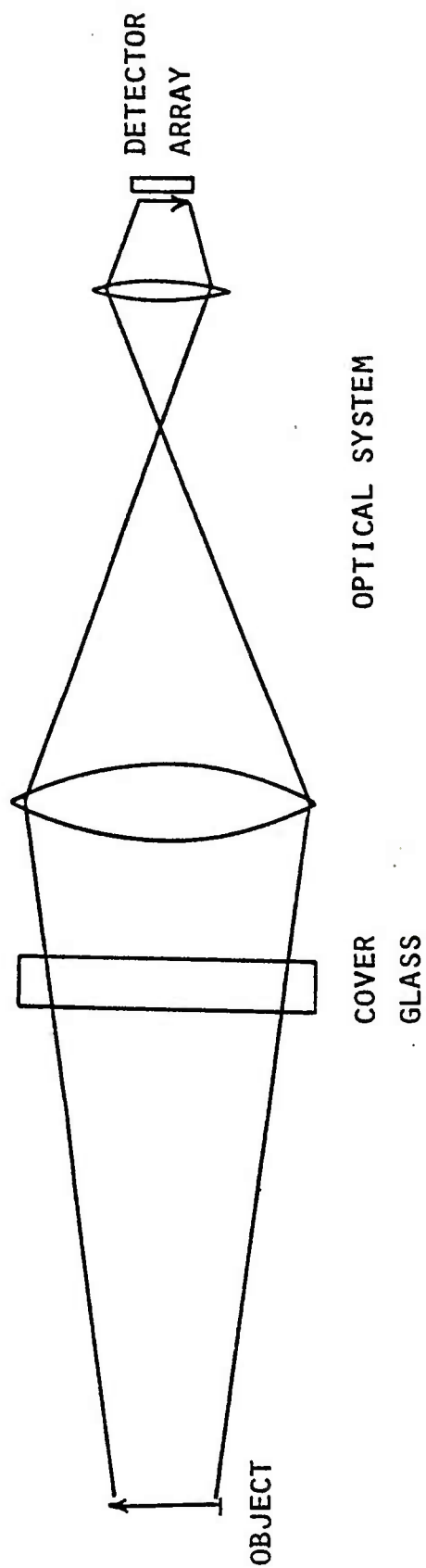
Fig. 1.1 Imaging capability of optical system determined by optical transfer function.
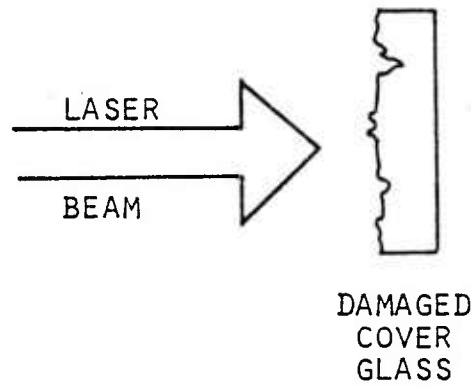
(A)   LASER IRRADIATION DAMAGES OPTICAL ELEMENT
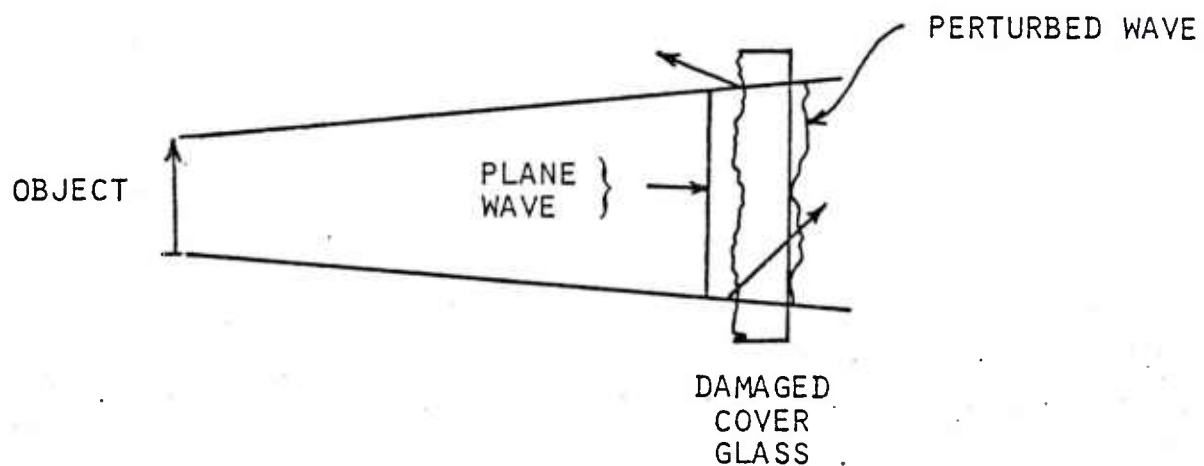
(B)   DAMAGED ELEMENT PERTURBS WAVEFRONT
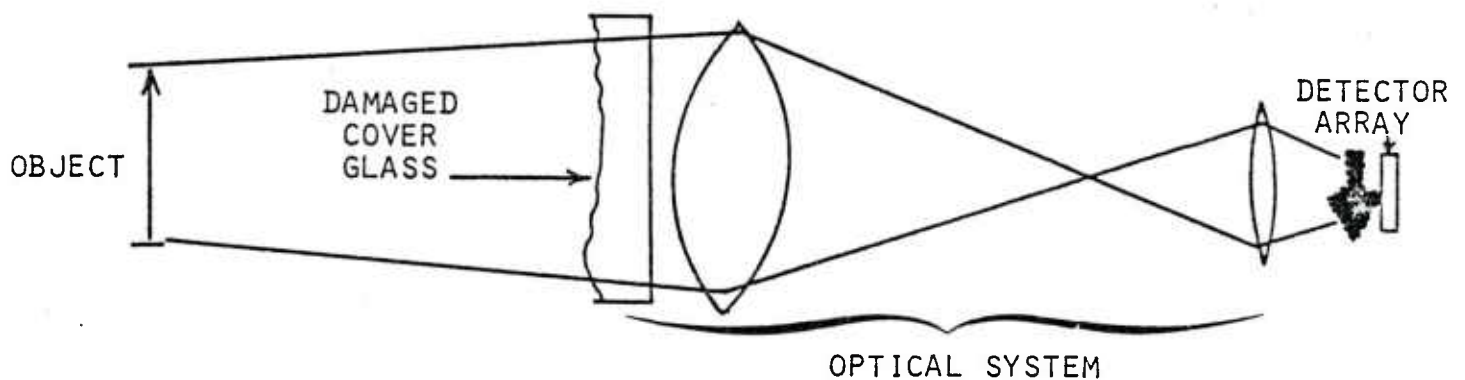
(C)   IMAGING CAPABILITY DETERMINED BY OPTICAL TRANSFER FUNCTION OF
      SYSTEM INCLUDING DAMAGED ELEMENT

      SYSTEM PERFORMANCE INCLUDES DETECTOR RESPONSE, OPTICAL SYSTEM
      RESPONSE AND OBJECT CHARACTERISTICS

Fig. 1.2   Elements of optical damage modeling.

features of the damaged transfer function must be faithfully reproduced. For the given scenario, the image and the system performance are determined by following the same procedures as for the undamaged system (Fig. 1.2c), with the only substitution being the replacement of the undamaged optical transfer function with the one for the damaged system. This last step involves many separate models and analyses; they are consolidated under one task in the methodology outlined above because no new modeling is required for the damaged system.

Thus, the system performance assessment can be conveniently categorized into four elements; namely,

1) determining the physical damage inflicted by the laser

2) relating physical damage to optical aberrations

3) calculating the optical transfer function (or its equivalent) for the damaged system

4) assessing the performance of the system in a given scenario and for a given detector.

The first step was initiated in Ref. 1; improvements to the models which further quantify the damage are described in Section 2. In Section 3, a general methodology for describing optical performance is established and its relationship to both laboratory experiments and system performance analysis are summarized. Models that are required to implement the methodology are formulated in Section 4; they include first estimates of the optical aberrations caused by the three most important types of physical damage and detailed calculations of the point spread function for a simple damaged optical system. However, no conclusions about system performance can be made without specifying a realistic optical system, the scenario, and the detector characteristics. Nevertheless, in Section 5, after the major results of the previous sections are summarized, some implications for system performance are suggested.

2. PHYSICAL DAMAGE MECHANISMS

2.1 Introduction

Previous investigations have modeled the threshold laser parameters required to damage glass. These investigations considered nine damage mechanisms (catastrophic fracture, melting, phase separation, viscoelastic stress relaxation, surface crazing, exfoliation, bubble formation, vaporization, and fracture of the antireflection coating), four glasses (BK7, ZKN7, soda lime, and fused silica), and three laser systems (RP 10.6 µm, CW 3.8 µm and RP 3.8 µm). The threshold predictions of the models were consistent with the available data, but quantitative predictions of the amount of physical damage were not made nor were quantitative measurements of physical damage available. In addition, several issues remained concerning the interpretation of the data. This section begins with brief review of the status of the theory developed previously, its comparison with the available data, and the major unresolved issues. Then the physical damage models are updated to predict the amount and nature of the damage, and to include the latest data on the glass absorption coefficients and coefficient of thermal expansion. The models are also applied to Vycor, a type of glass not studied previously. Finally, the available data are reinterpreted in the context of the improved and extended models, thereby resolving many of the issues.

2.2 Status of Models

The status of the models developed under the previous program and the major unresolved issues can be succinctly reviewed by reexamining the comparison between the data and the theoretical predictions. The details of the models are adequately described in Ref. 1 and need no further elaboration. The predictons of Ref. 1 for RP 10.6 µm damage thresholds are compared to the contrast ratio data in Fig. 2.1-2.3; the main features of damage to glass irradiated by CW 3.8 µm radiation are displayed in Fig. 2.4.

The previous work concentrated on predicting thresholds for various damage mechanisms. Thus, in Fig. 2.1 for example, the theory defines the values of pulse fluence above which new damage mechanisms will occur, but it
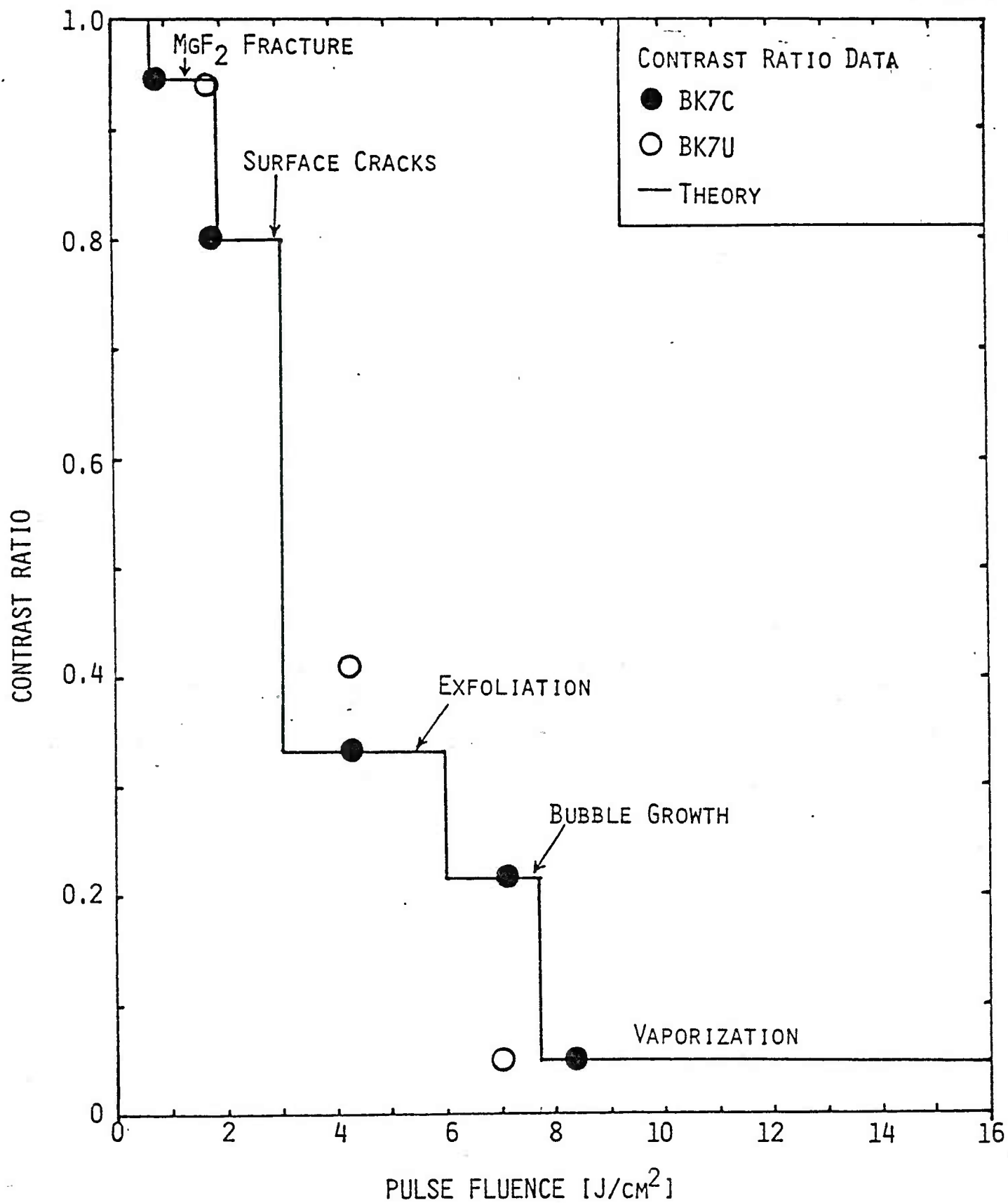
Fig. 2.1 Qualitative interpretation of contrast ratio data for BK7 exposed to 5 pulses of 10.6 μm radiation at 10 Hz repetition rate. From Ref. 1.
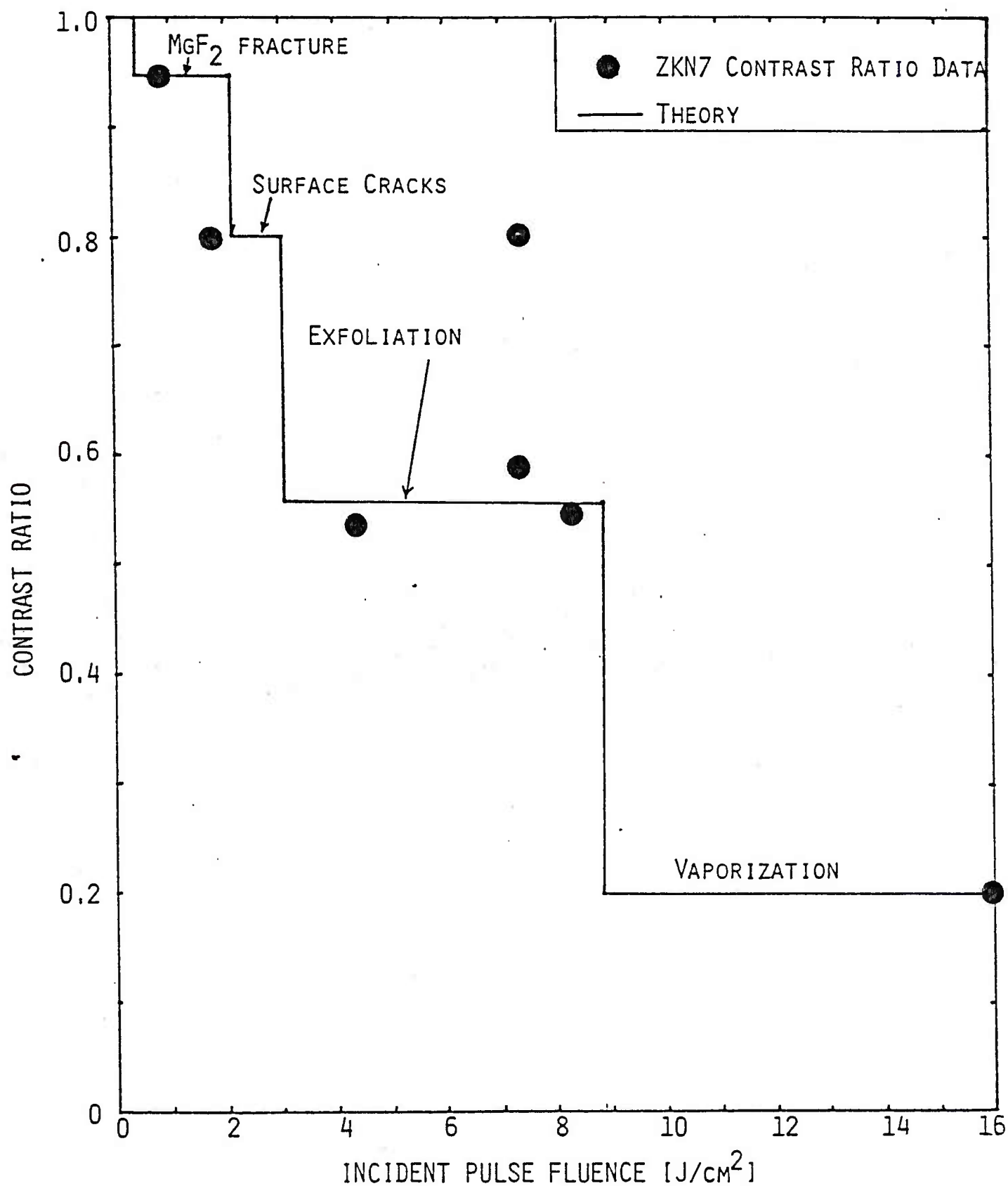
Fig. 2.2 Qualitative interpretation of contrast ratio data for ZKN7 exposed to 5 pulses of 10.6 μm radiation at 10 Hz repetition rate. From Ref. 1.
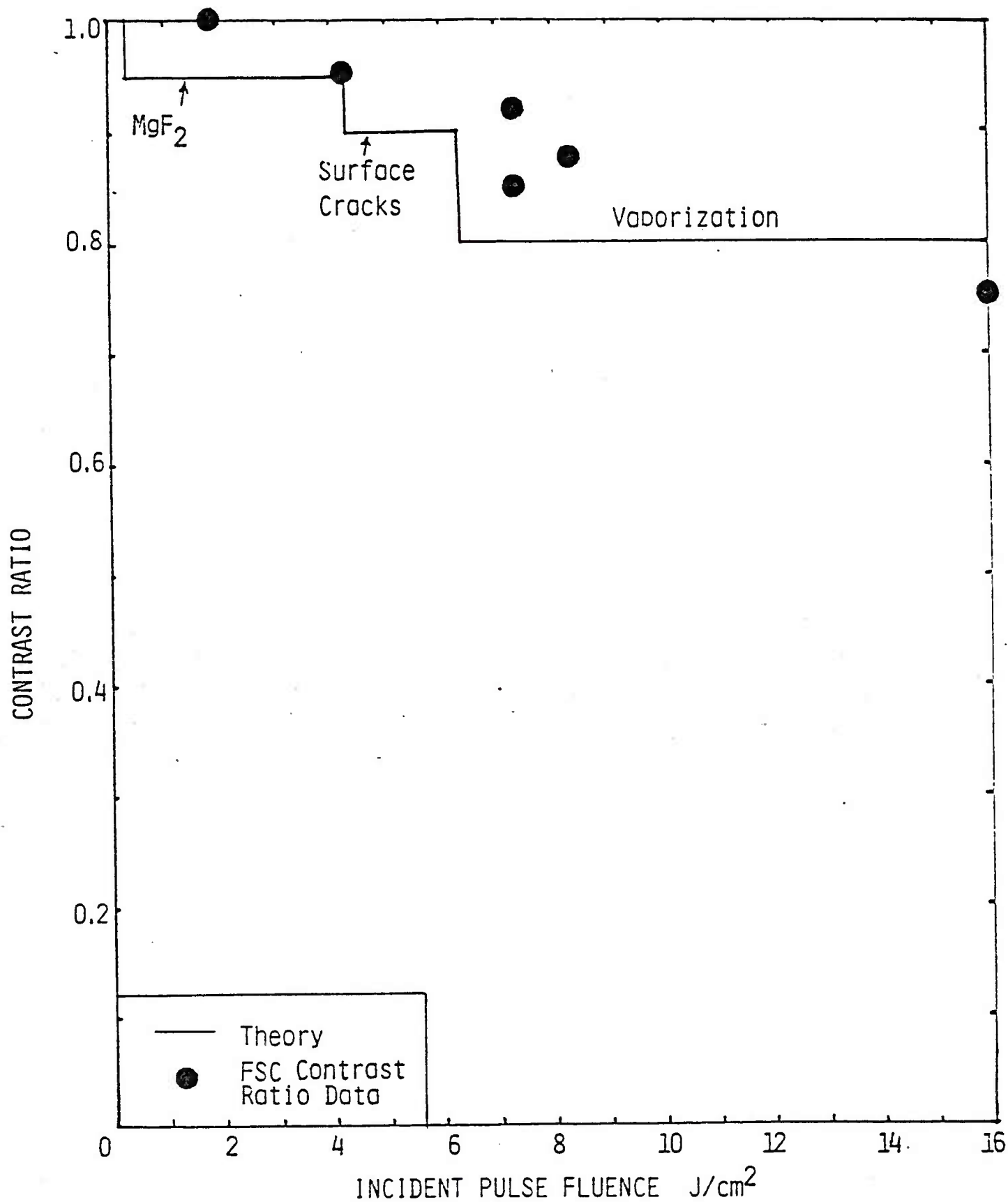
Fig. 2.3 Qualitative interpretation of contrast ratio data for FSC exposed to 5 pulses of 10.6 μm radiation at 10 Hz repetition rate. From Ref. 1.
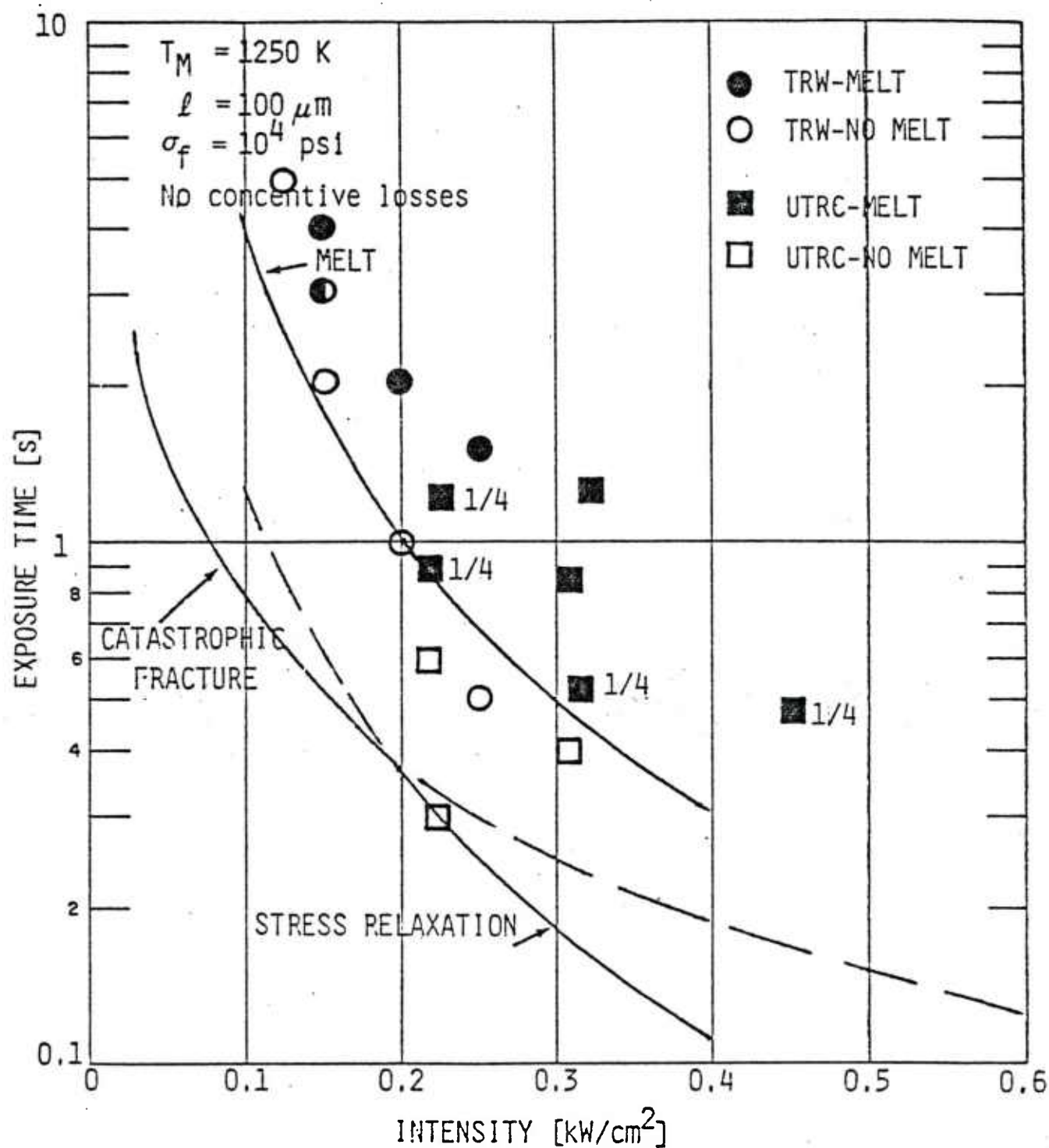
Fig. 2.4 Comparison of predicted melt times with melt and no melt data for CW 3.8 μm laser irradiation. From Ref. 1.

does not determine the magnitude of the damage. In Figures 2.1-2.3, the quantitative measurement of damage is the ratio of the contrast of an object (a black bar on a white background) when observed by a vidicon through a damaged glass sample as compared to observation through an undamaged glass sample. Interpretation of these damage measurements involves both a quantitative model of the amount of damage as well as a model of how the physical damage changes the contrast ratio. Neither of these issues were addressed under the previous program. Thus, for the purpose of comparison, the magnitude of the reduction in the contrast ratio associated with each damage mechanism was chosen so that the horizontal lines in Fig. 2.1 were consistent with the observed contrast ratio for BK7C samples. Despite the qualitative nature of the comparison, it does dramatically demonstrate that whenever a new damage mechanism was predicted, the sample did indeed show more damage, i.e., a reduction in contrast ratio. Furthermore, visual inspection of damaged samples confirmed the predicted hierarchy -- at the lowest fluence, only the surface coating was damaged; surface cracks appeared at their predicted threshold; exfoliation occurred only in samples irradiated above the predicted exfoliation threshold; bubble-like features were observed at high pulse fluence; and at the highest fluence a new damage feature, presumably caused by vaporizaton, was observed. The major issue associated with the comparison shown in Fig. 2.1 is the prediction of the quantitative level of damage (reduction in contrast ratio).

A similar comparison of the model predictions with contrast ratio data for ZKN7 is presented in Fig. 2.2. Again, the threshold predictions are consistent with the data and the major shortcoming is the lack of a quantitative model for the damage.

The comparison for fused silica is displayed in Fig. 2.3. The data give no strong evidence of the predicted threshold behavior. The predictions employ an absorption length of 6 µm for 10.6 µm radiation, whereas literature values of the absorption coefficient at 10.6 µm vary from 4 µm to 24 µm. Thus, for fused silica, the threshold calculations and data interpretation warrant further study.

18

The main features of CW 3.8 μm damage predictions are shown in Fig. 2.4, along with some earlier data pertaining to melting of the surface. Three features are predicted -- fracture of an 1/8" thick piece of BK7 when the rear surface tensile stress exceeds 10,000 psi; stress relaxation at the front surface; and melting at a temperature of 1250 K. The melting temperature and the absorption length of 100 μm at the laser wavelength were values recommended by other investigators (see Ref. 1). The available fracture data was ambiguous and could not clearly validate (or invalidate) the model. The melt prediction was in excellent agreement with the available melt data; in Fig. 2.4 it separates the tests in which melt was observed at the end of the run from those in which melt was not observed. However, there was no independent confirmation of either the melt temperature or the absorption length. In fact, photospectrometric measurements and consistent interpretation of the radiometer data both indicate that the absorption depth is approximately 0.1 cm. The major issues in the CW 3.8 μm interactions are thus validation of the catastrophic fracture predictions and resolution of the absorption length discrepancy.

Having reviewed the achievements and unresolved issues from the last program, we can now extend the modeling with the following goals in mind:

(1) to quantify the amount of physical damage

(2) to relate the physical damage to the contrast ratio data

(3) to reexamine the interpretation of RP 10.6 μm interactions with fused silica

(4) to resolve the absorption depth uncertainty in the 3-5 μm band

(5) to extend the model to Vycor.

2.3 Damage to Antireflection Coating

In the model for damaging the antireflection coating, thermal stresses are produced in the coating because its coefficient of thermal expansion is larger than that of glass. It is expected that the coating fails due to compressive stresses, and once fracture occurs a portion of the coating will be separated from the underlying glass. As a result of the thin air gap between

19

the coating and the glass, reflections can now occur at the inner and outer sides of the coating and at the glass surface. In the worse case, the coating remains and the reflection is increased to 0.06; if the coating is removed, the increase is 0.04. Although there are many cracks in the coating too, when the glass cools back to room temperature the width of the cracks is expected to be small (no change in size) and their contribution to the degradation in contrast ratio should be negligible. Thus, MgF_2 fracture is predicted to cause a 4 to 6 percent reduction in contrast ratio -- the data in Fig. 2.1 and 2.2 shows a reduction of 5 percent which is consistent with this interpretation. However, fused silica does not behave as predicted. The reason for the inconsistency has not been clearly identified. Two speculations are (1) that MgF_2 is not the antireflection coating for fused silica or (2) that the absorption coefficient of fused silica at 10.6 µm may be less than the value of 1667 cm^{-1} which is appropriate for the other glasses.

2.4 Surface Cracking

It was demonstrated in Ref. 1 that viscoelastic stress relaxation could lead to a tensile stress being frozen into a surface as it cools down after being heated by laser. This stress is large enough to initiate surface cracks at pre-existing defects called Griffith microcracks. The coefficient of thermal expansion is critical in determining the maximum tensile stress frozen into the surface. Although evidence was presented in Ref. 1 to demonstrate that the coefficient of thermal expansion increased by a factor of five when the glass temperature exceeded the glass transition temperature T_g, the viscoelastic stress relaxation model accepted only a constant coefficient of thermal expansion. The room temperature value was used in the earlier calculations. The model has now been improved to accept two coefficients of thermal expansion, one value below T_g and a larger one above T_g (see insert in Fig. 2.5). The new values of maximum surface tensile stress for BK7 are plotted in Fig. 2.5 as a function of pulse fluence. The earlier predictions which used a single coefficient of thermal expansion are also displayed for comparison. Although the temperature at which viscoelastic stress relief ceases during cool down is only about 100°C above the glass transition temperature of 559°C, the dramatic increase in the thermal expansion coefficient makes the high temperature (above T_g) contribution to the tensile stress as

20

INCREASED COEFFICIENT OF THERMAL EXPANSION ABOVE TRANSITION

TEMPERATURE ENHANCES STRESS
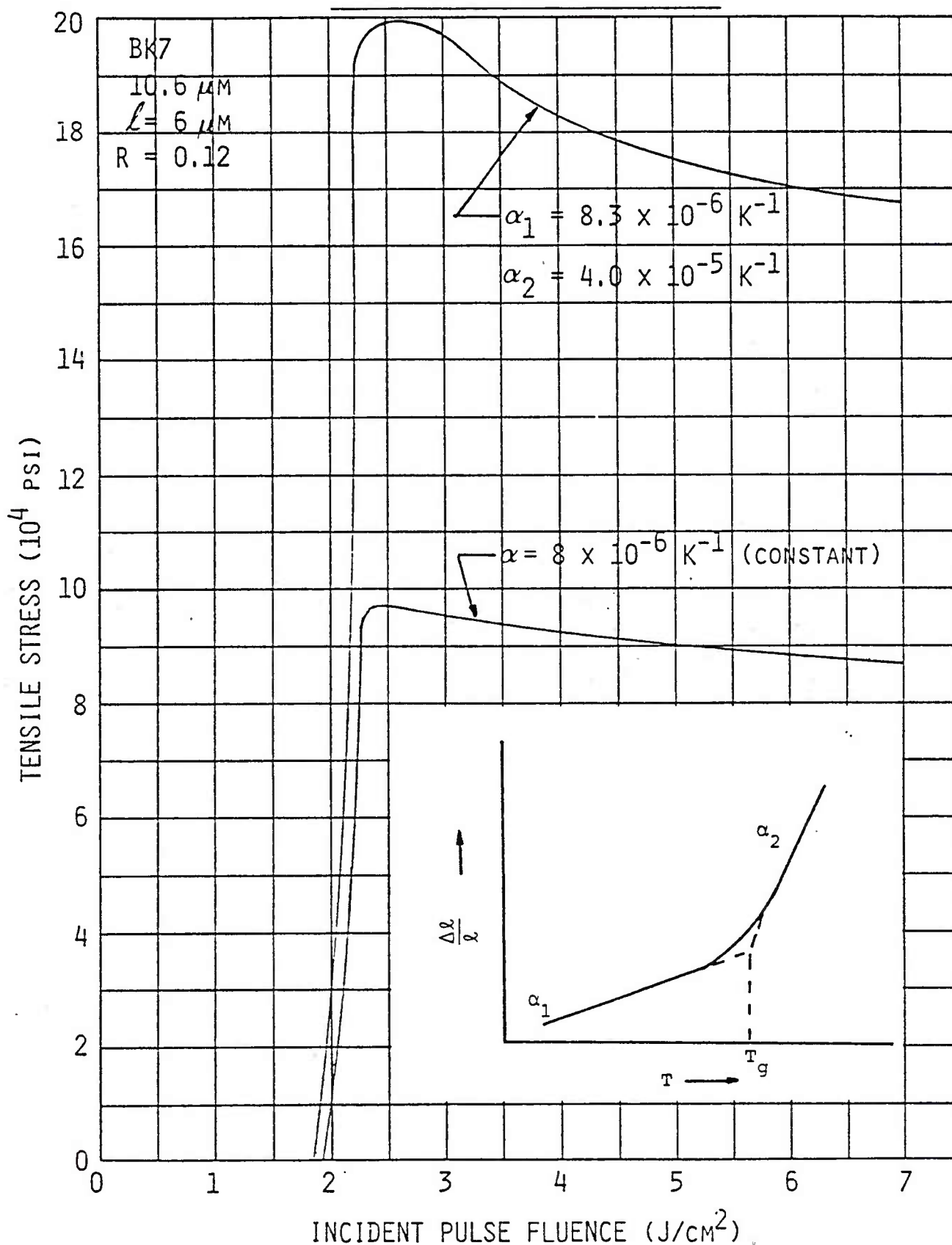
Fig. 2.5 Predicted tensile stress frozen into BK7 after irradiation by 10.6 μm laser pulse. Predictions for two choices of the coefficient of thermal expansion are compared.

large as the low temperature (between room temperature and T_g) contribution. The predictions of crack width and average intercrack spacing which were made in Ref. 1 can now be updated. The models developed in Ref. 1 now predict for BK7 a crack width of 1 µm, an intercrack spacing of 45 µm, and a total area covered by cracks which is 0.04 of the surface area. The few available photomicrographs of BK7 irradiated at 1.8 J/cm^2 are consistent with these predictions; they show intercrack distances of approximately 50 µm and crack width of 1-2 µm. It will be shown in Section 4 that cracks are expected to scatter visible light and to reduce the transmitted intensity by two times the fraction of the surface covered by cracks. Therefore we predict that cracks reduce the contrast ratio by an additional 8 percent, leading to a total reduction of 13 percent in the surface cracking regime. This is slightly less than the observed degradation, but it is of the correct magnitude.

We do not have values for the coefficient of thermal expansion of ZKN7 above its glass transition temperature; however, if it displays the same factor of 5 increase, and the same microcrack distribution function, the model predicts an average separation of surface crack of 80 µm, a 1 µm crack width and that 0.02 of the surface area is covered by cracks. The few available photomicrographs are consistent with these estimates. However, the data shown in Fig. 2.2 indicate that in the surface crack regime the contrast ratio suffers about the same amount of degradation for ZKN7 as for BK7, whereas the theory predicts only half as much. The logical next step in resolving this discrepancy is to examine in detail the physical damage features of ZKN7 irradiated at approximately 2 J/cm^2 to see whether or not the extent of physical damage is larger than predicted.

Fused silica develops little stress and it is not expected to display a large increase in the coefficient of thermal expansion at high temperature. Thus, the previous predictions of maximum tensile stress remain valid. For the nominal microcrack distribution, the predicted distances between surface cracks is large (0.3 mm). The predicted crack width is also large (3 µm), but only 0.002 of the surface is covered by cracks. Photomicrographs show no evidence of cracks on fused silica for experiments in the far field. The lack of cracks does not contradict the theory since few cracks are expected. In

22

fact, the predicted number of cracks is very sensitive to the details of the microcrack distribution near the threshold for cracking. Since only a small fraction of the surface is covered with cracks, they have little effect on the contrast ratio. This is consistent with the data shown in Fig. 2.3.

As a final note on surface cracks, photomicrographs of BK7 irradiated at 4.3 J/cm^2 display larger cracks than those irradiated at 1.8 J/cm^2. At the higher fluence, the average separation between cracks is 150 µm and the crack width is 2 to 5 µm. This increase in the separation between cracks as the fluence increases can be dramatically seen in individual tests at high fluence -- moving from the center of the spot to the edge crosses both the immediate ($\approx$ 4.3 J/cm^2) and low (1.8 J/cm^2) fluence range, thereby permitting the different crack patterns to be viewed simultaneously. A potential explanation for this behavior will be offered in the discussion on exfoliation in subsection 2.6.

In summary then, the improved predictions of crack separation and crack width for BK7 and ZKN7 are in good agreement with the photomicrophic observations on near threshold fluence. The reduction in contrast ratio in BK7 is of the magnitude predicted, but ZKN7 exhibits a decrease which is twice the predicted size. Surface cracks are expected to have little effect on fused silica.

2.5 Melting as Stress Relaxation

As glass cools, the transition from the regime of high coefficient of thermal expansion to low coefficient of thermal expansion occurs at the temperature at which viscoelastic stress relaxation (structural rearrangement) ceases. This temperature depends on the cooling rate. The nominal glass transition temperature corresponds to a cooling rate of 5°C min. During the rapid cooling following laser irradiation, the transition takes place at higher temperature and the glass thus formed is less dense than the original glass. This effect is shown qualitatively in Fig. 2.6 where the volume of glass if shown as a function of temperature. Initally, at temperature T_o, the glass has a volume V_o. As the glass is heated above the glass transition temperature, the rate of expansion with temperature increases dramatically. When irradiation ceases, the glass has attained a final temperature T_f, and the

23
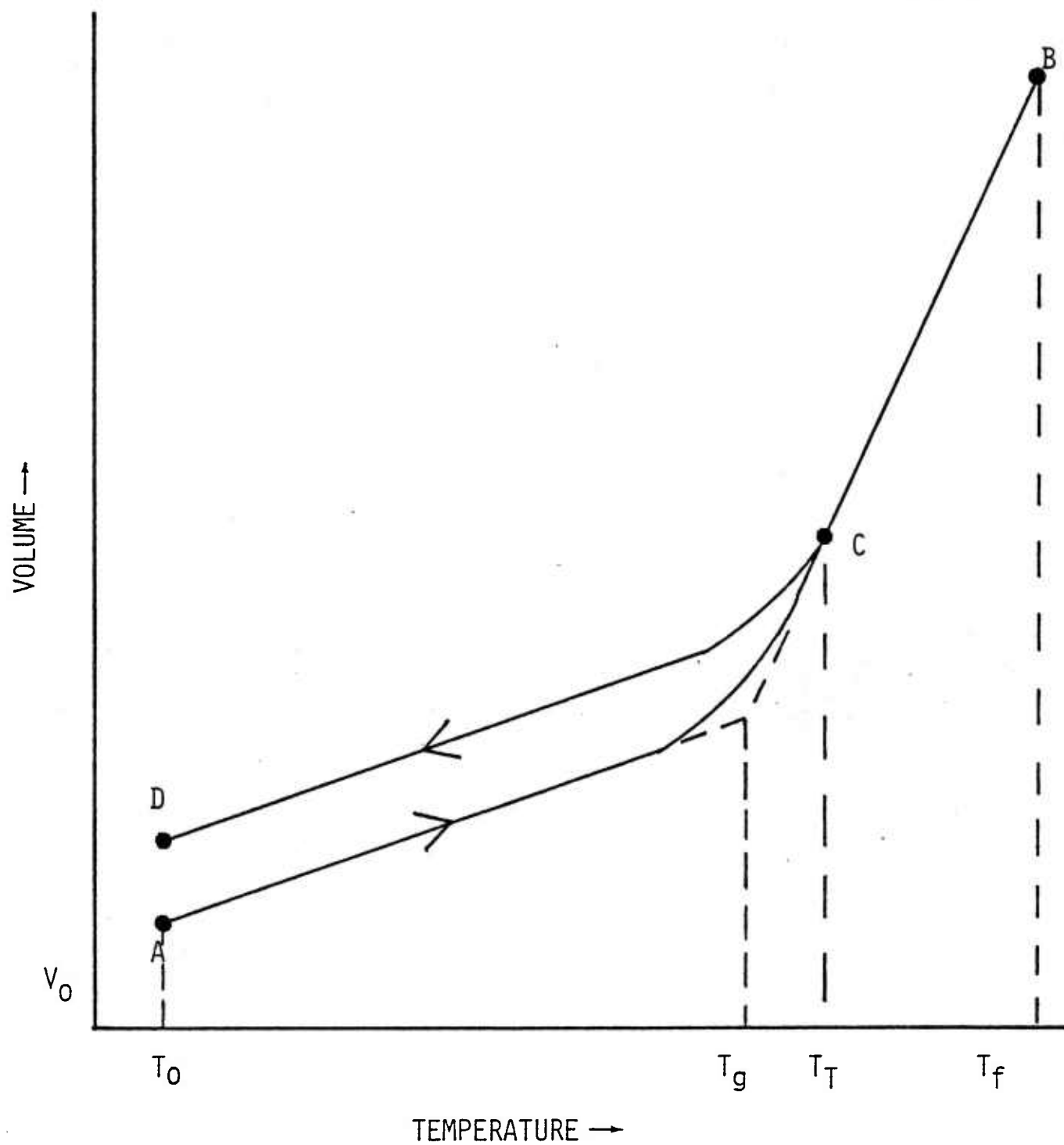
Fig. 2.6 Volume of glass as a function of temperature for a rapidly heated and cooled sample.

state of the glass is represented by point B. Two separate phenomena contribute to this large apparent coefficient of thermal expansion. The first is the normal expansion of a fixed structure with temperature; for glass this term is approximately given by the coefficient of thermal expansion below the transition region. The other contribution is structural rearrangement of the glass. At high temperature (low viscosity), rearrangement occurs at the same rate as the heating and dominates the thermal expansion, whereas at low temperature (high viscosity), rearrangement cannot proceed and there is no additional contribution to thermal expansion.

During subsequent cooling, structural rearrangement keeps pace with the temperature decrease until the glass attains temperature T_t (and state C); below this temperature, structural rearrangement ceases and the decrease in volume with temperature follows the much shallower slope characteristic of normal thermal contraction without structural rearrangement. When the temperature of the glass falls to the initial temperature T_0, the volume (density) of the glass is larger (smaller) than it was originally. This change in volume (density) is permanently frozen into the glass. The density change also results in a change in the index of refraction. Thus, this change may well be noticeable in the optical characteristics of the glass after irradiation, especially if the glass has suffered fracture which would lead to unequal expansion in different directions. It is proposed here that the state of the glass identified as melt in some of the experiments is in reality glass that has been heated above the transition temperature and is now in a state of lower density. Furthermore, this state will be detrimental to optical performance since it changes the index of refraction nonuniformly across the whole irradiated area.

2.6 Exfoliation

The tensile stresses frozen into glass as it cools down lie in the plane of the surface. When Griffith microcracks fail, the cracks that are formed propagate vertically into the glass until there no longer are any stresses causing them to grow. The first cracks propagate vertically because of symmetry. However, once a vertical crack is formed, as sketched in the cross section shown in Fig. 2.7a, components of stress are generated at the

25

ORIGINAL   SURFACE
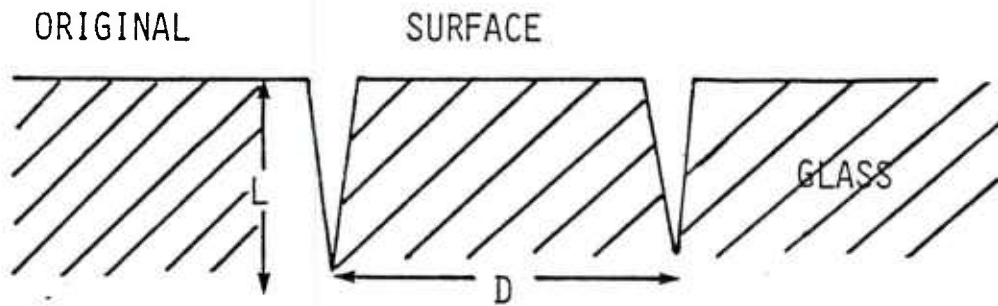
GLASS

(a) cross section of glass surface which has vertical cracks

σ_X

σ_Z σ_Z σ_Z σ_Z
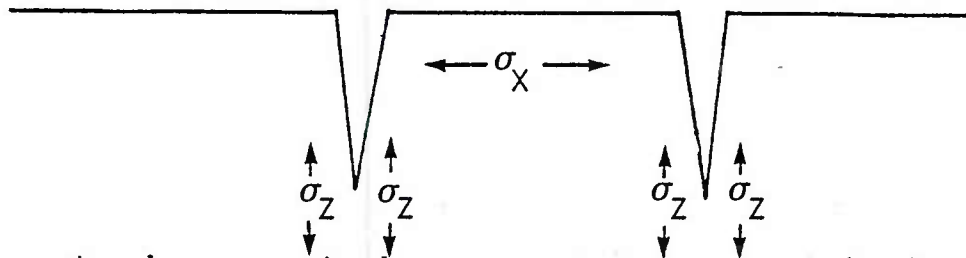
(b) stress develops vertical component σ_Z near crack tip

(c) cracks propagate horizontally causing exfoliation

Fig. 2.7 Exfoliation of glass.

26

tip of the crack which are perpendicular to the orginal surface. These are shown in Fig. 2.7b. In the previous work, it was demonstrated that the crack depth D was greater than 0.07 of the distance L between cracks, the stresses tending to produce horizontal cracks parallel to the surface were larger than the stresses which tend to initiate new vertical cracks at the surface. This translated into a criterion for exfoliation (flaking), namely D/L > 0.07.

The previous work gave a criterion for exfoliation to occur somewhere on the surface -- it did not indicate the fraction of the surface area which would experience exfoliation.

The number of exfoliations which will occur can be estimated as follows: Cracks initiated at surface defects propagate vertically into the glass as deep as viscoelastic stress relaxation has occurred. If the distance is less than the critical depth required for exfoliation (i.e., D/L < 0.07), no horizontal cracks are formed. If the depth is larger than the exfoliation criterion, the crack develop a horizontal component as shown in Fig. 2.7c. The number of cracks which do not lead to exfoliation can be calculated, for any given pulse fluence, from the stress σ_T which is frozen into the surface before stress relaxation reaches the critical depth for exfoliation. The stress σ_T is shown as σ_T in Fig. 2.8 as a function of 10.6 μm pulse fluence for BK7 and assumed depths of 5 μm, 7.5 μm and 10 μm. The transition from no exfoliation (no stress relaxation at a given depth) to complete exfoliation ($\sigma_T \ll 10^5$ psi) occurs rapidly. Therefore the model predicts either that exfoliation does not occur or it occurs throughout the whole area subjected to the incident pulse fluence (assumed uniform). This behavior is observed qualitatively in the irradiated samples. Furthermore, exfoliation, as illustrated in Fig. 2.7c, results in more effective stress relief in glass than is possible by the vertical cracks illustrated in Fig. 2.7a. Thus, once exfoliation is initiated, it is unlikely that further cooling of the flake will result in more vertical fractures. In other words, the onset of exfoliation terminates further vertical cracking, and the number of vertical cracks becomes less. For BK7 irradiated at 4.3 J/cm^2, Ref. 1 predicts that viscoelastic stress relaxation occurs to a depth of 9 μm. From the criterion D/L > 0.07 for exfoliation, the distance between cracks at the onset of exfoliation is expected to
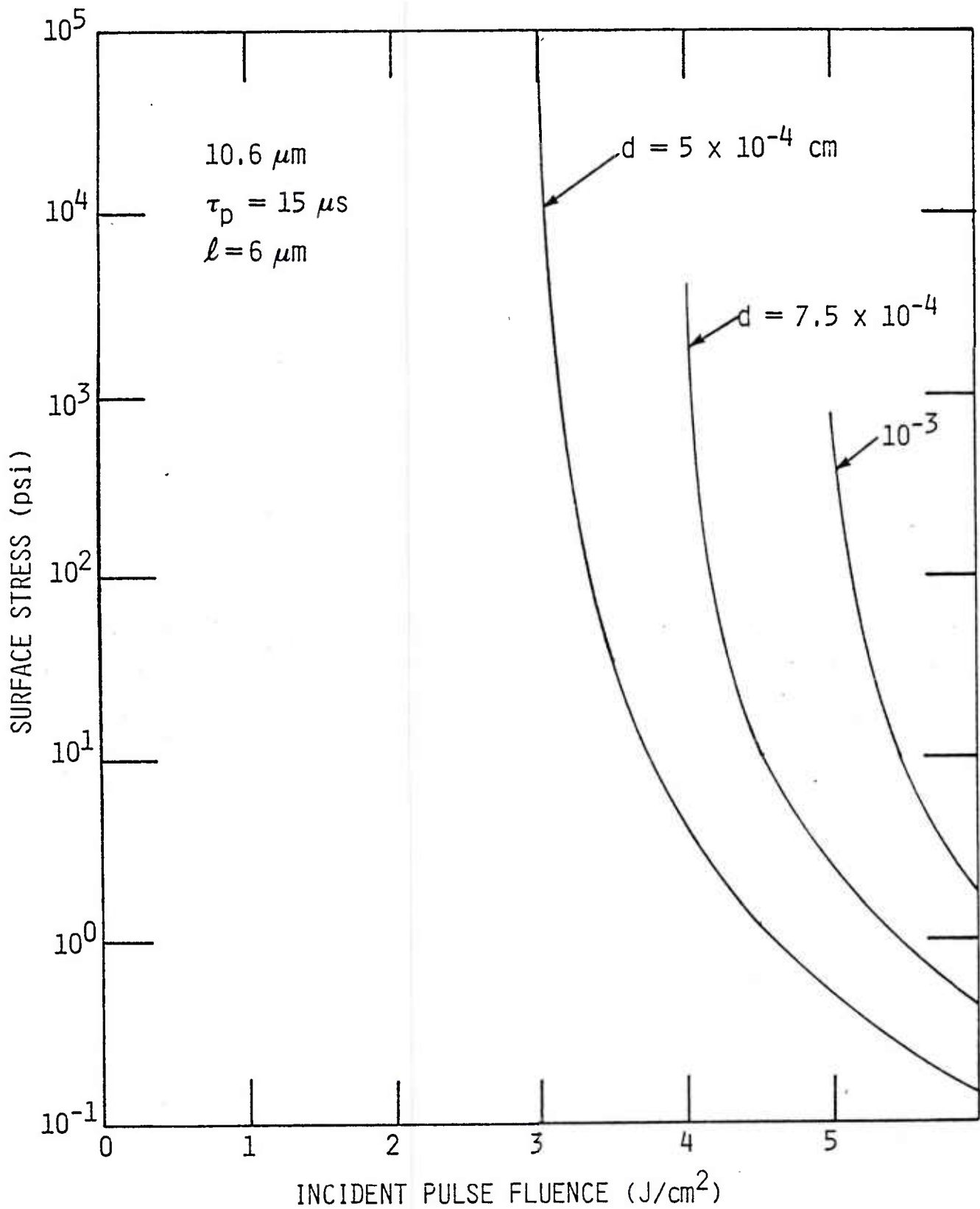
Fig. 2.8 Tensile stress frozen into surface of BK7 irradiated by 10.6 μm laser
pulse at the time when tensile stress first develops at a specified
depth d.

be 135 μm, and no further vertical cracks are generated because the exfoliations relieve the lateral stresses. This is in excellent agreement with the available photomicrographs of BK7 irradiated at 4.3 J/cm^2 -- they display an average crack separation of 150 μm.

In this model, increasing the pulse fluence results in larger inter-crack separations in the exfoliation regime. Furthermore, the exfoliation threshold is reduced from 3 J/cm^2 to almost 2 J/cm^2 because of the decreased minimum distance between cracks predicted with the updated BK7 thermal expansion properties. (For L = 45 μm, D ≈ 3.1 μm).

At least two mechanisms contribute to optical degradation by exfoliated glass. First, there are two more reflecting surfaces, which decrease the constrast by a total of 8%. In addition, if the phase change caused by the exfoliation is large, each element creates its own diffraction pattern. In repetitively pulsed interactions, where the flakes have a chance to trap air bubbles during the cycles of structural rearrangement (on heating) and freezing (on cooling), the phase difference should be large. The effect of exfoliation on optics will be discussed in detail in Section 4. Here some simple calculations are presented to show that the diffraction effect can, in fact, reduce the contrast ratio, but that accurate predictions of the magnitude of the reduction require more detailed knowledge of the optical system used to make the measurements. The object in the contrast ratio measurement is approximately 0.3 cm wide and approximately 1.0 m from the camera; thus, it subtends an angle of approximately 3×10^{-3} radians, as shown in Fig. 2.9a. The diffraction pattern of a 150 μm square subtends an angle of approximately 8×10^{-3} radians between the first zeros as sketched in Fig. 2.9b. If the camera has a magnification of 1, the contrast ratio is found by convoluting the diffraction pattern with the object. For the geometry described, the convolution will result in a contrast ratio reduction of approximately 35%. The total predicted reduction from exfoliation is 45% which is in good agreement with the data presents in Fig. 2.2. Of course, the values used in the calculations are approximate -- more accurate details of the object size and location, and camera optics are essential for accurate predictions. Exfoliation is predicted to decrease the contrast ratio an additional 0.45 more than surface cracking.

29

(b) diffraction pattern for 600 nm light from 150 μm flake

(a) approximate measurement configuration
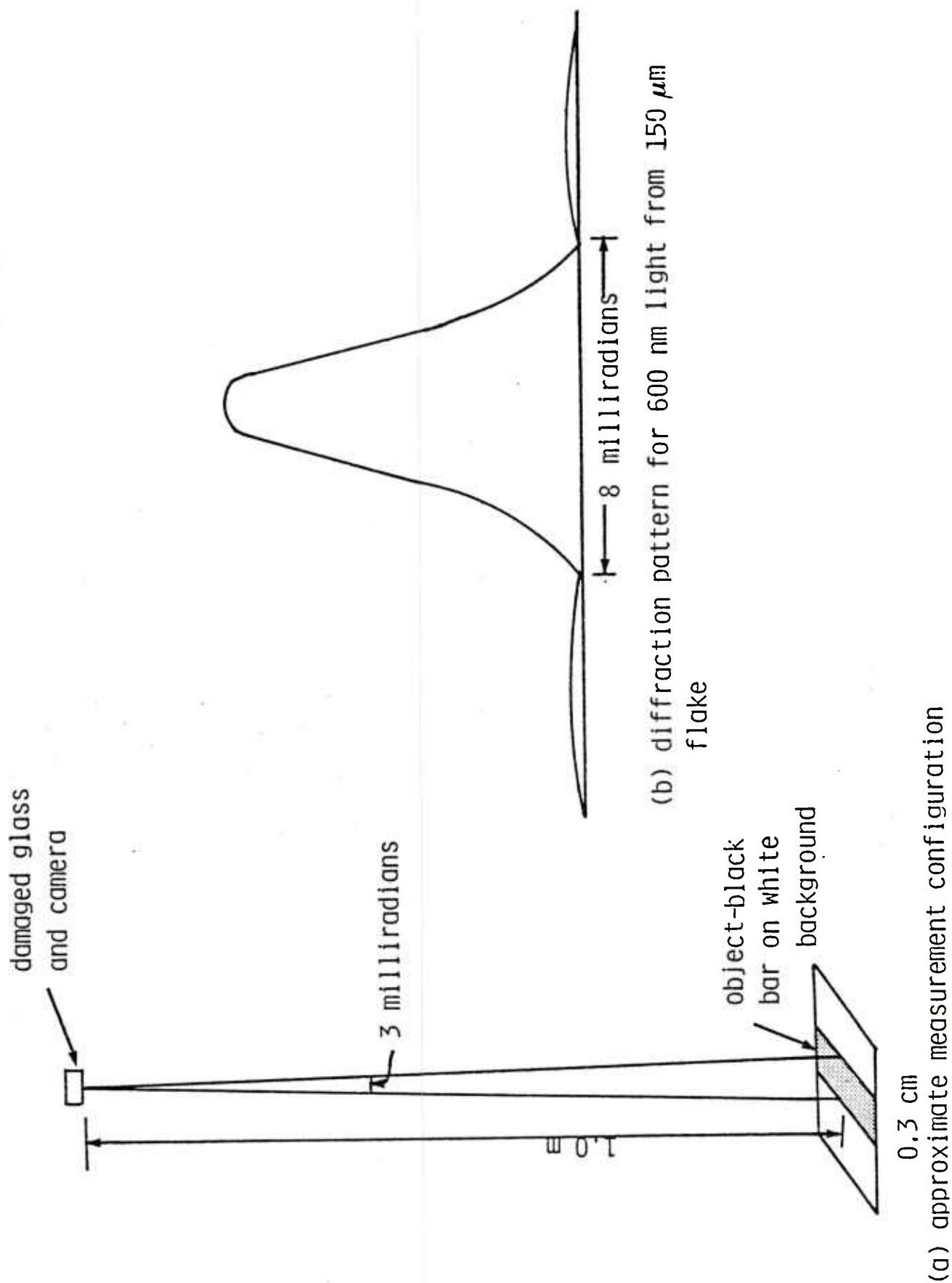
Fig. 2.9 Important parameters in contrast ratio measurement.

30

For ZKN7, the reduction is expected to be the same since the size of the exfoliation is approximately the same. Thus, the smaller degradation observed in ZKN7 interactions (compare Figs. 2.2 and 2.1) cannot be explained on the basis of larger exfoliation zones -- rather it must be caused by a smaller phase change. Note, however that the data shown in Fig. 2.2 support the prediction that the damage does not change much as the fluence is increased within the exfoliation regime.

The most important characteristic of exfoliation for optical damage estimates is that it damages the whole surface and that it can lead to large random phase changes.

2.7 Vaporization

Most glasses are mixtures (except for fused silica) and the various components of the mixture have different vapor pressures at a fixed temperature. Since the vapor pressure in pulsed laser interactions usually is much larger than the background pressure, the mass loss rate is almost linearly proportional to partial pressure. Therefore, the different components of the glass mixture vaporize at different rates, and the surface composition of the glass is changed. The magnitude of the composition change and the depth to which this modification occurs depend upon the laser pulse fluence (and pulse time for long pulses). The index of refraction is sensitive to changes in composition. It is proposed that vaporization leads to a nonuniform index of refraction. Inspection of damage BK7 suggests that the variations occur over scales of approximately 10 µm. Furthermore, the changes are expected to produce a large phase change, for example, a composite change of 20% over a depth of 2 µm will cause a phase change of 2π. This random variation in phase is disastrous for optical performance (see Sec. 4). In Fig. 2.1 and 2.2, the same analysis which led to an estimated reduction in contrast ratio of 45% for exfoliation yields a reduction of 90% for scale sizes of 10 µm and 80% for scale sizes of 20 µm. ZKN7 and BK7 exhibit small contrast ratios in the vaporization regime consistent with expectations. Fused silica does not experience differential vaporization, thus its optical degradation in the vaporization regime is expected to be small. The data in Fig. 2.3 are consistent with these qualitative predictions.

31

2.8 Vycor Damage

The models developed in the previous report have been applied to Vycor 7900. The basic material properties are listed in Table 2.1. The predicted tensile stress frozen into the surface of Vycor 7900 is compared to fused silica in Fig. 2.10; both predictions assume an absorption length of 6 μm. The threshold for crack formation is the same for both materials -- approximately 5 J/cm^2. The number of cracks is expected to be twice as large for Vycor as fused silica, but both are predicted to have only a few cracks. For the nominal distribution of Griffith microcracks, the predicted average separation between surface cracks for Vycor 7900 is 0.08 μm, and the fraction of the area covered by cracks is 0.004. Of course the results for a particular irradiation are very sensitive to the details of the microcrack distribution near the threshold. For the nominal distribution, the predicted reduction in contrast is less than 0.01.

The vaporization thresholds for silica and Vycor are also noted in Fig. 2.10. The change in fluence required to initiate vaporization is dominated by the difference in the equilibrium vapor pressure as a function of temperature. The predicted vapor pressure of Vycor 7900 in the ideal mixture approximation is compared to the results for fused silica in Fig. 2.11.

2.9 Absorption Length in Fused Silica

Many of the features of the data shown in Fig. 2.3 can be understood as a result of the updated modeling discussed earlier in the section. For example, surface cracks and vaporization are predicted to cause much less optical degradation in fused silica than in glassess. However, there is a mounting mass of evidence that the absorption depth in fused silica at 10.6 μm may be considerably longer than in other glasses. Literature values[2] of the absorption depth vary from 4 to 20 μm. Recent measurements[3] suggest a value between 16 and 24 μm. Some experimentalists[4] have observed significant scatter in experiments; this suggests that the response of fused silica differs from one sample to another. To assess the implication of a long absorption depth, the stress and vaporization threshold for fused silica has been calculated for

32

TABLE 2.1

Properties of Vycor 7900

	Symbol	Units	Vycor 7900
Density	ρ	g/cm^3	2.15
Coefficient of linear expansion (average 20°C-300°C)	α	K^{-1}	8.1×10^{-7}
Transformation Temperature	T_g	°C	875
Modulus of Elasticity	E	psi	10^7
Poisson's Ratio	ν		0.19
Specific Heat at 300 K	C	J/g-K	0.74
Thermal Conductivity at 300 K	k	W/cm-K	1.26×10^{-2}
Viscosity, expressed	η_0	poise	0.1
as $\eta_0 \exp \dfrac{Q}{T-T_0}$	Q	K	34310
	T_0	K	100
Vaporization Temperature	T_v	K	3150
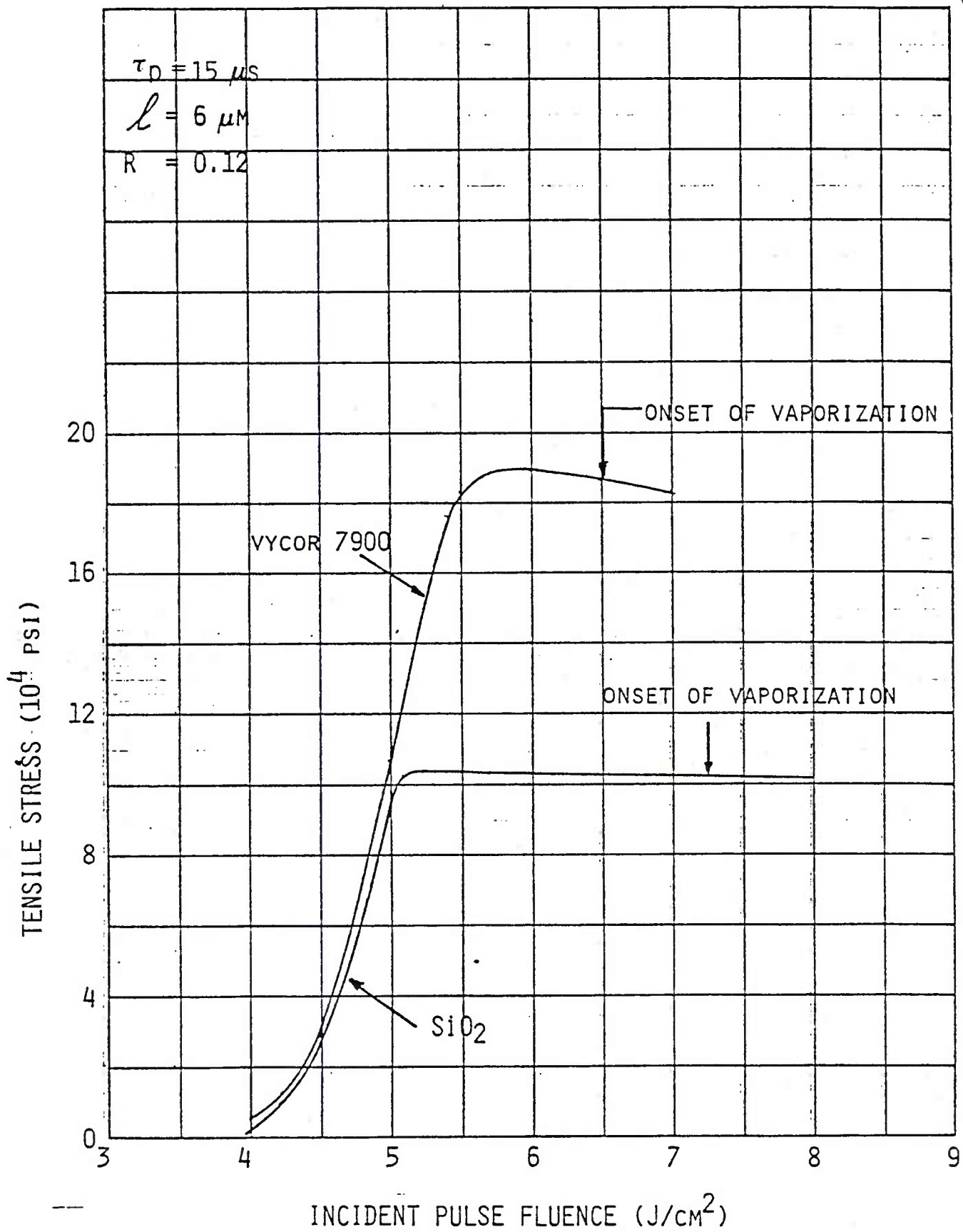
Fig. 2.10 Comparison of response of Vycor 7900 and fused silica to 10.6 μm
laser pulse.
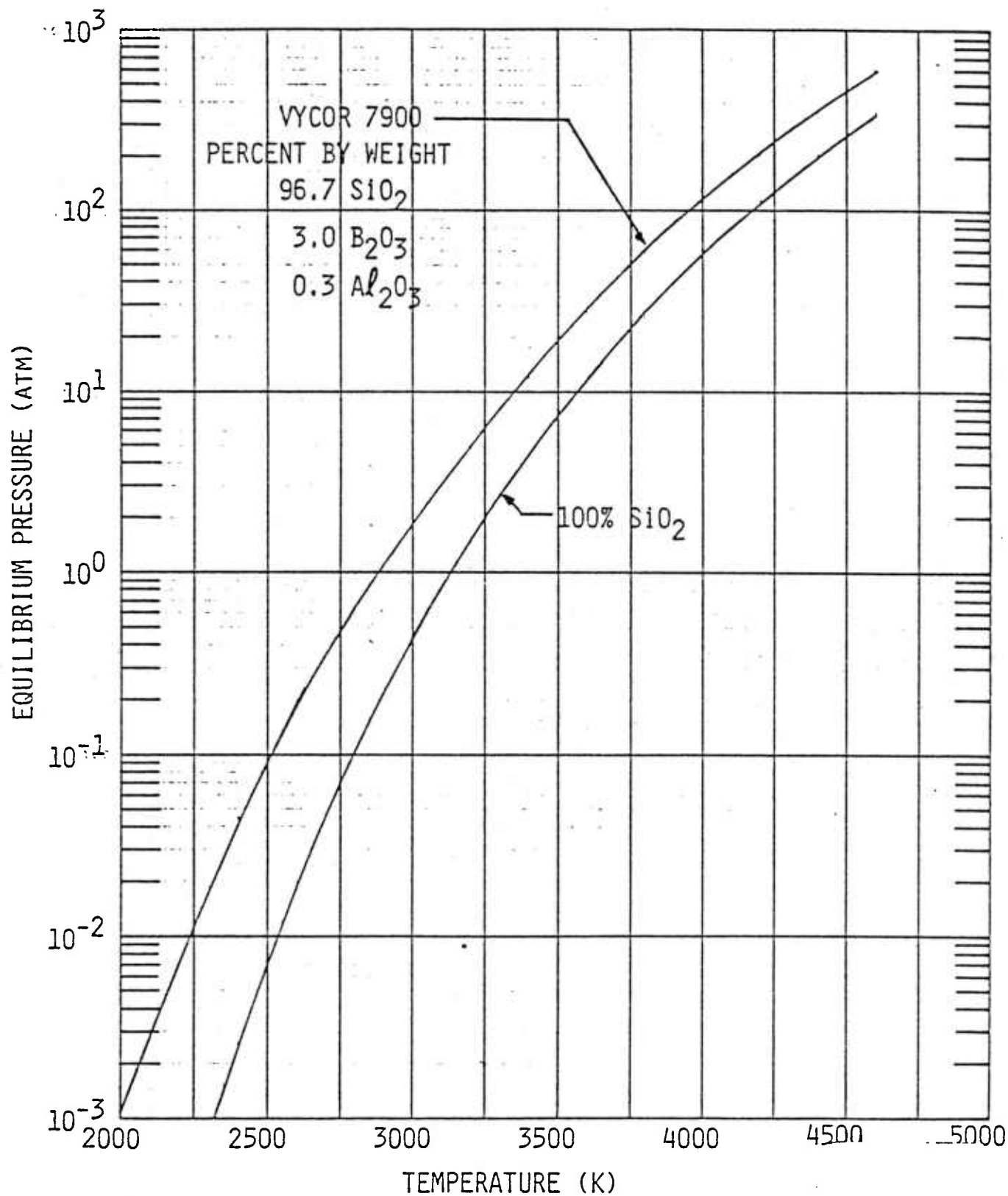
Fig. 2.11 Equilibrium vapor pressure of Vycor and fused silica.

an absorption depth of 20 μm; the results are plotted in Fig. 2.12 where they are compared to the predictions for an absorption length of 6 μm. The fracture criteria (10,000 psi) is met at 12.2 J/cm^2 rather than 4.8 J/cm^2. It should be noted that even if surface cracks are not formed (for example, because of a dearth of microcracks), this threshold also corresponds to reaching the melt temperature (2000 K) of silica. Similarly, the onset of vaporization is shifted from 6.7 J/cm^2 to 17.8 J/cm^2.

2.10. <u>RP Contrast Data Reinterpretation</u>

The extensions to the glass damage modeling, which were presented above, can be used to reinterpret the contrast ratio data. These updated reassessments are given in Figs. 2.13-2.15 and the first predictions for Vycor are presented in Fig. 2.16. For BK7 (see Fig. 2.13) the only change in the threshold behavior is the shifting of the exfoliation threshold to lower fluence. The major improvement is that the damage levels for MgF_2 fracture, surface cracks and exfoliation are now predicted rather than arbitrary. Bubble growth predictions have not been updated. But the vaporization prediction is qualitatively consistent with the interpretation given in subsection 2.8 for damage by vaporization.

The prediction for ZKN7 have been updated in Fig. 2.14. The thresholds have not changed, but the magnitude of the damage has been predicted. The agreement with the data is adequate but not inspiring. It may indicate that the phase shift in exfoliation has been over estimated.

For fused silica, two predictions are shown in Fig. 2.15 -- one for an absorption length of 6 μm, the other for 20 μm. Neither value gives an entirely satisfactory interpretation of the data, but both give reasonable explanations of why fused silica suffers less damage than other glasses. (Alternatively, the data can be correlated by assuming ℓ = 6 μm and that the contrast ratio decreases in proportion to the melt layer thickness.) This correlation is shown in Fig. 2.16 for the predicted performance of Vycor with a 6 μm absorption depth. The major difference from the fused silica prediction is that differential vaporization will degrade Vycor substantially in the vaporization regime.
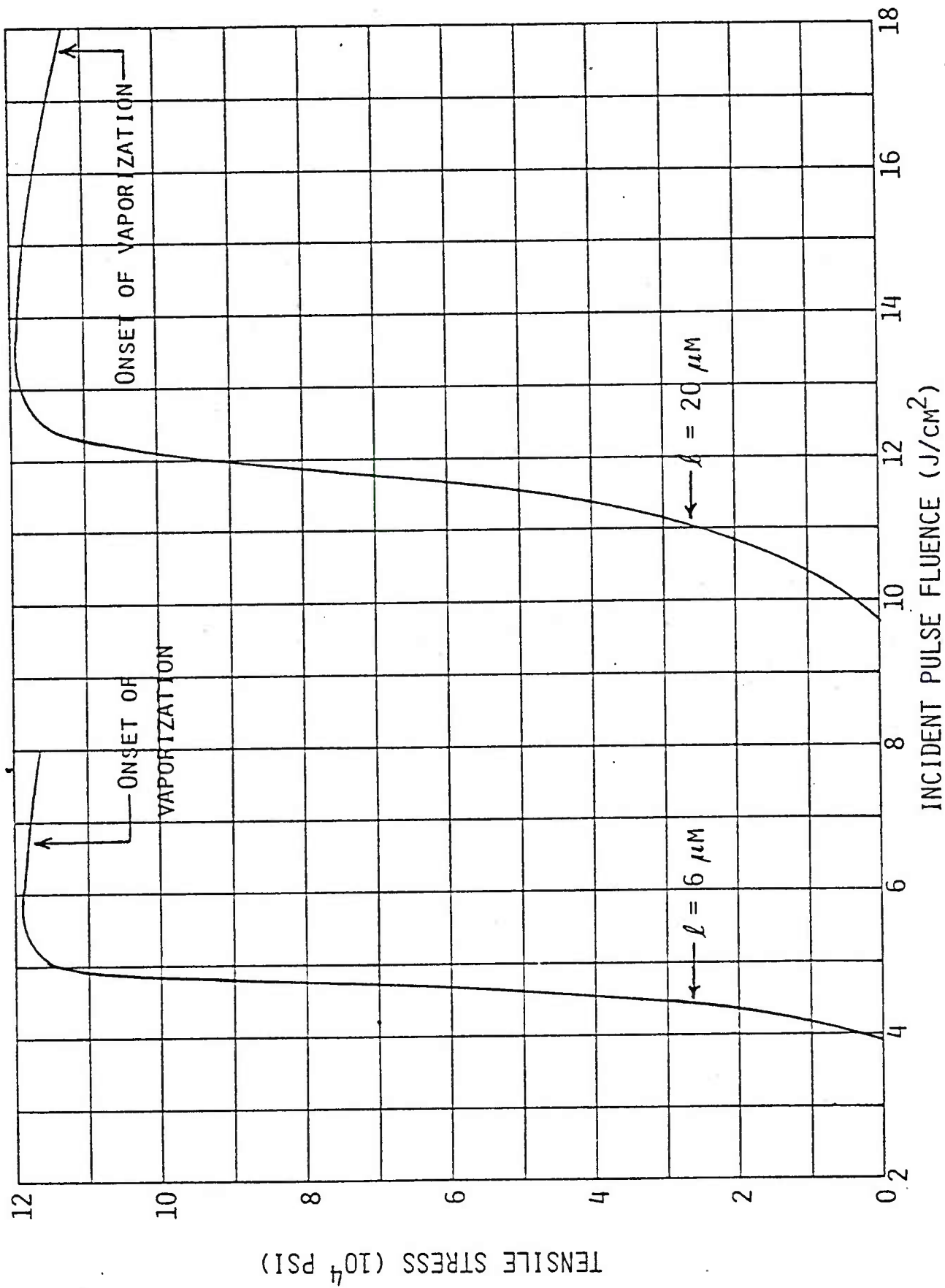
Fig. 2.12 Comparison of tensile stress at surface of silica after 10.6 μm laser pulse for two different absorption lengths.
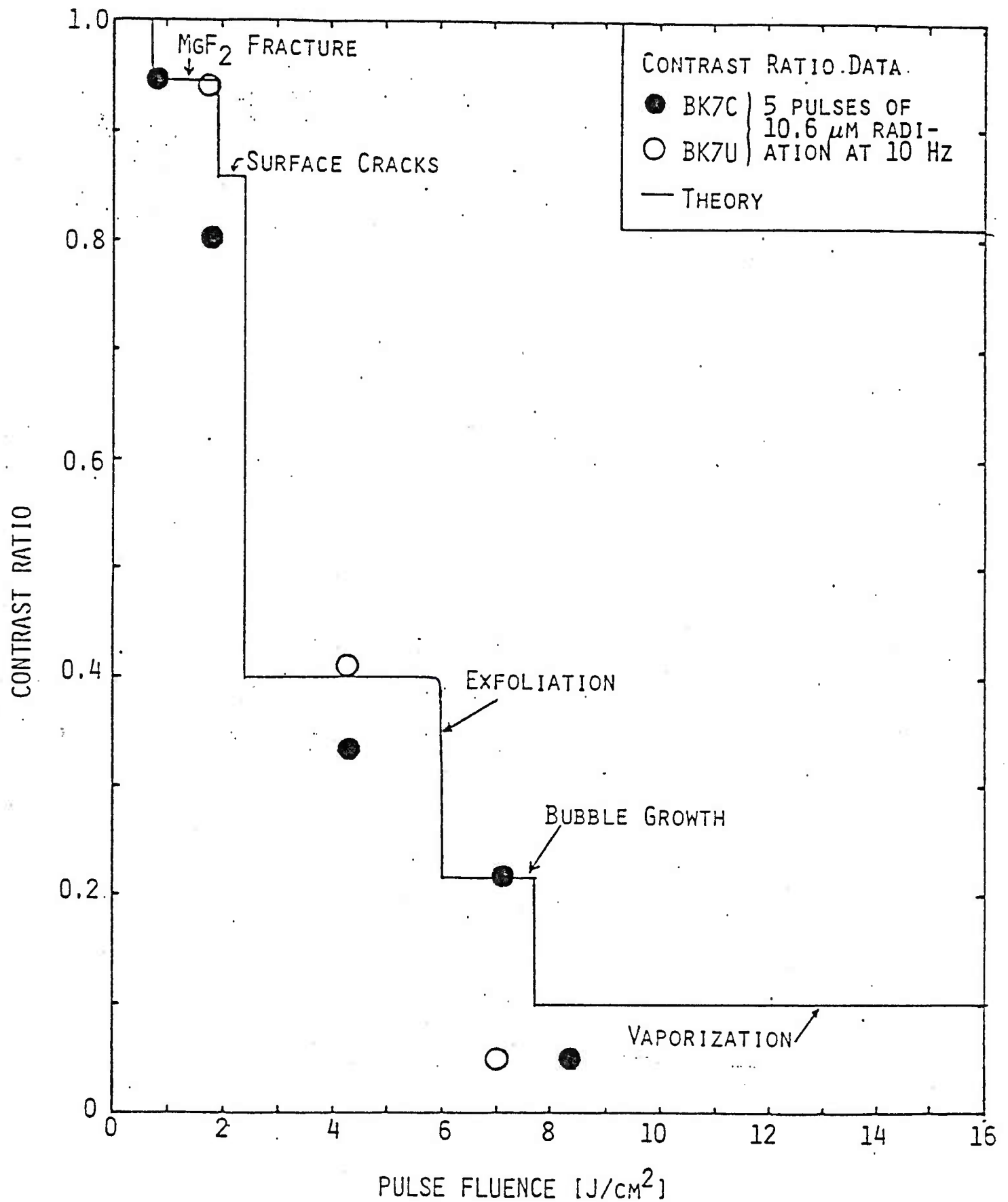
Fig. 2.13 Quantitative predictions of contrast ratio data for BK7 damaged by
5 pulses of 10.6 μm radiation at 10 Hz repetition rate.
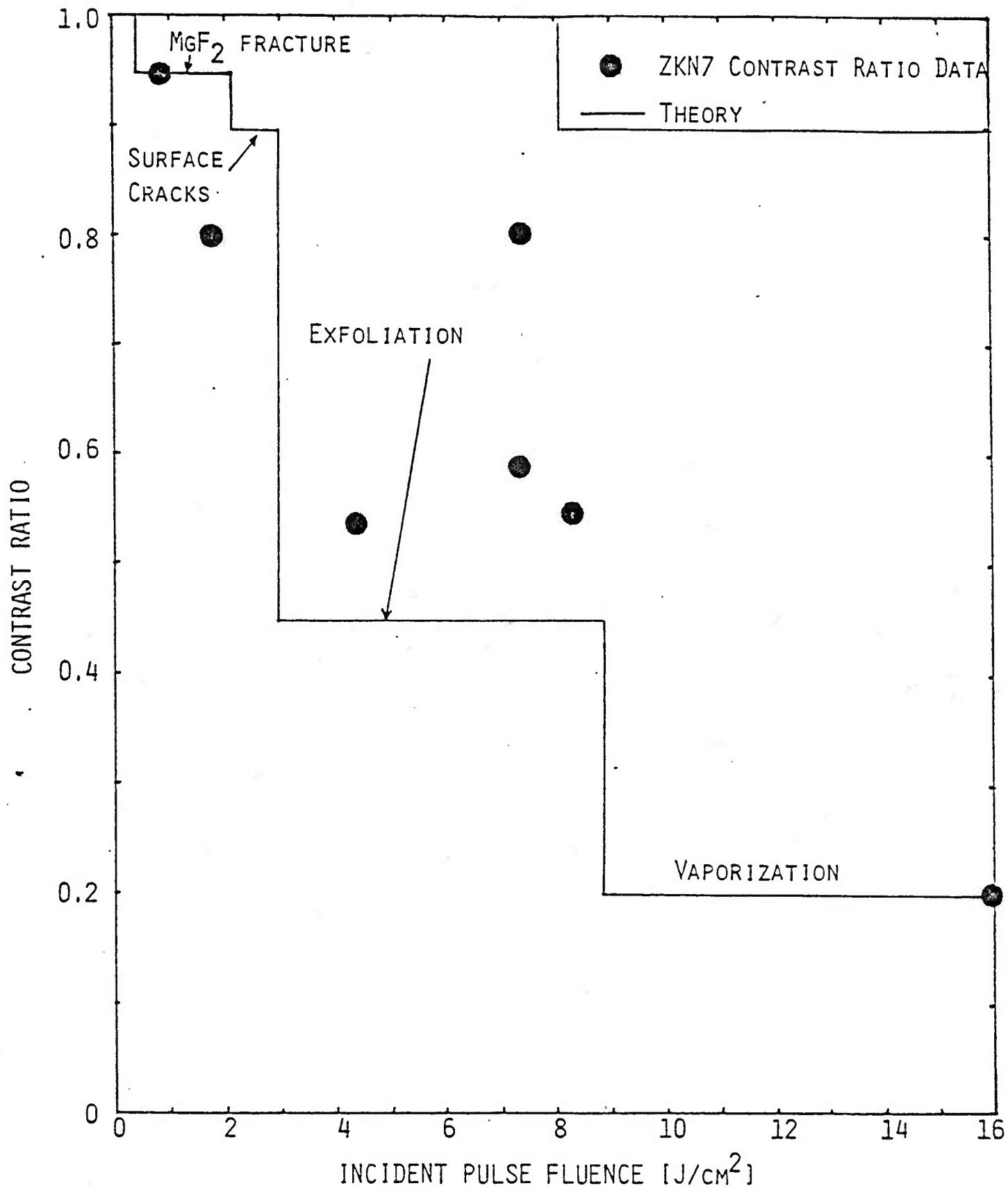
Fig. 2.14 Quantitative predictions of contrast ratio data for ZKN7 exposed to 5 pulses of 10.6 μm radiation at 10 Hz repetition rate.
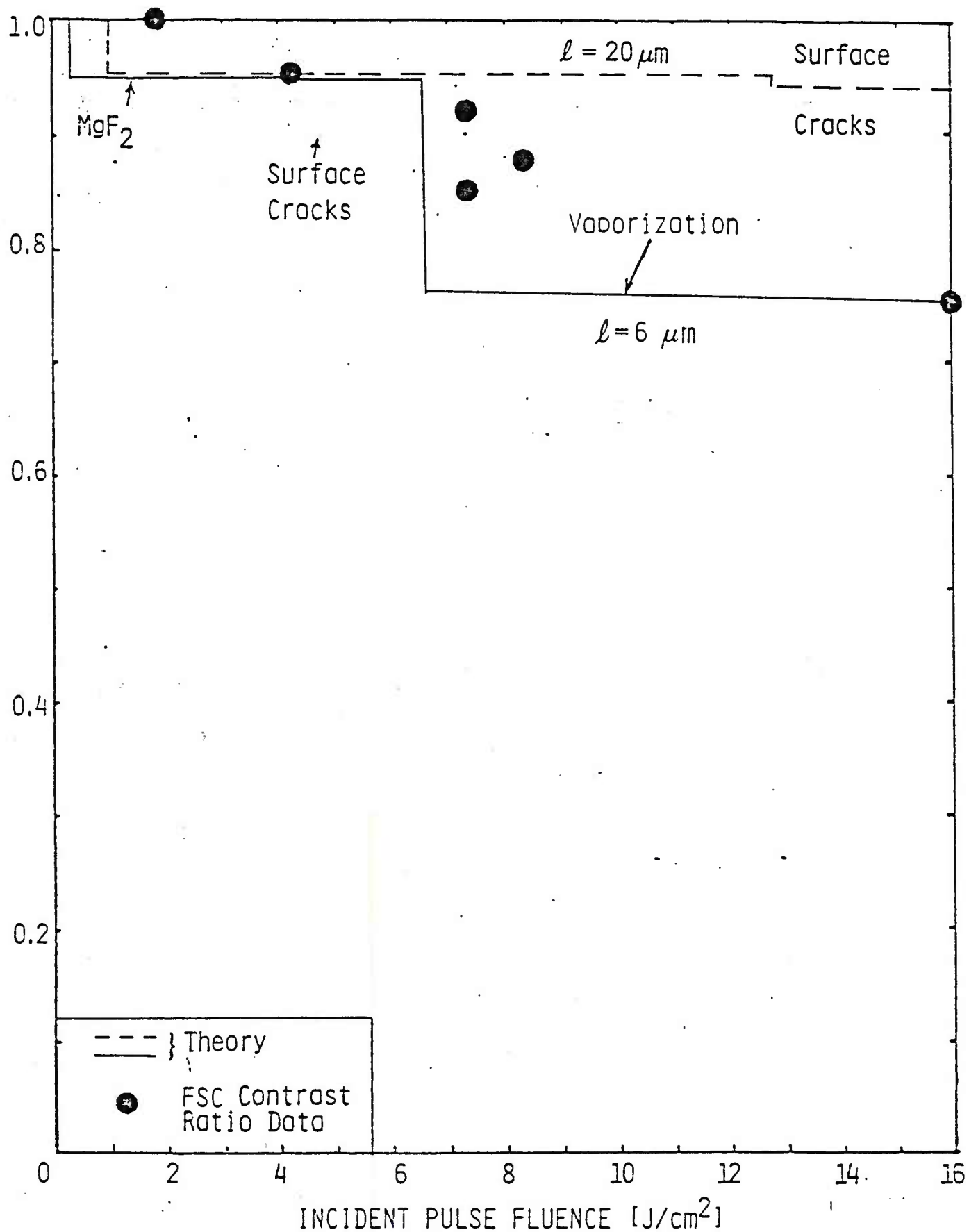
Fig. 2.15 Quantitative interpretation of contrast ratio data for FSC exposed to
5 pulses of 10.6 μm radiation at 10 Hz repetition rate. Predictions
corresponding to two choices of absorption depth are shown.
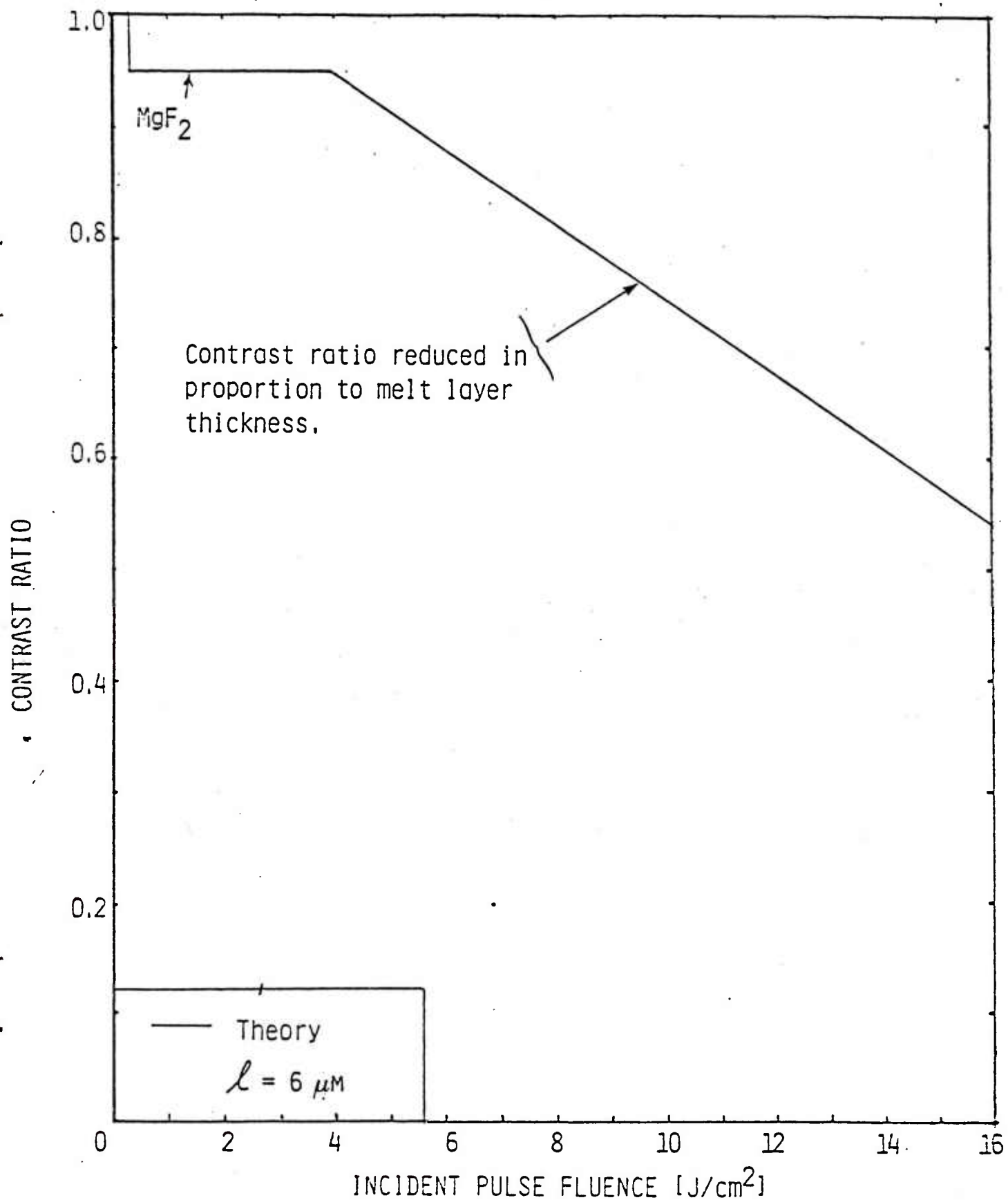
Fig. 2.16 Predictions of contrast ratio for Vycor based on melt layer thickness. Effect of melt layer is estimated to be twice as large for Vycor as for fused silica.

2.11 CW 3.8 μm Interactions

Recent measurements[3] of the absorption depth of glasses at 3.8 μm confirm that the value of 100 μm used in early calculations is incorrect. Since there is evidence[5,6] that the absorption length can change with temperature, however, we can not be certain of the appropriate value to use in our calculations. To help choose a value, we have calculated, for various absorption lengths, the time required to cause stress relaxation in BK7 for 3.8 μm CW irradiation at 200 W/cm^2. The results are plotted in Fig. 2.17. Diffusion is important, thus the exposure time does not increase linearly with absorption depth. The "melt" prediction shown in Fig. 2.4 at 200 W/cm^2 could be duplicated by using an absorption depth of 0.08 μm and the stress relaxation criterion. Since the measured values tend to be slightly larger, we have used a value of 0.1 cm for the updated calculations shown in Fig. 2.18. This comparison shows that the melt data are consistent with predictions based on the measured absorption length and the interpretation of melt as the permanent density change accompanying stress relaxation.

The fracture predictions are insensitive to absorption depth but they do depend on the thickness of the glass and the fracture criterion. "As is," glass usually fails at 5,000 psi, carefully handled glass at 10,000 psi, and the nominal microcrack distribution function used in Ref. 1 corresponds to a first failure at 7,500 psi. The effect of failure criterion on exposure time to first fracture is illustrated in Fig. 2.19 for 1/8" thick BK7. As the laser intensity is varied, the required exposure time corresponds approximately to a constant fluence (see Ref. 1), the value of the fluence is approximately proportional to failure stress. Calculations for fracture of various thicknesses of glass at 10,000 psi are shown in Fig. 2.20. Again as the laser intensity varies, the required exposure time corresponds approximately to a constant fluence, but the value of the fluence is approximately proportional to the thickness.

The time of first fracture has been measured for glass exposed to CW 3.8 μm laser irradiation. The BK7C fracture data for 3/8" thick sample are compared to the predictions for the three failure criteria in Fig. 2.21. The
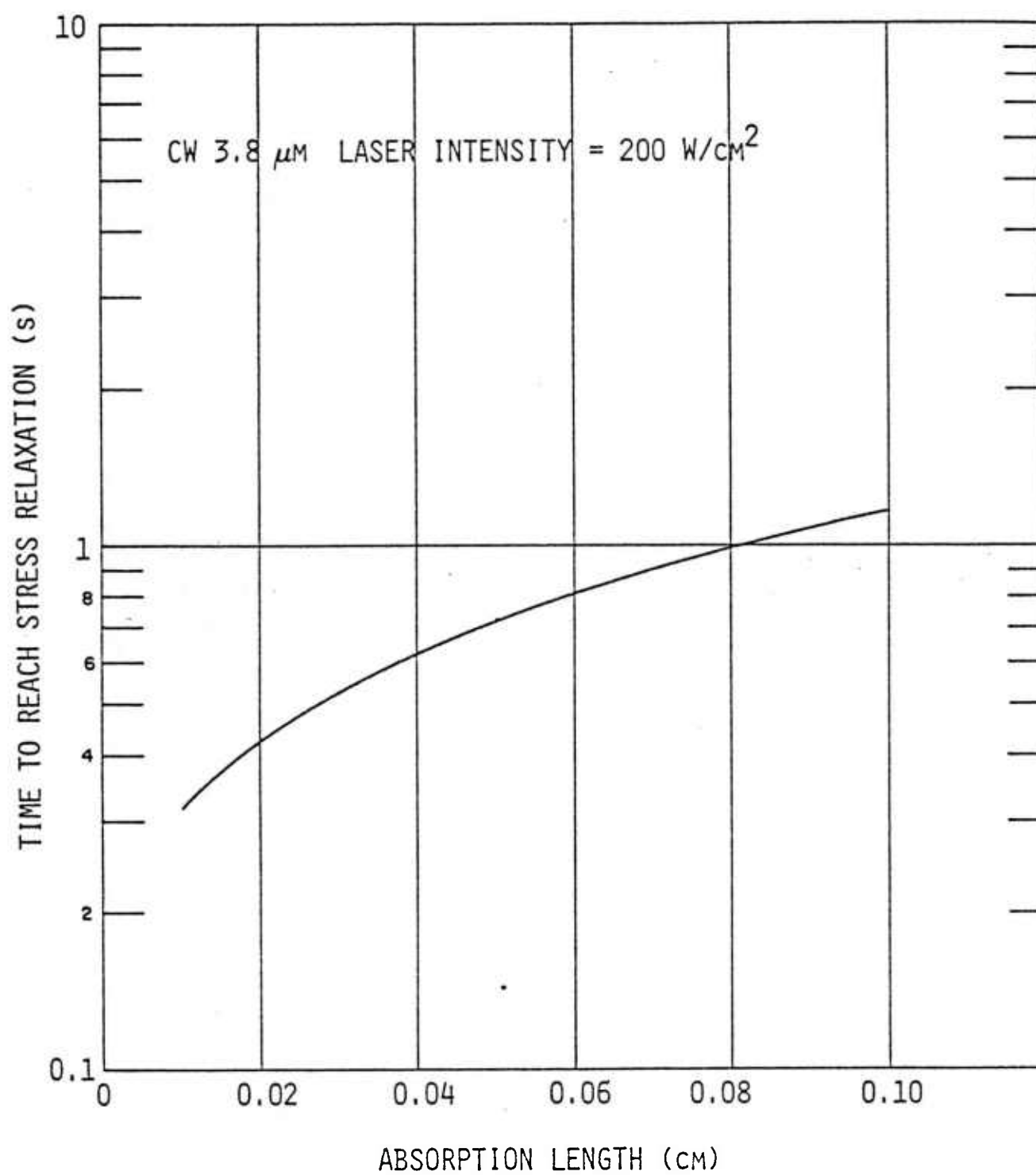
Fig. 2.17 Effect of absorption length on predicted stress relaxation time of EK7 irradiated by 200 W/cm² at 3.8 μm.

10 ⊣

BK7
$\ell = 1000\ \mu m$
R = 0.04

● TRW-MELT
○ TRW-NO MELT
■ UTRC-MELT
□ UTRC-NO MELT

STRESS RELAXATION

EXPOSURE TIME (s)

1

FRACTURE
$\sigma_F = 10,000$ psi
1/8" thick

0.1

0   0.1   0.2   0.3   0.4   0.5

INCIDENT LASER INTENSITY (kW/cm^2)
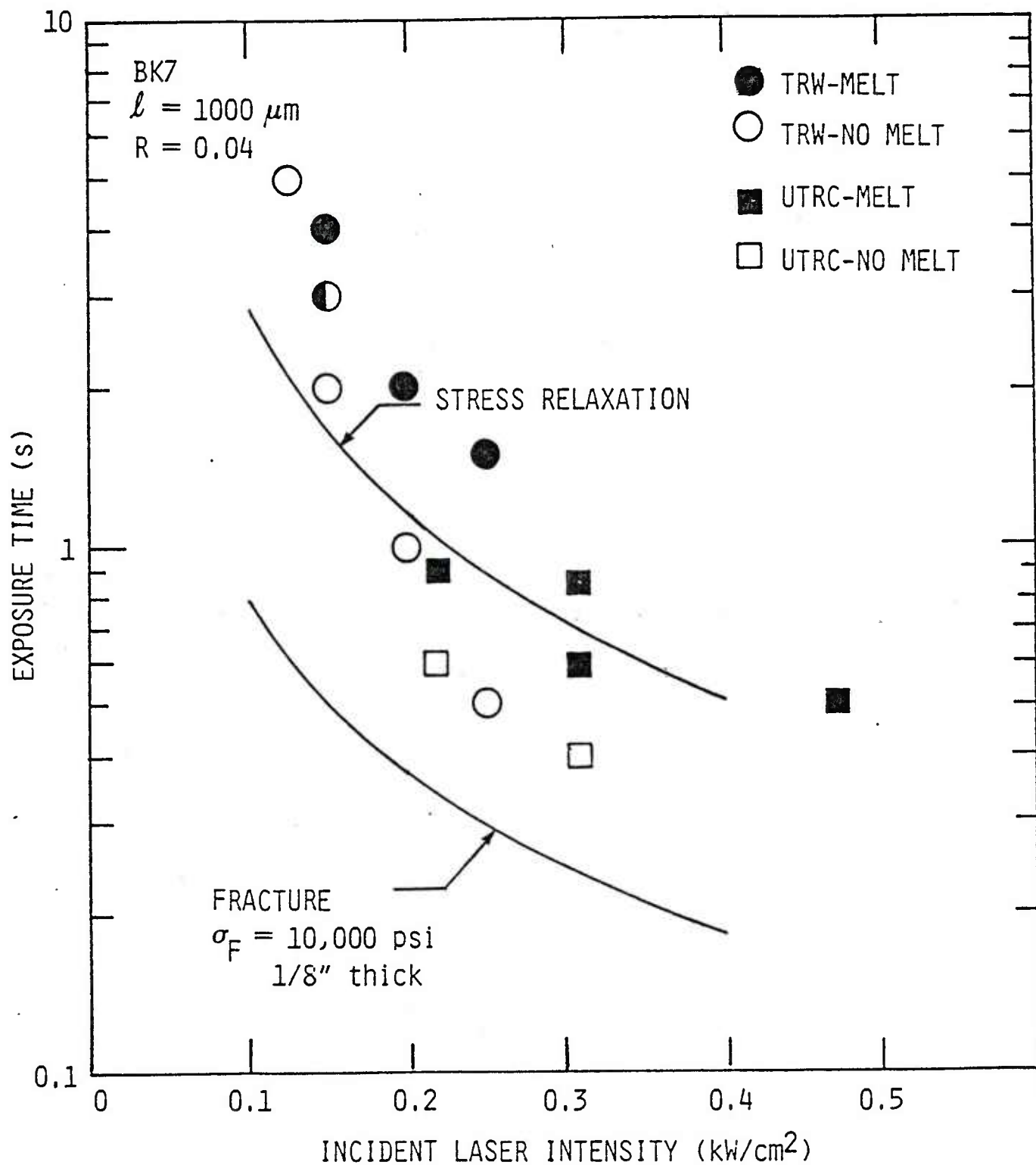
Fig. 2.18 Predicted damage times for BK7 irradiated by CW 3.8 μm for an absorption length of 1000 μm.
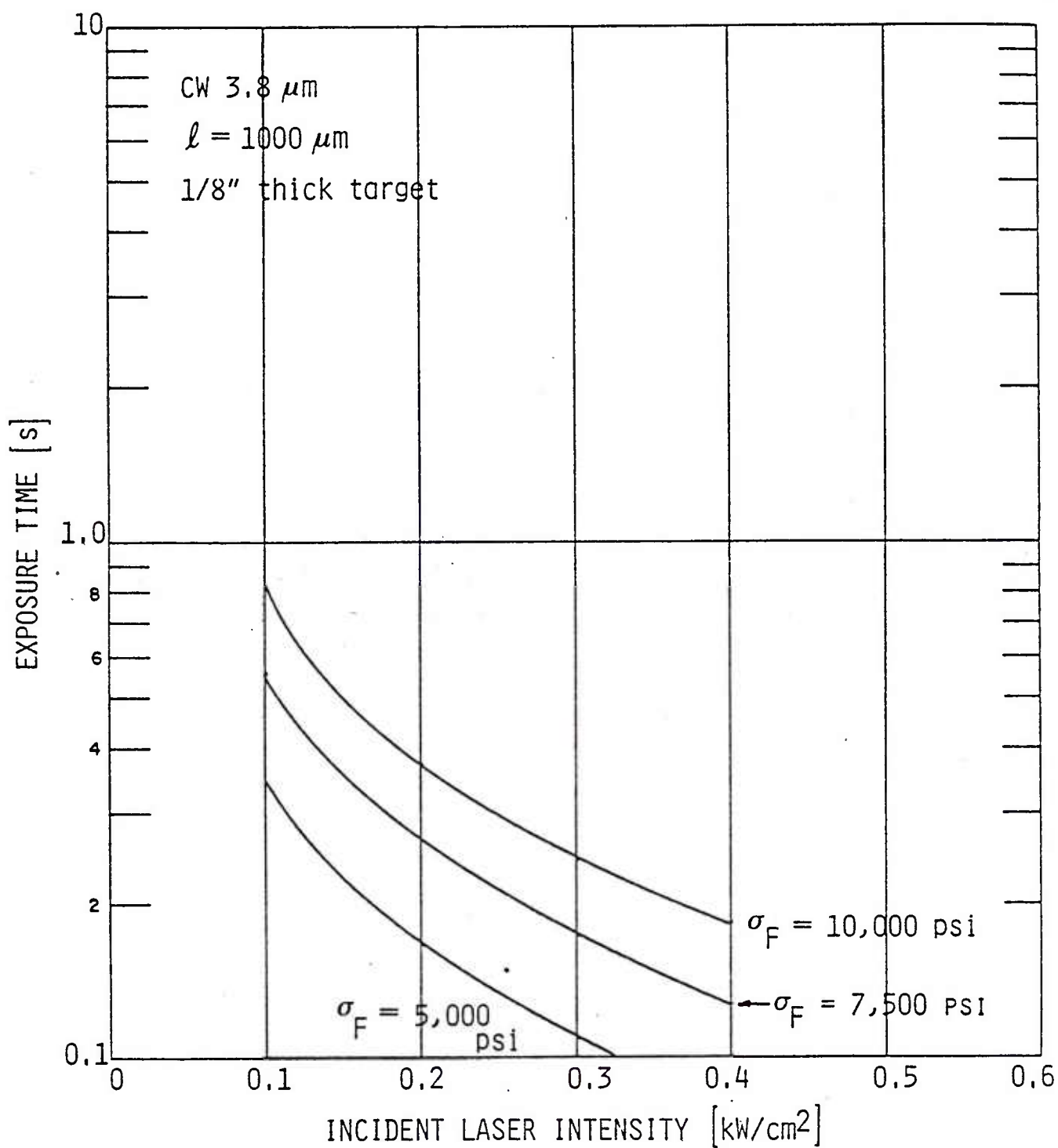
Fig. 2.19 Effect of failure criterion on time for first fracture of 1/8" thick BK7 irradiated by CW 3.8 μm laser.
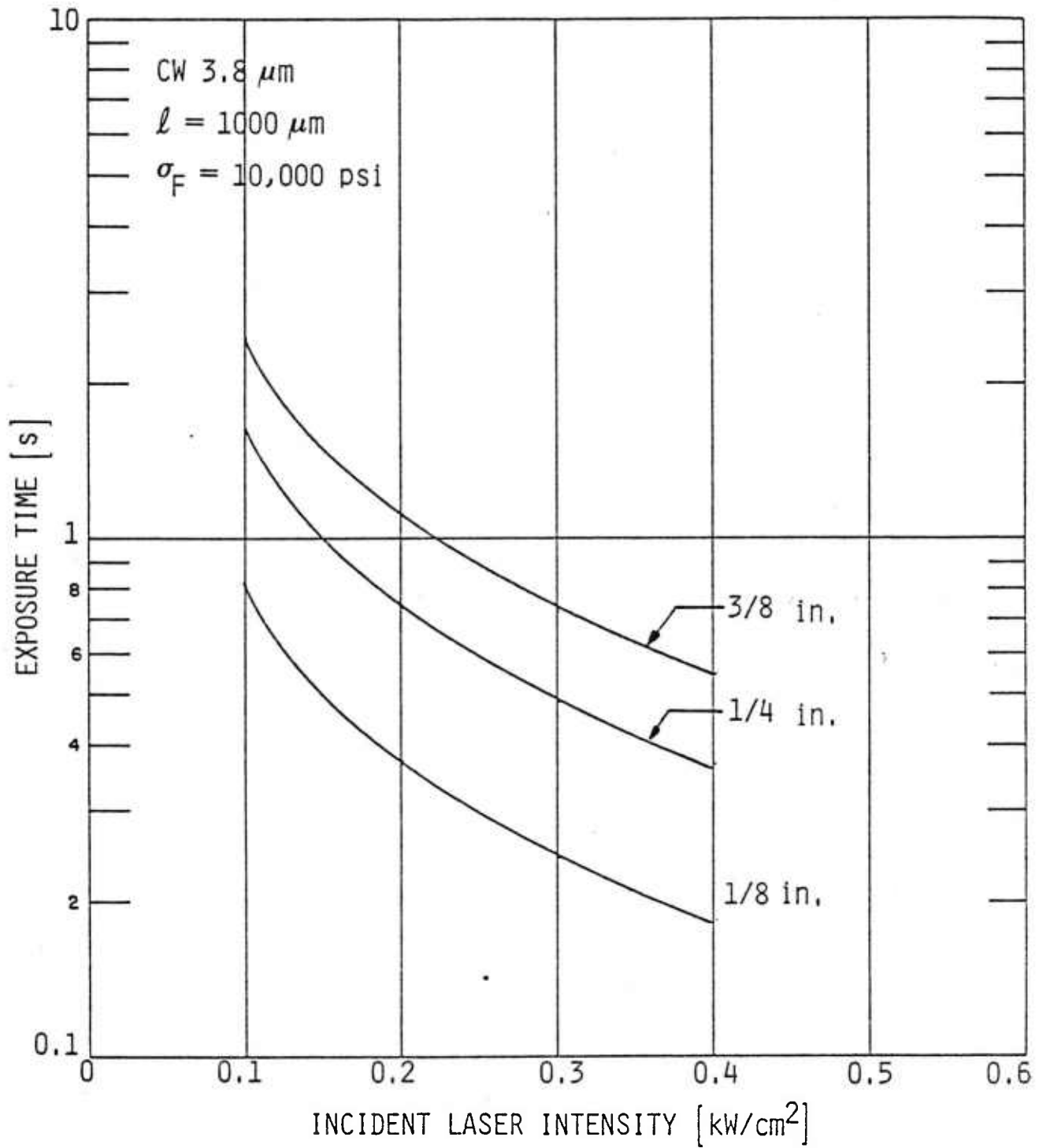
Fig. 2.20 Effect of target thickness on time for first fracture for BK7 irradiated by CW 3.8 μm laser. Failure stress is 10,000 psi.
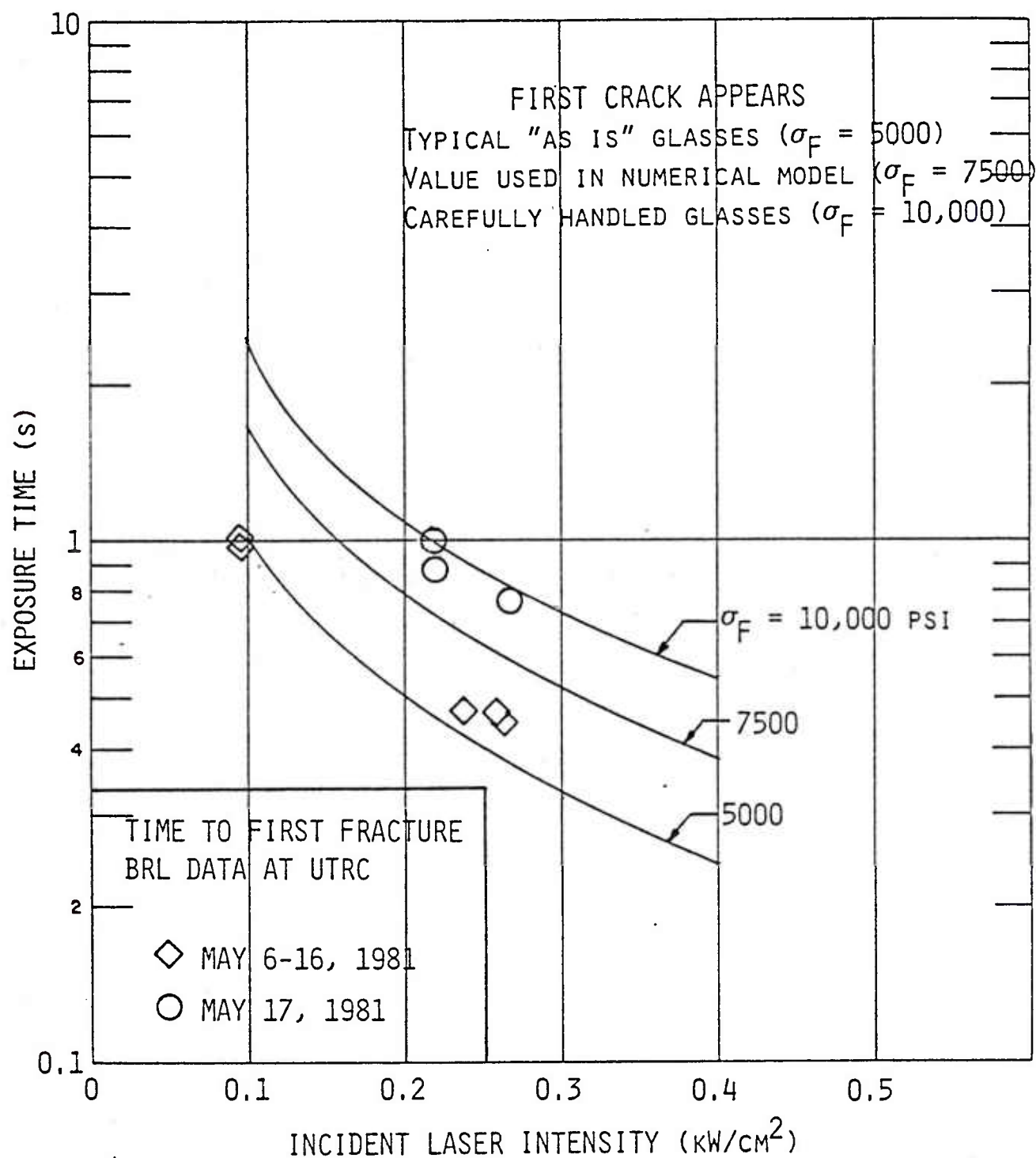
Fig. 2.21 Data/theory comparison for first fracture of 3/8" BK7C under CW 3.8 μm irradiation.

data taken during May 6-16 correlates well with failure at 5,000 psi. Data taken on May 17 correlates with failure at 10,000 psi. This variation from one test to another falls within the potential variability in the fracture criteria, but the additional correlation with date of test is surprising. However, in lieu of other information on the samples which can explain the difference in the failure criteria, the most plausible explanation is the variability of failure stress. The flagged datum point at 211 W/cm^2 fractured on cooling after the exposure was terminated. The absence of fracture during irradiation can be explained by the variability in failure stress and/or thickness. The failure on cool down, however, must be explained by a different fracture mechanism. The mechanisms that leads to surface cracking in RP interactions can also cause catastrophic failure -- front surface failure is initiated by the tensile stress frozen into the surface during cooling of glass that has undergone stress relaxation. The calculation shown in Fig. 2.18 indicates that the flagged point should have experienced viscoelastic stress relaxation and should have cracked on cool down. Furthermore, once stress relaxation begins at the front surface during heating, the rear surface tensile stress no longer increases linearly with fluence (exposure time); rear surface failure becomes increasingly more difficult.

The predicted CW 3.8 μm laser irradiation requirements to melt ZKN7 are shown in Fig. 2.22. The absorption depth is 667 μm. The melt (stress relaxation) prediction separates the limited no melt data from the melt data for intensities above 150 W/cm^2 (where radial cooling effects are small). The prediction for rear surface fracture of a 3/8" thick piece of ZKN7 at a failure stress of 5,000 psi is also plotted as the dashed line. Note that for ZKN7 these two damage mechanisms compete. The ZKN7 data on fracture are compared to the theoretical predictions in Fig. 2.23. When failure occurs during heating, the data are shown as solid circles and the exposure time corresponds to the time at which fracture first occurred. Tests for which failure occurred on cool down are plotted as solid squares; they are plotted versus total exposure time and the observed failure times (in seconds) are written beside the data points. If no failure occurred, the points are plotted as open symbols. There is an excellent correlation between the predicted failure

48
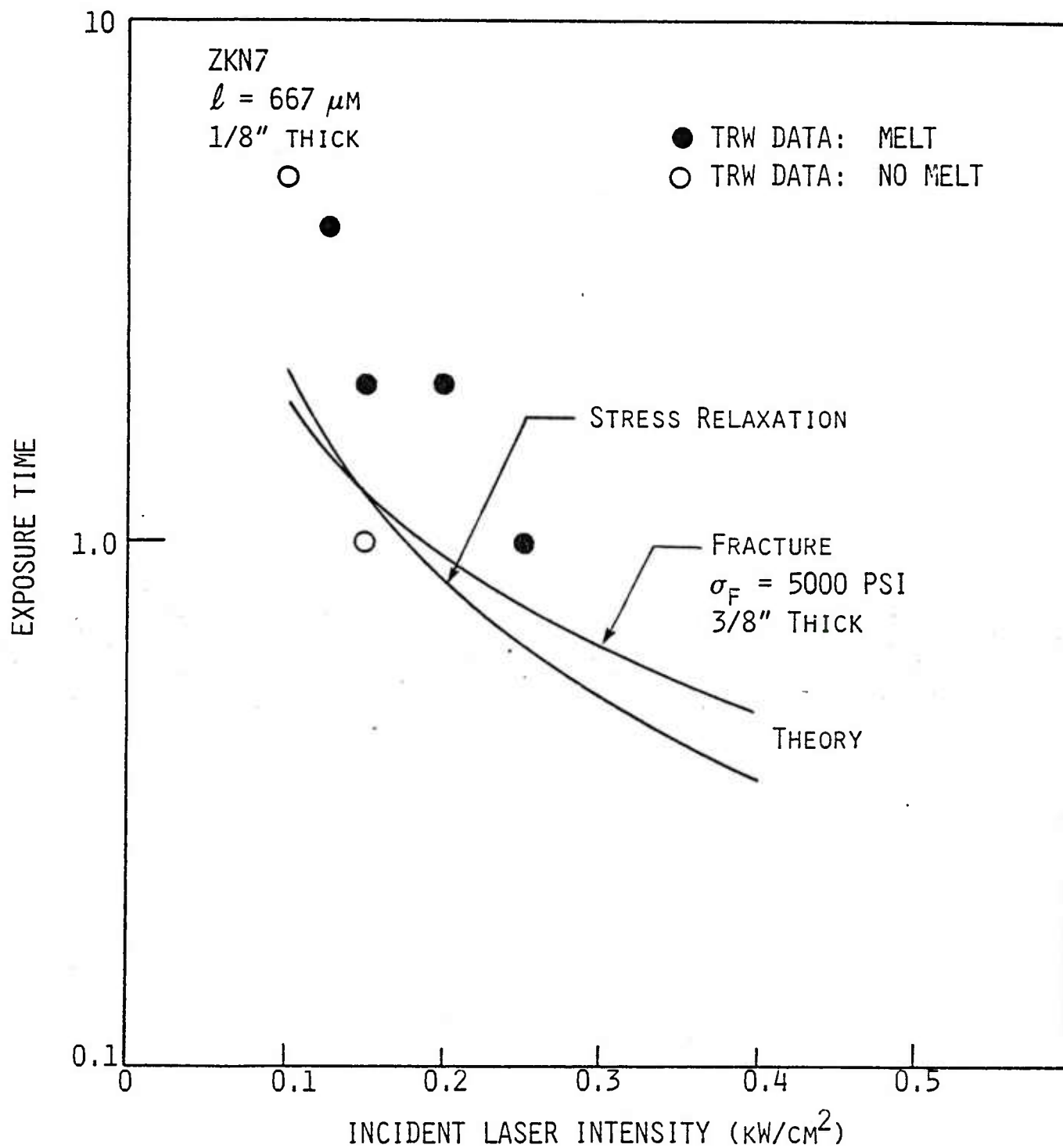
Fig. 2.22 Predicted damage times for ZKN7 glass irradiated by 3.8 μm and
comparison with melt data.

Fig. 2.23 Comparison of data and predicted fracture time for 3/8" thick ZKN7 irradiated by CW 3.8 μm laser.

50

times and the observations. One sample tested at 211 W/cm^2 fractures well before the three other samples tested at that intensity -- most likely this sample was damaged during handling.

2.12   RP 3.8 μm Interactions

Because of the long absorption depth for 3.8 μm radiation, the pulsed 3.8 μm interactions at low pulse fluence exhibit the same basic damage mechanisms as CW 3.8 μm interactions. Only when the single pulse fluence is large enough to cause vaporization (and pressure) is the interaction expected to vary. The predicted low fluence requirements to damage BK7 with 50 Hz RP 3.8 μm laser radiation are shown in Fig. 2.24. Failure at 5,000 psi requires an almost constant fluence of 80 J/cm^2. Recent data[7] have been taken at lower pulse fluence (5-10 J/cm^2) and lower pulse repetition frequencies (25-50 Hz). The data are compared to failure predictions in Fig. 2.25. The data offer excellent support for the fracture theory for a 5,000 psi failure stress. The contrast ratio data is compared to the fracture and melt (stress relaxation) predictions in Fig. 2.26. Severe degradation in contrast ratio -- a contract ratio less than 0.5 -- correlates well with the onset of melting, and the degradation is worse for samples which are melted to a deeper depth (i.e, which exceed the minimum melting requirement by more fluence). Below the predicted fracture fluence, no damage is predicted and the contrast ratio is essentially unity. Above the fracture threshold, the number of fractures expected increases with fluence. In general the data confirms this behavior -- the contrast ratio decreases with increasing fluence for most samples.

2.13   Summary

The glass damage models have been upgraded to include improved material properties and to predict the fraction of the surface damaged by the various mechanisms. Simple models have been used to relate the damage to the reduction in contrast ratio. In general, the models predicted the observed trends in contrast ratio; however, further quantification of damage, requires the details of the optical system used in measurements. The main results of the modeling are:
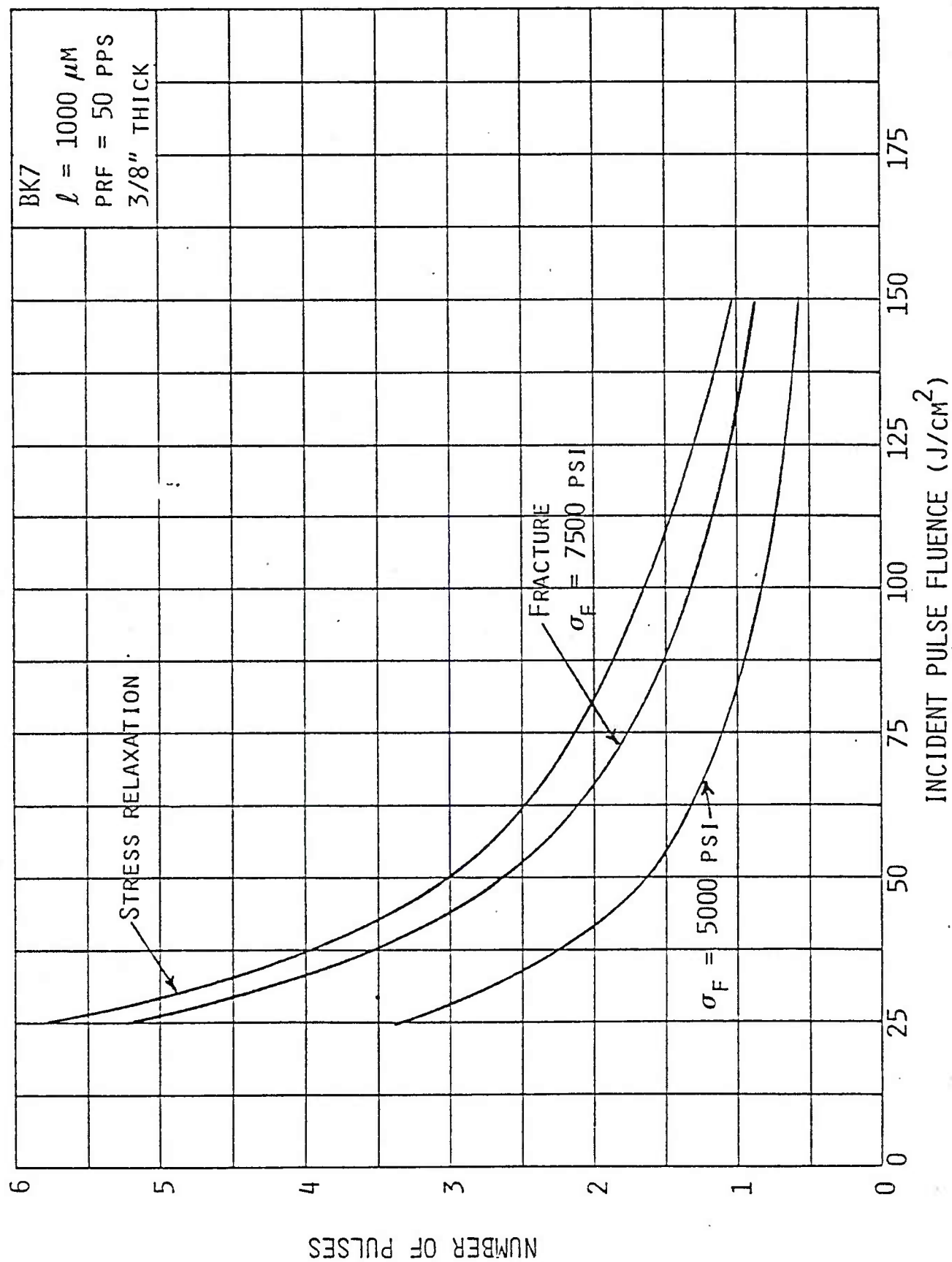
Fig. 2.24 Predicted damage times for BK7 irradiated by pulsed 3.8 μm.
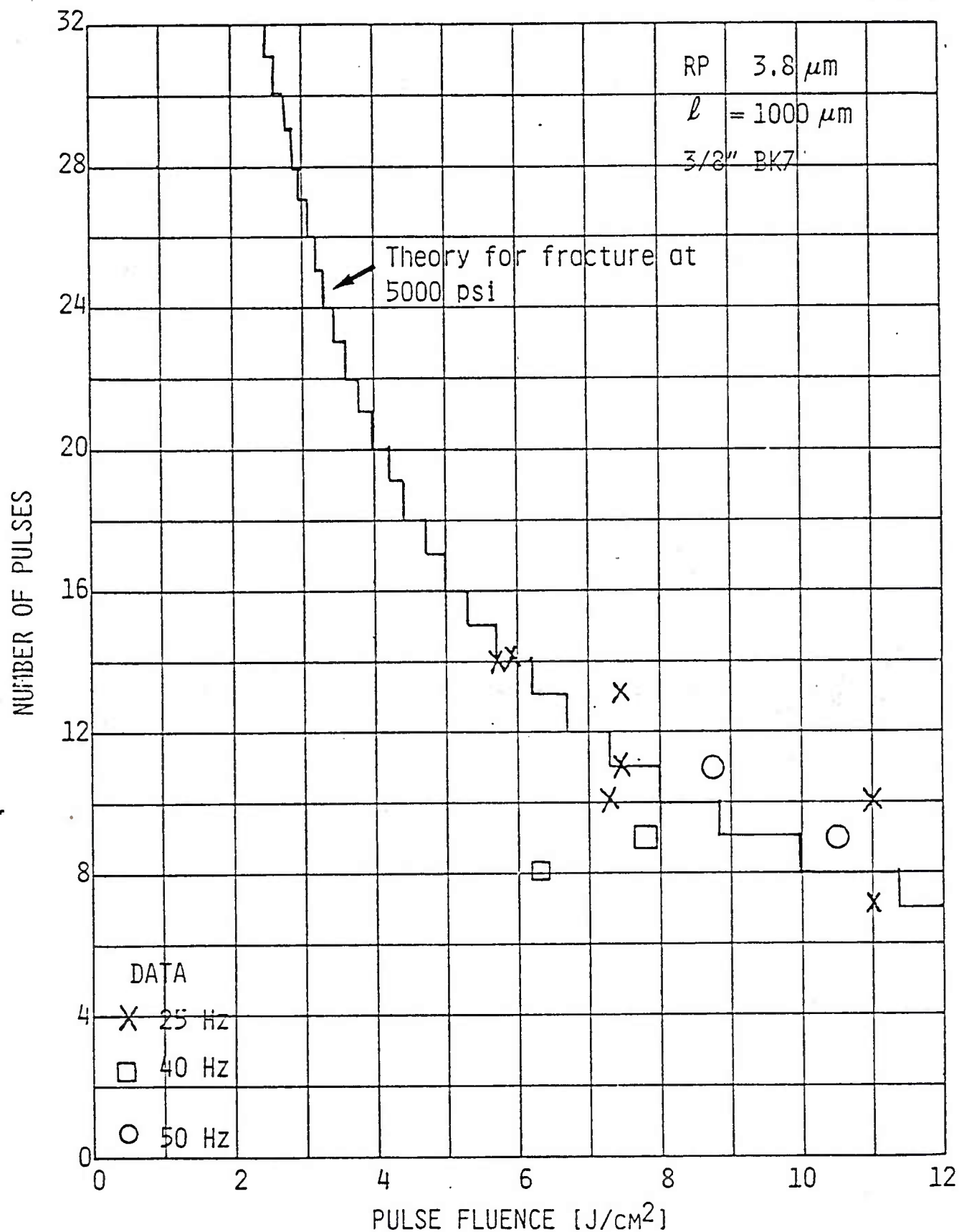
Fig. 2.25 Comparison data and theoretical prediction for number of 3.8 μm pulses required to fracture 3/8" BK7.
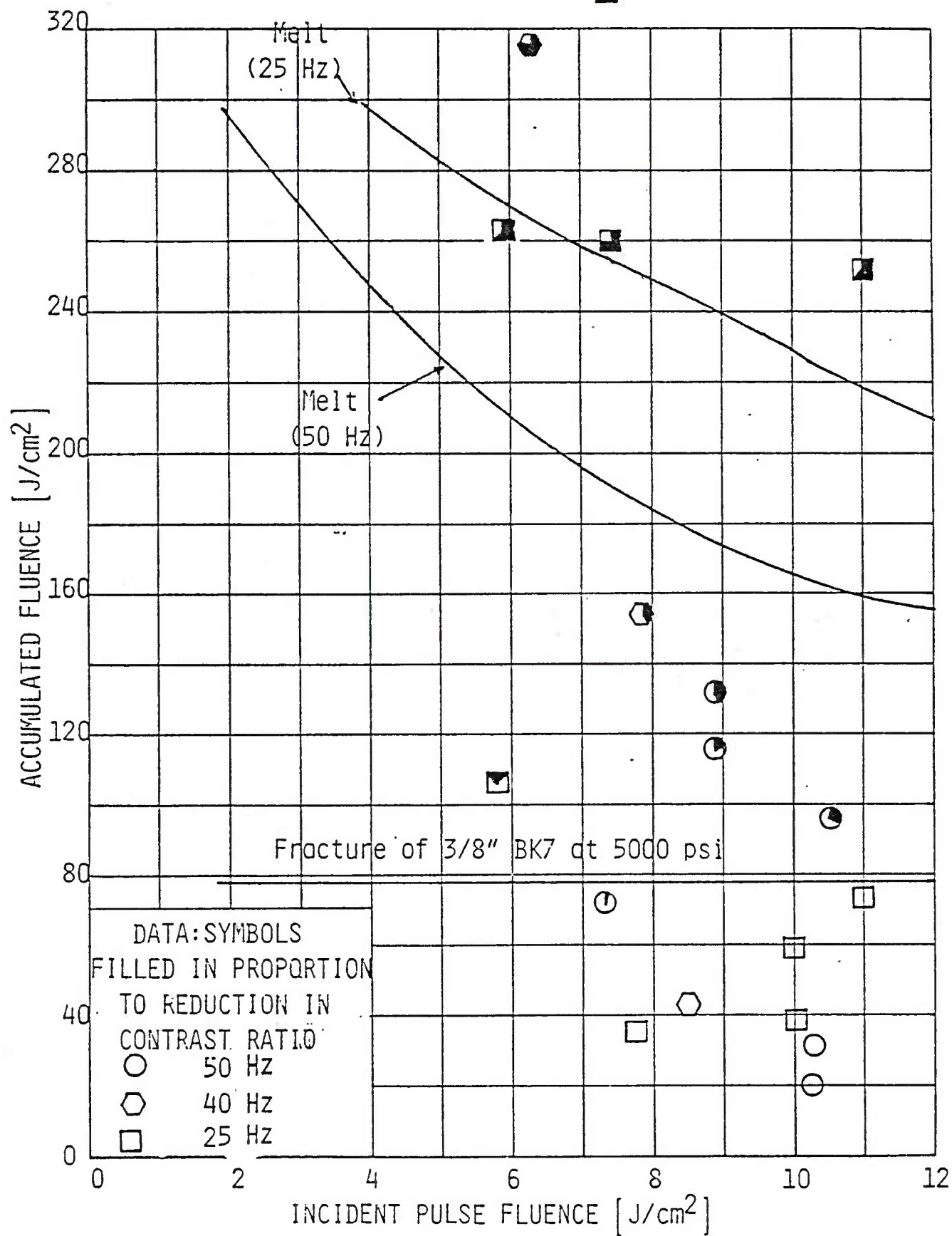
Fig. 2.26 Correlation of contrast ratio data[7] with fracture and melt predictions
for RP 3.8 μm laser irradiation of BK7.

54

1) Surface cracks can be adequately predicted for RP 10.6 μm interactions, but the cracks cover only a small fraction of the surface. They cannot cause extensive optical degradation.

2) Exfoliation occurs over the whole surface. It relieves lateral stresses, thereby increasing the intercrack distance. If the phase difference introduced by different flakes (exfoliations) is large and random, significant optical degradation may result.

3) Melting in CW 3.8 μm interactions correlates well with stress relaxation when reasonable values of the laser absorption coefficient are used. Melting occurs over the entire surface; therefore, it has the potential to cause significant optical damage when the melt depth is sufficient to produce large random phase changes.

4) Vaporization results in a change in surface composition for glasses that are mixtures (i.e., all glasses but fused silica). Since vaporization takes place over the entire surface, it can produce severe degradation when the phase change is large.

5) First fracture of BK7 and ZKN7 are well predicted for CW and RP interactions.

6) The damage models have been extended to Vycor. It is predicted to respond much as fused silica does, but it will display more damage in the vaporization regime.

7) The main damage feature of fused silica - namely, its resistance to severe optical degradation - can be understood on the basis of the damage models, but the details of the threshold behavior have not been well characterized. It is not known whether this represents an inadequacy in the damage mechanism models or merely reflects the uncertainty in the absorption coefficient.

Some of the conclusions presented above rely on the following assertion which is justified in the subsequent sections: severe optical degradation requires large random phase changes over short distance.

3. OPTICAL PERFORMANCE CONSIDERATIONS

3.1 Introduction

A detailed analysis of the impact of laser glass damage on optical system performance can be divided into three distinct aspects: physical damage, optical aberrations, and degraded performance. The first is the mechanical damage which is caused by laser irradiation. The physical damage must then be related to optical aberrations which control the performance of the system. The analysis requires a rather detailed characterization of the optics, a model of system performance, and a quantitative criteria which adequately describes those aspects of the system which are key to accomplishing the defined mission. This section provides an overview of optical performance modeling for damaged optics; detailed calculations are deferred to the next section.

A complete program designed to develop the capability to evaluate laser glass damage requires both theoretical modeling and laboratory evaluation of key parameters. A general methodology and approach to this task are shown in Fig. 3.1. The laser causes physical damage to one or more optical elements which results in optical aberrations. The Optical Transfer Function (OTF) is a particularly convenient format for determining how these aberrations and other important characteristics of the optics impact system performance. A complete systems model will depend not only on the OTF, but also on object characteristics and propagation effects. Performance quantification must also account for detector characteristics and is usually specified in terms of an image quality criteria. A laboratory evaluation is most often required to define several key parameters which cannot be defined from first principles, and, of course, to validate the model.

3.2 Optical System Characterization

The OTF, which is key to the methodology of Fig. 3.1, is defined as the Fourier Transform of the Point Spread Function (PSF) which describes the response of the optical system to a point source. For a focused, isoplanatic, incoherent imaging system, the image plane intensity is given by

$$I(\underset{\sim}{x}) = \int P(\underset{\sim}{x} - \underset{\sim}{y}) \, O(\underset{\sim}{y}) \, d\underset{\sim}{y} \quad , \tag{3.1}$$

where $O(\underset{\sim}{y})$ = object plane intensity and $P(\underset{\sim}{x} - \underset{\sim}{y})$ = point spread function.
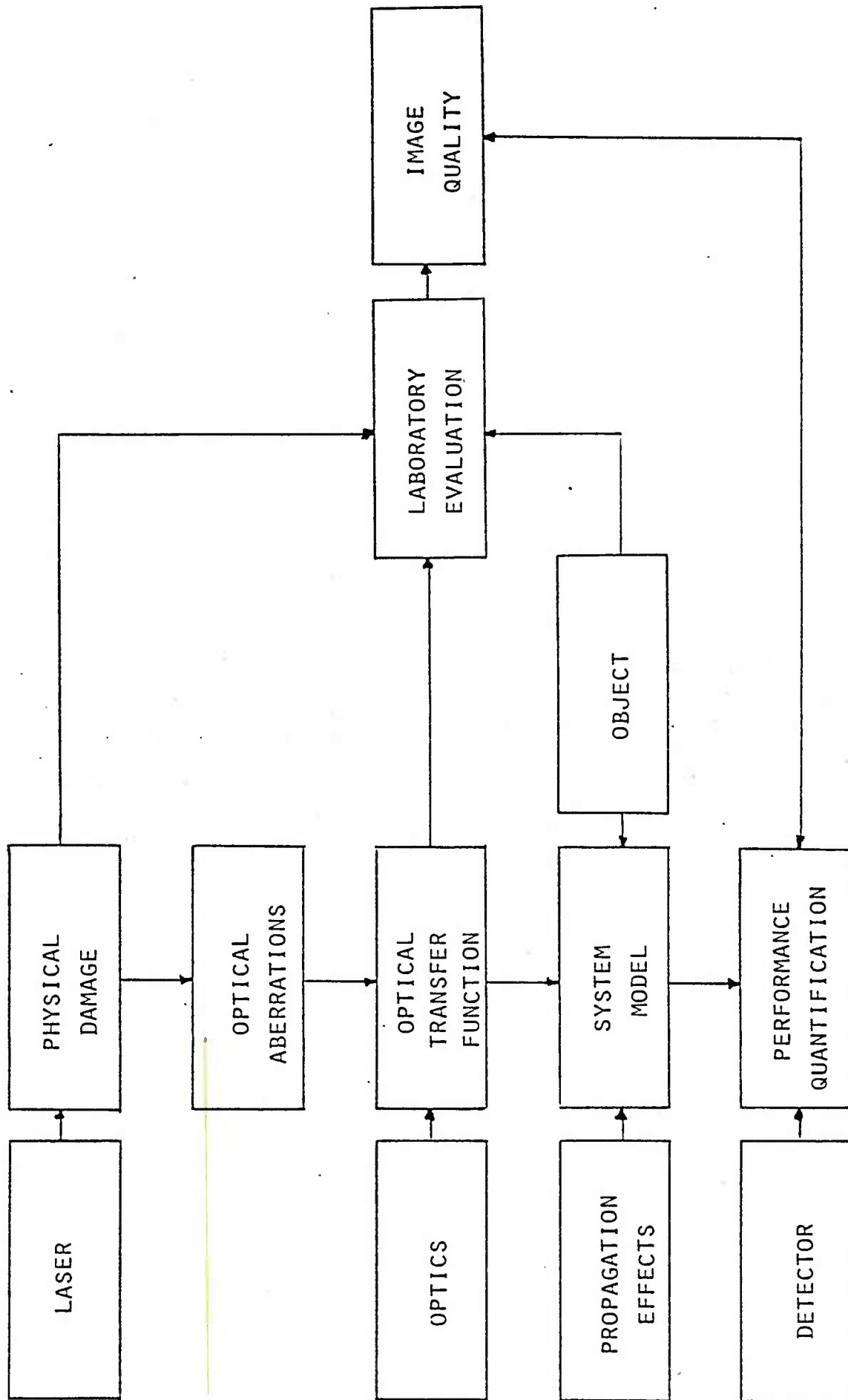
Fig. 3.1 Methodology.

If the object is a point ($\sim \delta(\underset{\sim}{y})$) then $I(\underset{\sim}{x})$ is equal to $P(\underset{\sim}{x})$. Provided Eq. (3.1) is valid, the performance of the system for any object is completely specified by $P(\underset{\sim}{v})$ or its Fourier Transform, $\tau(\underset{\sim}{f})$ (OTF).

$$\tau(\underset{\sim}{f}) = \int P(\underset{\sim}{v})\ e^{2\pi i(\underset{\sim}{f}\cdot\underset{\sim}{v})}\ d\underset{\sim}{v}\ , \tag{3.2}$$

$$\widetilde{I}(\underset{\sim}{f}) = \tau(\underset{\sim}{f})\ \widetilde{O}(\underset{\sim}{f}), \tag{3.3}$$

where $\widetilde{I}(\underset{\sim}{f})$ and $\widetilde{O}(\underset{\sim}{f})$ are the Fourier Transforms of the image and object intensities, respectively. For a diffraction limited circular clear aperture of diameter D, the PSF is $[J_1(ax)/ax]$,[2] where J_1 is the first order Bessel function and a is an appropriate scaling factor. The OTF is given by

$$\tau(\underset{\sim}{f}) = \frac{2}{\pi}\left\{\cos^{-1}\left(\frac{\lambda Rf}{D}\right) - \left(\frac{\lambda Rf}{D}\right)^2\left[1 - \left(\frac{\lambda Rf}{D}\right)^2\right]^{1/2}\right\} \tag{3.4}$$

$$\text{for } (\lambda Rf/D) \leqslant 1,$$

where λ is the wavelength of the radiation and R is the effective focal length of the optical system.

For more general cases, the OTF is conveniently defined by

$$\tau(\underset{\sim}{f}) = \frac{1}{A}\int \beta(\underset{\sim}{v})\beta^*(\underset{\sim}{v} - \lambda R\underset{\sim}{f})W(\underset{\sim}{v})W(\underset{\sim}{v} - \lambda R\underset{\sim}{f})d\underset{\sim}{v}\ , \tag{3.5}$$

where

$$W(\underset{\sim}{v}) = \text{Aperture Window Function} = \begin{cases} 1 \text{ Inside Aperture} \\ 0 \text{ Outside Aperture} \end{cases} \tag{3.6}$$

$$\beta(\underset{\sim}{v}) = \text{Complex Pupil Function}$$

$$= A(\underset{\sim}{v})\ e^{i\phi(\underset{\sim}{v})} \tag{3.7}$$

and A is the total area of the aperture.

58

The complex pupil function describes the effects of the optical system on a plane wave in terms of an apodization, $A(\underset{\sim}{v})$, and phase shift, $\phi(v)$. Common cases for which results are given in standard references are as follows:

- Diffraction Limited: $\beta(v) = 1$

- Central Obscuration: $\beta(v) = \begin{cases} 0 \text{ for } |v| < \varepsilon D \\ 1 \text{ otherwise} \end{cases}$

- Defect of Focus: $\beta(v) = \exp(iav^2)$

- Spherical Aberration: $\beta(v) = \exp[ia(v^4 + bv^2)]$

- Primary Astigmatism: $\beta(v) = \exp[iav^2\cos^2\theta]$,

where v is the magnitude of a two-dimensional vector in the aperture plane (i.e., integration variable of Eq. (3.5)) and θ is the phase angle of this vector.

Based on the above definitions, it is obvious how laser glass damage can be included in the model. The physical damage caused by laser irradiation results in optical aberrations which yield a specification in terms of a complex pupil function. Having specified the complex pupil function, the OTF can be evaluated from Eq. (3.5). This approach requires a model to relate the damage to $\beta(v)$; the subsequent evaluation of the OTF is then, in principle, straightforward, although in practice it can be computationally complex.

There is, however, an effect which makes laser-induced damage distinctly different from the previously discussed aberrations. Because of the nature of laser interactions with glass, the resulting damage and aberrations will be random in nature, i.e., repeating a given experiment multiple times will not yield identical results, but rather different statistical realizations which are members of an ensemble. Consequently, the evaluation of a single realization, while in principle is possible in some cases, is of little utility. Rather a characterization in terms of average properties is of more practical value. The most obvious property of interest is the average performance, i.e., average OTF defined by

$$\langle \tau(\underset{\sim}{f}) \rangle = \frac{1}{A} \int \langle \beta(\underset{\sim}{v})\beta^*(\underset{\sim}{v} - \lambda Rf) \rangle W(\underset{\sim}{v})W(\underset{\sim}{v} - \lambda Rf)d\underset{\sim}{v} , \tag{3.8}$$

where <...> indicates a statistical average and all statistics are assumed to reside in the damage related pupil function. If the statistics are stationary (a reasonable assumption for the case of interest here), then the pupil correlation function will be independent of the integration variable; that is,

$$\langle \beta(\underset{\sim}{v}) \beta(\underset{\sim}{v} - \lambda R \underset{\sim}{f}) \rangle = \tau_\beta (\lambda R \underset{\sim}{f}) \ , \tag{3.9}$$

and therefore the average OTF is given by

$$\langle \tau(f) \rangle = \tau_\beta(\underset{\sim}{f}) \tau_o(\underset{\sim}{f}), \tag{3.10}$$

where $\tau_o(\underset{\sim}{f})$ is the OTF of the undamaged system. We note that if the undamaged optical system is not diffraction limited, the appropriate aberrated pupil function should be included in $\tau_o(f)$. Furthermore, in terms of the methodology of Fig. 3.1, it can be seen that the laser-induced damage and optics couple into the OTF via the multiplication of Eq. (3.10).

For a number of cases of interest, more than one damage mechanism may be present. If these multiple processes are statistically independent, then the average OTF will be given by

$$\langle \tau(f) \rangle = \left[\underset{i}{\pi} \tau_i (\underset{\sim}{f}) \right] \tau_o(f) , \tag{3.11}$$

where $\tau_i(\underset{\sim}{f})$ is the correlation function associated with the ith process. This is a particularly powerful result because any combination of damage mechanisms can be easily evaluated once the effect on each mechanism is determined.

An example of the type of behavior to be expected for diffraction-limited performance and random aberrations is given in Fig. 3.2. The diffraction-limited response to a point source is the classical $[J_1(x)/x]^2$ PSF which has most of the energy concentrated in a peak whose width is proportional to D^{-1}. Small Airy rings are also present. When a random aberration is present, the energy in the image plane will be spread over an area with characteristic dimension Δ^{-1} where Δ is the scale of the aberrations in the aperture plane. Provided the aberrations are of sufficient strength, the interior of this region will be comprised of a number of randomly located bright spots of dimension D^{-1}. When averaged over many realizations, the diffraction-limited image will, of course, remain unchanged. In contrast, for the damaged optics,

QUANTIFY

- SINGLE REALIZATION IMAGE

- AVERAGE IMAGE

- AVERAGE TRANSFER FUNCTION

- CONTROLLING SCALES ARE D AND Δ

DIFFRACTION LIMITED

I_0 ~1/D

I_0 ~1/D

$f_D \sim D$

RANDOM ABERRATION

I_R ~1/D ~1/Δ

$\langle I_R \rangle$ ~1/D ~1/Δ

f_D

$f_R \sim \Delta$

$\langle I_R \rangle < I_0$
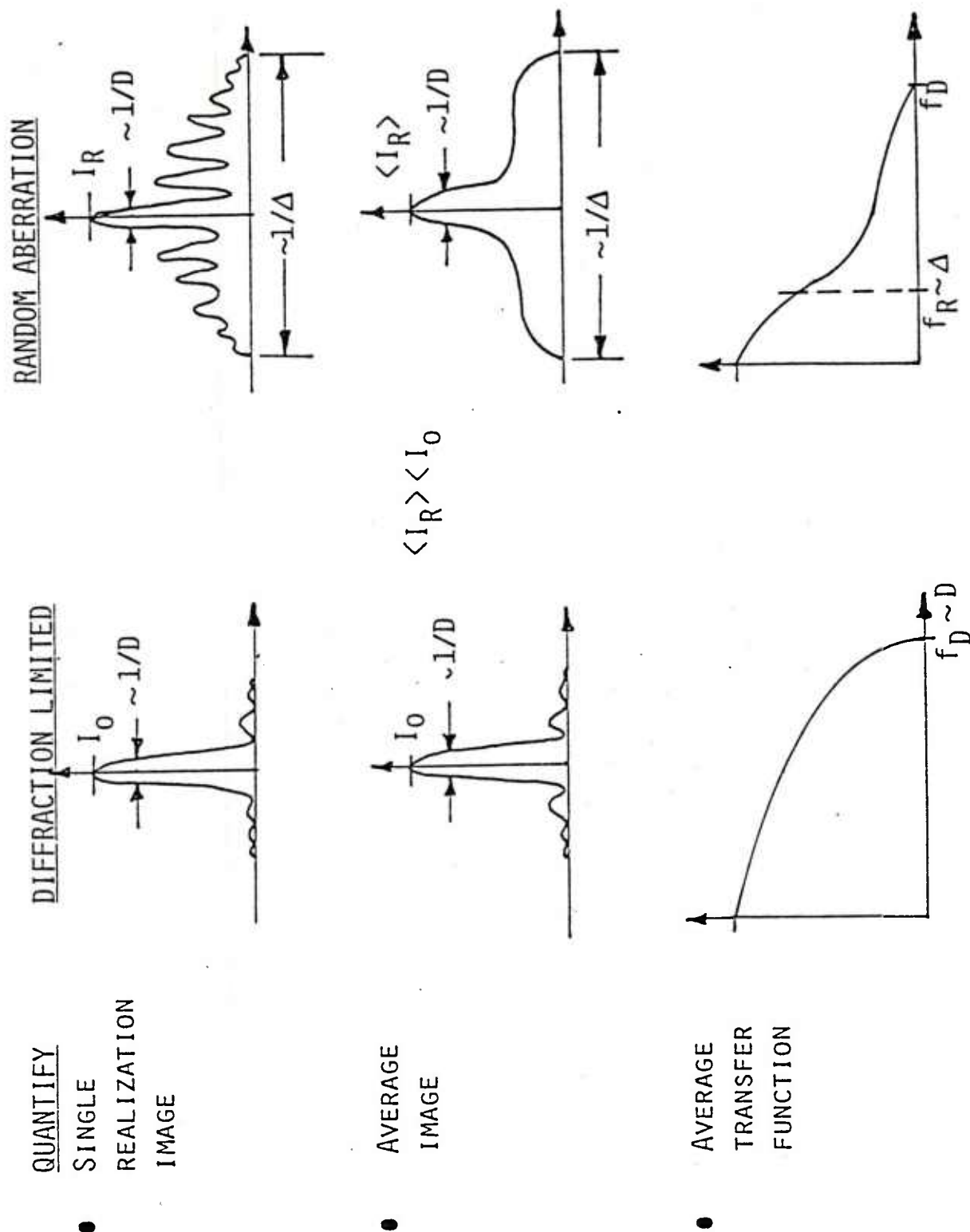
Fig. 3.2 Image comparison.

because of the random locations of the spots associated with random aberrations, these local fluctuations will be smoothed upon averaging, resulting in a large diffuse image of size Δ^{-1} with, perhaps, a somewhat brighter peak in the center of size D^{-1}. The on-axis intensity, $\langle I_R \rangle$ will always be less than that of the corresponding diffraction-limited case because the energy has been spread.

The Fourier Transform of the diffraction image yields the OTF given in Eq. (3.4). The OTF associated with a single random aberration will, in general, be complex. The average OTF for random aberrations will have the approximate form indicated in Fig. 3.2. Generally, it will have a non-zero value out to the diffraction limit ($f = f_D \sim D$), but will fall off dramatically at spatial frequencies above that associated with the scale of the aberrations: $f > f_R \sim \Delta$. The effect of this attenuation at higher frequencies is to reduce object frequencies in this range. This results in loss of resolution, contrast, etc., which degrade performance of the optical system.

A final point which is important is that the analysis discussed above only considers a single characterization of the damage system, i.e., its average performance. In actual practice, the system will receive a specific spatial distribution of damage, i.e., a single realization, which may result in greater or lesser performance than that specified by the average. For a system level analysis, it is often important to associate statistics with performance; for example, the probability of performance better (or worse) than a given value. Such an analysis can be carried out theoretically by evaluating other moments of the statistical ensemble of random aberrations associated with the laser-incuded damage. In some cases, it is appropriate to do this in terms of the OTF; in others, an image quality parameter is more appropriate. While the evaluation of higher order statistics and probability distributions can be more computationally complex, there are no fundamental issues which must be overcome to institute such an evaluation.

Another aspect of statistics which must be considered results from the comparison of the model with laboratory or field data. In most cases, the

data will correspond to specific statistical realizations. The cascading of OTF contributions, which is described in Eqs. (3.10) and (3.11), is a property of the ensemble average; it need not be true for a specific realization. Hence, in the laboratory experiments it is essential to evaluate the OTF as a property of the whole optical system rather than as a product of OTF's of separate components. Furthermore, even for the OTF of the whole system, the measured results for a specific realization will not, in general, agree in detail with the model of average performance. To deal with this situation, one of two approaches must be employed. The most direct one is to carry out multiple measurements with a fixed physical configuration, thereby generating an adequate statistical ensemble from which the appropriate average performance can be empirically determined for comparison with the model. Alternately, theoretical estimates of higher order moments and distributions can be generated and then compared with a limited set of measurements and consistency evaluated. Which approach is exploited depends on the situation. In any case, the important observation which must be remembered is that a single measurement of system performance associated with a single statistical realization is of little value in determining anticipated system performance.

3.3   Performance Characterization

The previous discussion of the optical transfer function concentrated on the specification of system performance from the point of view of the detailed characterization of the image plane distribution of energy. While this is a fundamental description of the physics involved which is entirely adequate for determining performance, it is not a particularly convenient parameter for characterizing specific aspects of performance related to detailed mission objectives. One reason for this is that the OTF is a function of spatial frequency in two-dimensional space and, hence, includes a substantial amount of detailed information. Depending on the applications, simpler descriptors of performance are of greater practical utility. Many such descriptors have been defined. Some are related to resolution, contrast or other similar concepts. Four common ones are Strehl ratio, edge response, frequency response and contrast.

The Strehl ratio is defined as the ratio of on-axis intensity for an aberrated system to the on-axis intensity for a diffraction-limited system.

63

In terms of OTF, the on-axis intensity is equal to the integral over all spatial frequencies. Hence, it eliminates the detailed frequency distribution and yields a single number characterization which is related to resolution and the peak energy to be found at a single point or within a small region.

The edge response is generally a one-dimensional description of resolution. Typically, edge response is evaluated in terms of the distance in the image plane associated with a specified drop in the PSF, for example, 90% to 10% of peak.

Frequency response is generally defined as the extent of the OTF in frequency space, i.e., the critical frequency, f_c, for which $\tau(f)$ is smaller than some value ε at any frequency above f_c. The implication of this is again related to resolution. The higher the value of f_c, the more detailed the information about the object which will be passed by the system.

Contrast is generally defined as the ratio of the difference in maximum and minimum value of intensity to the sum of these same two quantities for a sine object of specific frequency. It is closely related to standard bar targets which have been defined for use in evaluating optical system performance.

All of the parameters defined above, as well as others, are of greater or lesser value for quantifying the performance of a given optical system designed to meet specific measurement goals. The appropriateness of any parameter should be judged in terms of the application and should be part of the system requirements specification. Generally, those descriptors will depend on the aberrations present and optical system geometric parameters such as limiting aperture. Furthermore, they may also depend on object characteristics, the intervening propagation media and detector response. In this last case, the specification can become complicated due to the variations in eye response with observation conditions and observer.

64

3.4   Specific Damage Models

A number of damage models are of specific interest including coating removal, cracks, flakes, bubbles and vaporization. In each case the procedure is to define a distorted pupil function $\left(B = A \exp(i\phi)\right)$ with random apodization (A) and phase shift (ϕ), and to evaluate the correlation function which provides the basis for evaluating system performance in terms of the average OTF. System performance characterizers have not been defined because the results have not, at this time, been made system specific. Detailed models for three cases: cracks, flakes and vaporization, have been completed. The details of the models and computational procedures can be found in the next section.

In all three cases, the average OTF and PSF can be characterized as shown in Fig. 3.3. Consider first the OTF. Its zero frequency value, $T = \langle \tau(0) \rangle$, is reduced from the diffraction-limited case as a result of overall energy loss associated with the random apodization. For cracks, T is equal to (1-a) where a is the area coverage of cracks, whereas for flakes, it is equal to $t_o^2(1-a+a^2)$, where a is again the area coverage and t_o is the average transmission of a flake. For vaporization, T=1 as a result of the assumption of a pure phase aberration which appears to be an appropriate model.

In each case, the OTF becomes attenuated for frequencies above some critical value, Λ, relative to diffraction-limited performance. This scale is related to the correlation scale of the aberrations, i.e., crack width, flake length and vaporization scale length. At frequencies above Λ, the OTF takes on a roughly constant value (S) which is determined by the strength of the aberrations (rms sense). Finally, $\langle \tau(f) \rangle$ becomes zero at the diffraction frequency which depends on the limiting system aperture (D).

The average PSF can be characterized by two components: a diffraction peak and a damage halo. The diffraction peak has, as suggested, the spatial variation of the undamaged response, but is reduced in strength by the scale S of the high frequency OTF. The damage halo has a spatial scale ($\sim \Lambda^{-1}$) controlled by the scale of the aberrations and a maximum value controlled by S and the ratio of Λ to the aperture size, D.

65

Fig. 3.3 General characterization.
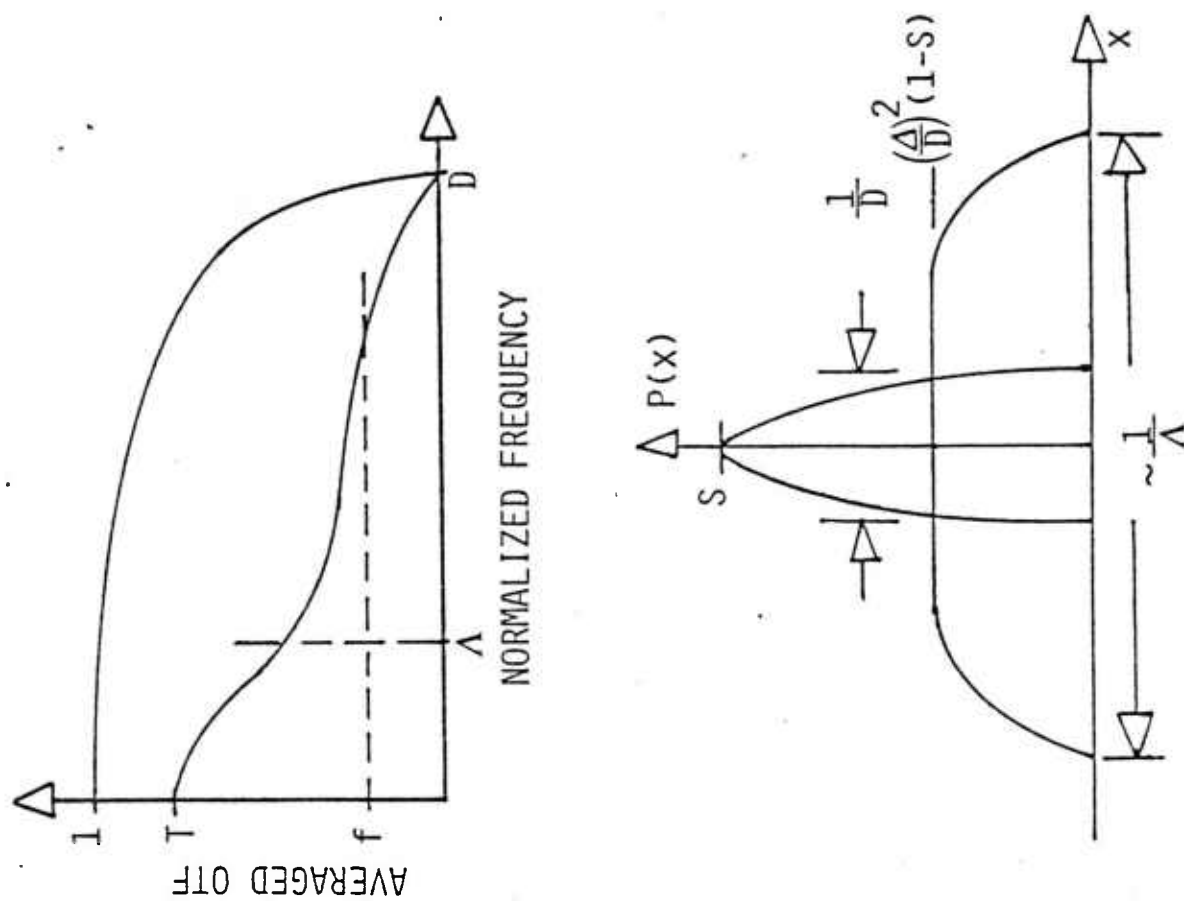
- All cases yield similar ⟨τ(f)⟩
  - T = ⟨τ(0)⟩ = FNC of transmission properties only
  - S = High frequency ⟨τ(f)⟩ = FNC of strength of aberrations
  - Λ = Characteristic scale of damage
- Point spread function has two identifiable components
  - Diffraction peak
  - Damage halo
- Damage specifies s & Λ
- Image quality ≃ FNC(S, Δ)

66

In summary, it can be seen from Fig. 3.3 that the average performance of the damaged system can be characterized, to first order, by determining two parameters, the scale of the aberrations, Λ, and the level of the high frequency OTF. Once these parameters have been determined from the physical damage models, the approximate forms of the damaged OTF and PSF are defined. Similarly, when suitable image quality or system performance descriptors are defined, they can also be evaluated in terms of S and Λ.

In terms of specific results for the three cases considered in detail, cracks were found to have only a modest effect, provided the amount of the surface covered is not excessive. For flakes, the damage scale appears to be of order 100 μm and a major effect can result because the area coverage can be large. However, if the rms phase distortion is small, the overall effect of the aberrations will be modest. Of the three cases considered, vaporization will probably have the largest effect. Estimated damage scales are of order 10-20 μm with rms phase shifts of greater than a half wave. These two parameters combine to cause substantial spreading of the image and severe attenuation of the diffraction peak.

3.5   Laboratory Measurements

As noted previously, laboratory measurements are of value for determining relevant scales (i.e., Λ), for validating theoretical models, as well as for empirically evaluating performance. However, such measurements must be carefully evaluated because of several effects. One effect is the statistical problem discussed previously, i.e., a few measurements will not adequately define performance without a supporting model. Another issue is that any laboratory measurement will depend on both the parameters of the damaged glass and the measurement systems.

As an example, consider the typical laboratory measurement shown in Fig. 3.4. For this measurement, a video system views a black and white contrast target with and without a piece of damaged glass in the optical line of sight. The video signal (single sweep) through the image starts at a baseline, corresponding to the white portion of the target which then increases to a higher

67

B/W CONTRAST TARGET

DAMAGED GLASS

TV

▷ VIDEO SIGNAL

UNDAMAGED

V_1 T_1

DAMAGED

V_2 T_2
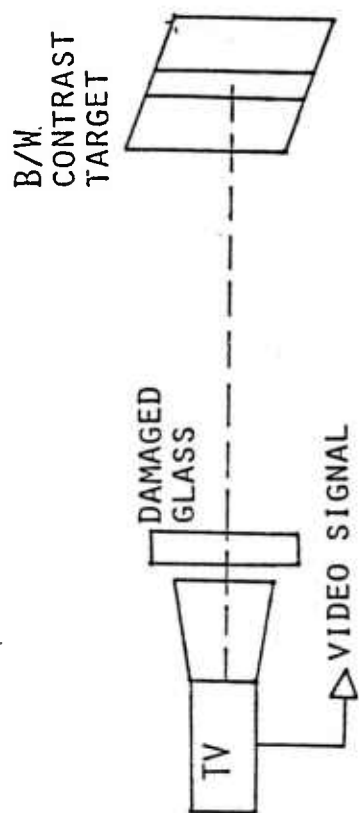
● CONTRAST

   $C = (V_2/V_1)$

● RESOLUTION

   $R = (T_2/T_1)$

● SINGLE REALIZATION

● MODEL REQUIRED BECAUSE RESPONSE DEPENDS ON SYSTEM PARAMETERS

$$C \approx \left[\int_{-\Delta/2}^{\Delta/2} P_D(x)dx \bigg/ \int_{-\Delta/2}^{\Delta/2} P_0(x)dx \right]$$

– INDEPENDENT OF OBJECT FOR VERY SMALL Δ

– ONE FOR VERY LARGE Δ
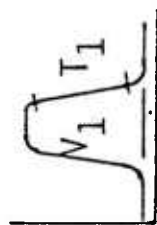
Fig. 3.4 Typical laboratory measurement.

level, corresponding to the black stripe, and then drops back to the baseline. The effect of the damaged glass is specified by comparing the change in signal level, i.e., contrast, and fall time, i.e., resolution. Typically, only single realizations are measured. This measurement could easily be extended to average properties by using a damaged sample larger than the optical field of view and moving the glass between successive measurements. This would yield an ensemble of results which could then be used to determine appropriate average properties.

A model of the measurement process is required because the measured parameters depend on system characteristics. For example, it is easy to demonstrate that the contrast is approximately equal to the ratio of the damaged and undamaged point-spread function integrated over the projected width of the black stripe ($\pm$ $\Delta/2$), including the response of the video system.

$$C \cong \left[\int_{-\Delta/2}^{\Delta/2} P_D(x)\,dx \bigg/ \int_{-\Delta/2}^{\Delta/2} P_O(x)\,dx \right]. \qquad (3.12)$$

If Δ is small compared to the scales of the damaged and undamaged PSF (P_D and P_O), then C is independent of Δ (i.e., the object) and, in fact, is equal to the Strehl ratio. While this may be optimal in terms of ease of interpretation of the results, there exists a fundamental problem, i.e., signal to noise. For a very small black stripe, the video sensor will not resolve the object and hence the change in signal levels (V_1 and V_2) will be extremely difficult to detect. In contrast, if the stripe is very broad (relative to P_D and P_O), each integral in Eq. (3.12) will be approximately equal to the total energy collected, i.e., the ratio will approach one. Hence, the measurement will be easy to make but the information content will be essentially zero.

In summary, laboratory measurements are valuable for determining the impact of damage on optical system performance. However, for this data to be useful, the experiments must be appropriately designed to account for statistical effects and a model must be generated to specify the experimental parameters and provide the means of reducing the data to a set of damage parameters of utility for evaluating the performance of a given system.

69

3.6 System Modeling

The prior discussion primarily concentrated on the evaluation and specification of the damaged optical component and its effect on the fundamental performance of the system. A complete evaluation and specification of a particular system designed to meet the requirements of a specific application requires a more extensive system model. Important aspects of such a model are shown in Fig. 3.5. Key aspects include the physical damage, optics, object, environment, detector and requirements. All of these impact the performance assessment and there exist several interactions between these various parts of the model.

Physical damage will depend on the type of laser employed, the damage modes involved and environmental effects which can modify the nature of the radiation which is incident on the optics. Important system parameters include aperture size, field of view, jitter and detector response. If a human observer is part of the system, the physiological response of the eye may play a key role in establishing performance. The requirements for system performance depend on the mission objectives and the type of objects which are likely to be encountered in actual practice. This will include not only the specific object of interest, but also other objects within the field of view, background and propagation effects such as attenuation and scatter.

All of these effects and issues must be included in the performance assessment model if valid conclusions are to be developed. Finally, the performance figure of merit should be designed to reflect the system mission requirements. Three generic missions are shown at the bottom of the figure. For detection, the key parameter is signal-to-noise ratio. For a system designed to provide data for pointing a weapon, the key issue is pointing accuracy, whereas for a recognition mission the range at which a given target can be identified is fundamental. In each case, it is desirable to quantify these parameters in terms of laser characteristics which determine the extent of damage. In this fashion the laser characteristics required to negate specific optical systems can be quantified as a function of mission requirements.

70
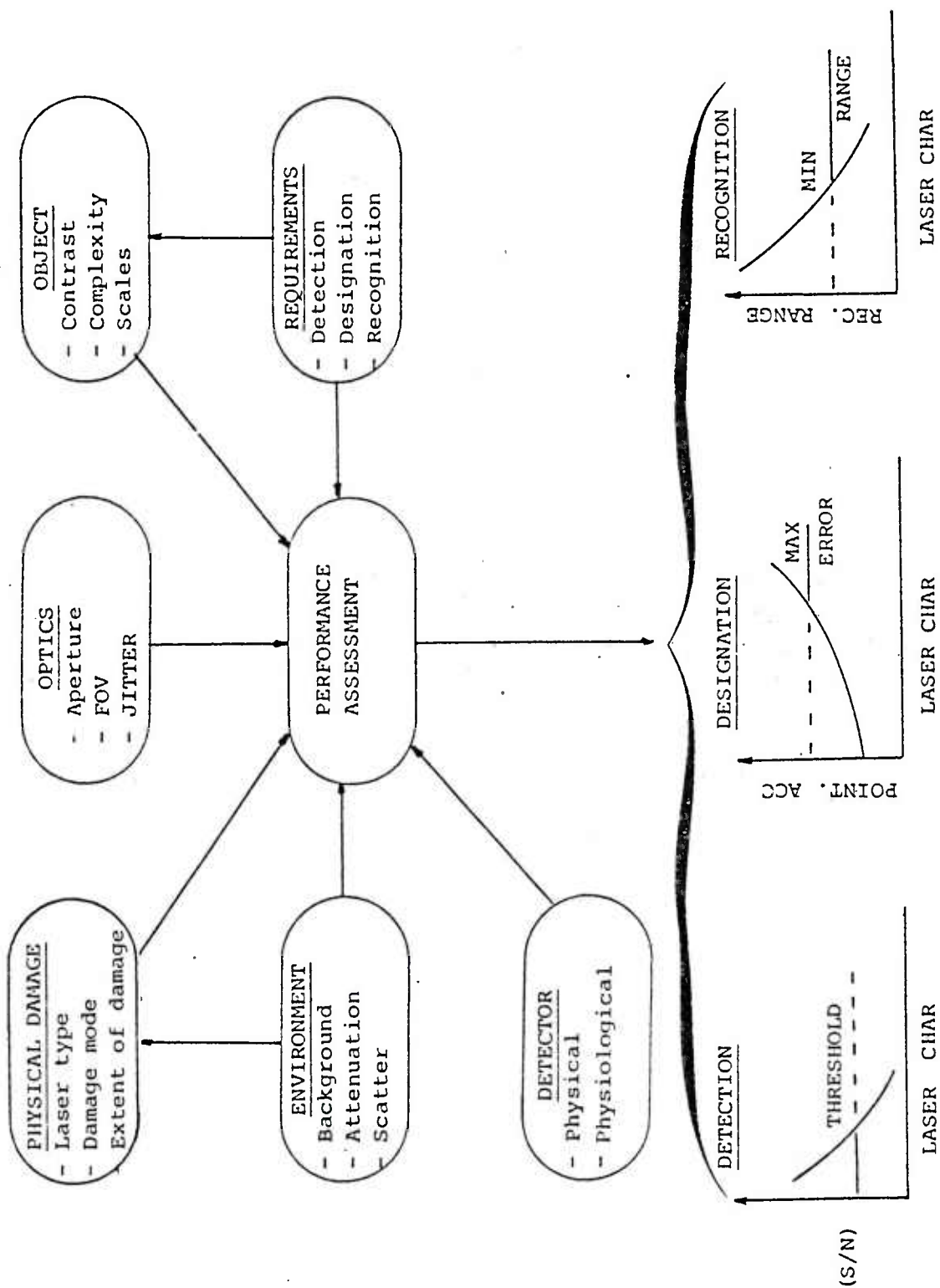
Fig. 3.5 System model.

3.7   Validity of Methodology

An aspect of the analysis summarized in the foregoing discussion which merits further consideration is the validity and utility of two fundamental assumptions. These are:

- Spatial statistical stationarity

- Appropriateness of the average OTF.

Spatial stationarity was assumed when evaluating the correlation function of the damaged related pupil function, Eq. (3.9):

$$< \beta (\underset{\sim}{v}) \beta^* (\underset{\sim}{v} - \lambda R\underset{\sim}{f})> = \tau_\beta (\lambda R\underset{\sim}{f}) \quad , \qquad (3.9)$$

where β is the pupil function, $\underset{\sim}{v}$ is a position variable in the aperture (integration variable), λ is wavelength, R is the system focal length, $\underset{\sim}{f}$ is the spatial frequency of interest and $<...>$ indicates a statistical average. Stationarity yields the result that the pupil function correlation (τ_β) is independent of integration variables ($\underset{\sim}{v}$ in Eq. (3.5)), and hence the total average OTF separates into a product of terms associated with the various independent damage mechanisms and the undamaged optical transfer function (Eqs. (3.10) and (3.11)). It is obvious that this assumption leads to a very powerful result, i.e., the effect of damage can be evaluated independent of the specifics of the optical system. Once evaluated, the damaged pupil correlation function can be used to determine the averaged OTF for any system by forming the product with the undamaged OTF for the system of interest.

Aside from the desire for a simple analytic description, there is physical rationale for assuming spatial stationarity. As noted previously, laser glass damage is a random phenomenon and thus, can only be characterized in statistical fashion. If the statistics were not stationary, then the correlation function would depend on two variables:

$$<\beta(\underset{\sim}{v}) \beta(\underset{\sim}{v} - \lambda R\underset{\sim}{f})> = fnc(\underset{\sim}{v}; \ \lambda R\underset{\sim}{f}) \ . \qquad (3.13)$$

72

In terms of a piece of glass irradiated by a laser, Eq. (3.13) would imply that τ_β depends on the location ($\underline{V}$) at which the correlation function is being evaluated. There are two physical effects that could cause this: variations in glass properties and variations in the laser radiation. The former would require that the response of the glass be a function of position. While this is certainly possible, there is no reason to assume such a characteristic in the systems of interest. Consequently, it is more reasonable to assume homogeneous glass properties which lead to spatial stationarity with regard to the response of the glass.

Because the extent and type of damage is dependent on the local strength of the laser field which irradiates the glass, it is quite possible that the correlation function may be non-stationary due to variations in laser irradiation. As suggested by Figs. 2.1 and 2.2, damage tends to be a step function of pulse fluence. Consequently, if the variation in laser radiation over the aperture is confined within the limits corresponding to a particular type of damage, then the assumption of spatial stationarity should be valid. If the variation extends over several damage regimes, then it would be necessary to account for the variation. This situation could be modeled by assuming

$$\langle \beta(\underline{V})\beta(\underline{V} - \lambda R\underline{f})\rangle = \sum_{ij} \langle \beta_i(\underline{V})\beta_j(\underline{V} - \lambda R\underline{f})\rangle W_i(\underline{V})W_j(\underline{V} - \lambda R\underline{f}), \qquad (3.14)$$

where β_i is the pupil function associated with the damage regime occurring in the ith region of the aperture defined by the window function W_i. The size, shape and location of the regions would be determined by the locations at which the magnitude of the laser fluence crosses the thresholds indicated in Figs. 2.1 and 2.2. With reference to Eq. (3.14), the various statistical averages can be assumed to be independent of the integration variable (V) if the statistics are spatially stationary within each subregion. Substitution of Eq. (3.14) into Eq. (3.8) would then lead to a separation which would allow the various damage factors ($\langle \beta_i \beta_j\rangle$) to be evaluated independent of the system but the complete separation of Eq. (3.10) would not occur because of the residual integrals over window functions and the sums of Eq. (3.14).

73

Another extension to the theory can be developed for situations in which the incident radiation has propagated through a random media such as atmospheric turbulence. In this case the incident field will have a random variation which will be statistically stationary and the total average optical transfer function will be given by

$$\langle \tau(f) \rangle = \tau_\beta(\lambda Rf) \tau_A(\lambda Rf), \tag{3.15}$$

where τ_β is the previously defined quantity (Eq. (3.9) or (3.14)) and τ_A is a correlation function associated with turbulence. Considerable analysis of this latter quantity has occurred over a number of years and there exist an extensive body of results which can be used to quantify this effect.

The preceding brief discussion suggests the manner in which the existing theory can be extended to include (1) situations in which the statistics are not spatially stationary, and (2) the impact of atmospheric turbulence. However, it is anticipated that for most scenarios of interest, the size of the incident laser beam will be large compared with the system aperture. Furthermore, the primary emphasis of this study is to evaluate the effect of glass damage. Consequently, the original result, Eq. (3.9), would seem to be more appropriate. If finite beam effects or atmospheric turbulence need to be incorporated into the model, it should be possible to do so in the manner indicated above.

The second assumption underlying the preceding analysis is that the evaluation of the average optical transfer function or the point spread function is an appropriate measure of performance. This approach assumes that the average image is of principal concern (i.e., Eq. (3.1)). As previously stated, an observer using the optical system will be viewing the object through a single realization of the damage. However, only statistical properties can be evaluated analytically. Thus, the fundamental issue is which statistical properties are most appropriate for characterizing performance.

In addresssing this issue it is important to realize that the entire scenario and system, from object to detection technique, must be considered. However, specific applications have not, as yet, been defined. Consequently,

74

a definitive assessment of this issue cannot be given. Nevertheless, it is instructive to consider several simple examples to highlight various aspects of the problem.

First consider the laboratory measurement discussed in Sec. 3.5 and Fig. 3.4. The contrast is defined by Eq. (3.12):

$$C \cong \left[\int_{\Delta/2}^{\Delta/2} P_D(x)dx \Big/ \int_{-\Delta/2}^{\Delta/2} P_O(x)dx \right], \qquad (3.12)$$

where P_D and P_O are the damaged and undamaged point spread functions, respectively, and Δ is the projected width of the black object stripe. For a single realization, as will likely be obtained in the laboratory, C is random. The average contrast is given by

$$\langle C \rangle = \left[\int_{-\infty}^{\infty} \mathrm{sinc}(\pi f\Delta)\langle \tau(f) \rangle df \Big/ \int_{-\infty}^{\infty} \mathrm{sinc}(\pi f\Delta)\tau_O(f)dt \right]. \qquad (3.16)$$

This result is obtained by expressing P_D and P_O in terms of their Fourier Transforms (τ and τ_O), carrying out the one-dimensional spatial integral ($\mathrm{sinc}X = \sin X/X$) and interchanging the order of the average and the frequency integral. No averaging of the denominator occurs because P_O is independent of the damage. From Eq. (3.16) it can be seen that an evaluation of the averaged OTF leads immediately to an evaluation of the average contrast via a straight-forward integral. Consequently, the average OTF is an appropriate quantity for characterizing this aspect of the laboratory measurement. However, it may be important to characterize the expected variation in contrast about its average value, i.e., the variance defined by:

$$\sigma^2 = \langle C^2 \rangle - \langle C \rangle^2. \qquad (3.17)$$

In similar fashion, the second moment of C is given by

$$\langle C^2 \rangle = \left[\int_{-\infty}^{+\infty} df_1 df_2 \mathrm{sinc}(\pi f_1 \Delta)\mathrm{sinc}(\pi f_2 \Delta)\langle \tau(f_1)\tau^*(f_2) \rangle \right] \Big/ \left[\int_{-\infty}^{\infty} df \tau_O(f)\mathrm{sinc}(\pi f/\Delta) \right]^2. \qquad (3.18)$$

75

From this result we see that in order to determine the contrast variance it is necessary to evaluate the second moment of the damaged optical transfer function, $\langle \tau(f_1)\tau^*(f_2)\rangle$. This quantity can be evaluated in a fashion similar to the first moment although it may be computationally more complex.

The other parameter of the laboratory measurement of Fig. 3.4 is the resolution defined by the characteristic fall time of the video signal. This parameter can also be related to statistical properties of the OTF. Consequently, a statistical description of this particular laboratory procedure requires the computation of several average properties of the OTF. Furthermore, if probability distribution or density functions are required, a more detailed computation must be carried out. However, the averaged damaged OTF does play a central role in the quantification of this laboratory evaluation technique.

As a second example, consider the contrast associated with the response of a damaged system to a sinusoidal object. It is straightforward to show that for an object defined by

$$O(X) = 1 + A \cos(2\pi f_o x), \tag{3.19}$$

the image is given by

$$I(X) = \tau(o) + \frac{A}{2}\left[\tau(f_o)e^{-2\pi i f_o X} + \tau^*(f_o)e^{+2\pi i f_o X}\right]. \tag{3.20}$$

The conventional image contrast is given by

$$C = \frac{I(max) - I(min)}{I(max) + I(min)} = \frac{A|\tau(f_o)|}{\tau(O)}, \tag{3.21}$$

where $|\tau(f_o)|$ is the modulus of the OTF at the object spatial frequency (i.e., the OTF is, in general, complex). If the damage yields phase aberrations only, the OTF at zero frequency will be equal to unity and the average contrast is given by

$$\langle C\rangle = A\langle|\tau(f_o)|\rangle \tag{3.22}$$

From this result it can be seen that the average contrast is related
to the average modulus OTF rather than the average OTF of the previous ex-
ample. The former quantity is difficult to evaluate analytically but several
approximate forms are available in certain limits. For example, if the extent
of the aberrations is modest or low frequency behavior is of primary interest
then

$$<C> \cong <\tau(f)> + \left[<\tau_I^2(f)> \,/\, <\tau(f)>\right], \qquad (3.22)$$

where $\tau_I(f)$ is the imaginary part of the OTF defined by

$$\tau_I(f) = \int d\underset{\sim}{X} P_D(\underset{\sim}{X}) \sin(2\pi \underset{\sim}{f} \cdot \underset{\sim}{X}). \qquad (3.23)$$

The average of τ_I^2 can usually be calculated in straightforward fashion.

If the aberrations are strong and high frequencies are of principal
interest, then $|\tau(f)|$ can be modeled as having an approximate Rayleigh dis-
tribution in which case

$$<|\tau(f)|> = \left[(\pi/4)<|\tau(f)|^2>\right]^{1/2}. \qquad (3.24)$$

The average value of the modulus squared OTF is easier to evaluate
because it is a complete square (as opposed to the square root of the sum of
the squares of the real and imaginary parts). It is also a reduced form
($f_1 = f_2$) of the OTF correlation function required for the second moment of
the contrast in the prior example (Eq. (3.18)).

The above brief discussion indicates that for the response of a system
to a sinusoidal object, the average contrast is proportional to the average
modulus OTF. In one regime which may be of interest, the average OTF does
enter the problem although in conjunction with another average property, and
thus is important to the analysis. However, in other limits or the general
situation, it does not play a central role.

As a final example, consider a human observer viewing an object through a damaged object system. Assuming small scale aberrations of reasonable strength, a single realization of the PSD (i.e., response to point object) will correspond to the upper right hand sketch of Fig. 3.2. For a resolved object, the resultant image seen through the optical system will be a convolution of this highly variable spatial distribution with the object distribution (Eq. (3.1)). If the object is very small (i.e., a few diffraction elements in size), the image seen by the observer will be spread over a region of size $(1/\Delta)$. Interior to this region will be multiple, randomly located bright spots. Each of the spots will have a characteristic size determined by the size of the object. In the limit of an unresolved object, the size of these "speckles" approach the diffraction limit of the undamaged optical system. In fact, the intensity distribution across a specific speckle is approximately determined by the convolution of the object with the undamaged optical transfer function. Consequently, it is entirely possible that an observer could identify detailed object structure at scales much smaller than the overall size of the image which is controlled by scale of the aberrations (Δ).

When multiple images of the type discussed above are averaged, the relatively smooth curve given by the center right sketch of Fig. 3.2 results because of the random location of the speckles in each realization. In effect, all locations are more or less equally probable and so the image is filled in when averaged. Consequently, unless the strength of the aberrations are small, the average image will be large and diffuse, and object details at scales below $(1/\Delta)$ will not be observable. If the aberrations are small then a substantial amount of the total collected energy will remain in the undistorted component of the field yielding the on-axis peak shown in Fig. 3.2. In this case it may still be possible to observe detail near the center of the image, but at reduced contrast because of the presence of the broad halo resulting from the damage related aberrations.

Now consider objects with overall sizes much larger than the diffraction limit, but still significantly smaller than the image size produced by the aberrations. It is also approximately valid in this case to characterize the

complete image as a summation of terms, each of which is the convolution of the object distribution with an undamaged PSD of reduced and random amplitude. As in the prior case, each of these terms is randomly located within the interior of the overall image.

The result of the convolution of two functions of limited spatial extent is a new function whose width is given roughly by the square root of the sum of the squared widths of the two convolved functions. Therefore, as the object increases in size, each of the image speckles increases in size by a corresponding amount. Hence the speckles begin to overlap and very quickly the image becomes filled-in in much the same manner as occurs when the PSD is averaged.

Based on the foregoing discussion it is reasonable to assume that for large objects, the image seen by an observer using the damaged optical system will be more characteristic of the averaged PSD. This, in turn, suggests that an appropriate measure of performance will be obtained by modeling the average optical transfer function which is just the Fourier Transform of the averaged point spread function. While this conclusion seems well justified on a physical basis, it should be noted that the development is heuristic and qualitative. A quantitative assessment could yield some modifications depending on the detailed characterization of the aberrations and the exact nature of the object. Consequently, it may be appropriate to carry out a laboratory evaluation to determine the detailed relationship between visual observations and the mathematical characterization of random images.

In summary, the brief examination of these examples clearly indicates that the specific statistical properties of the damaged optical system required to characterize performance depend on the details of the application being considered, including object properties and detection technique. While several different parameters may be required to describe a particular situation, it is clear that the averaged optical transfer function will play a central role in many cases.

3.8   Summary

A substantial body of results have been developed for analyzing the effects of laser radiation induced damage to optical systems. Specifically, a methodology has been established for translating physical damage into system performance, and a variety of analysis tools required in this methodology have been developed. Furthermore, in the next section several specific damage mechanisms have been evaluated in terms of their impact on the system Optical Transfer Function and Point Spread Function. It is clear from these results that system performance degradations depend not only on the properties of the damaged glass, but also on object properties, measurement objectives, detector characteristics and environmental effects.

However, further work on specified components of the methodology is required to provide a model of practical utility for evaluating system performance. This includes additional quantification of the several damage modes, the development, analysis and interpretation of laboratory data, and the establishment of a complete systems model. When these models are validated, the methodology will yield system performance predictions as a function of laser parameters.

4. OPTICAL PERFORMANCE MODEL

4.1 General Considerations

Laser induced damage to glass that was studied in a previous report[1] will result in degradation of the optical system considered. We analyze in this section the effect of physical damage on optical performance. For the purpose of simplicity, we reduce the optical system considered to a cover plate, objective lens and ocular lens as shown in Fig. 4.1. The damage is considered to have been inflicted on the first optical element which is the cover plate. In the absence of any damage, the image of a point source at infinity will be an Airy pattern in the focal plane (for a diffraction limited system) of angular width proportional to λ/D where D is the diameter of the entrance pupil (which we take here to be the objective lens) and λ is the wavelength. When the cover plate has been damaged under laser illumination, incident light will be scattered at the damage sites, each damage site creating its own diffraction pattern of angular size λ/δ where δ is a typical dimension of the damage site. Since $\delta \ll D$, the damage sites will, in effect, spread the image of the point source over a distance $\lambda F/\delta$, where F is the focal length. The image of the point source in the focal plane of the first lens is conveniently represented by the form (i.e., the point spread function of Sec. 3).

$$I(r) = \eta Ai(r) + (1-\eta)B(r) \tag{4.1}$$

where $Ai(r)$ is the Airy pattern of the undamaged objective, B is the spreading function of the damage sites and η is a parameter between 0 and 1 that is related to the spatial extent (and also possibly magnitude) of the damage ($\eta = 0$ corresponds to no damage and $\eta \lesssim 1$ corresponds to complete coverage by severe damage). The situation is shown schematically in Fig. 4.2. The object of the following analysis is to calculate η and $B(r)$ for the various types of damage observed on glass.

Image degradation will result in a decrease in system performance. The performance decrease will depend on the engagement scenario: angular width subtended by the target, contrast of target to background, level of illumination, etc. The response of the eye will also play a role whenever an observer is looking at the scene through the optical system.
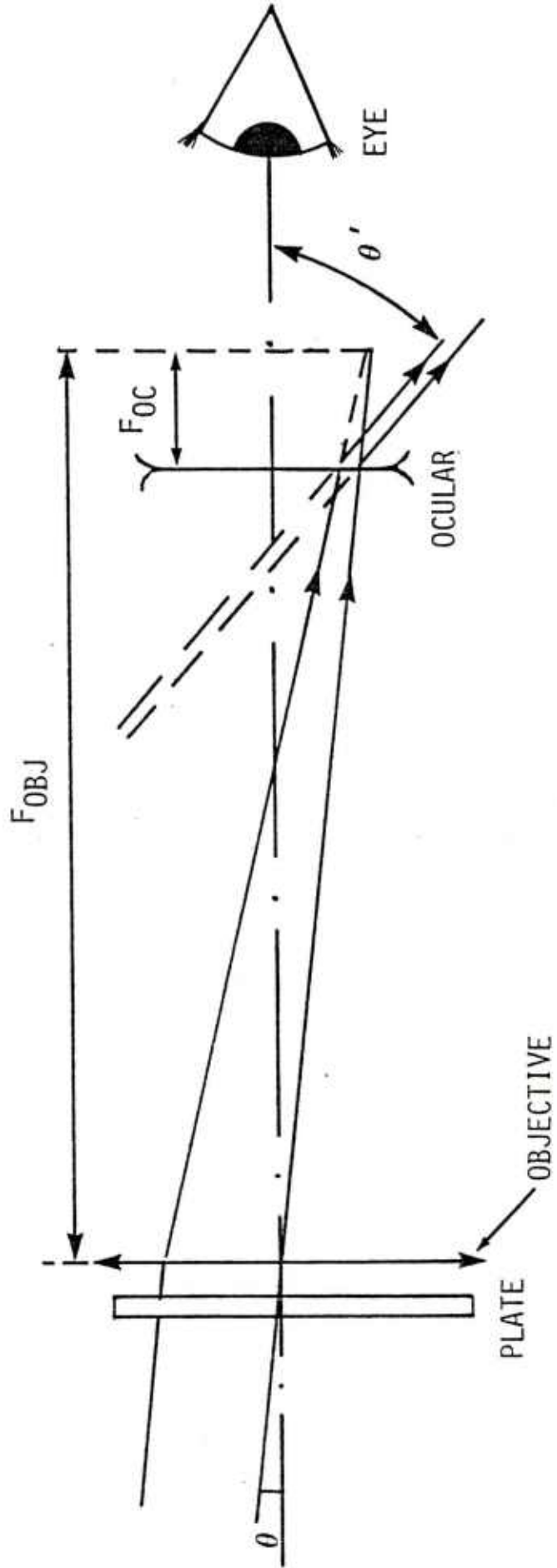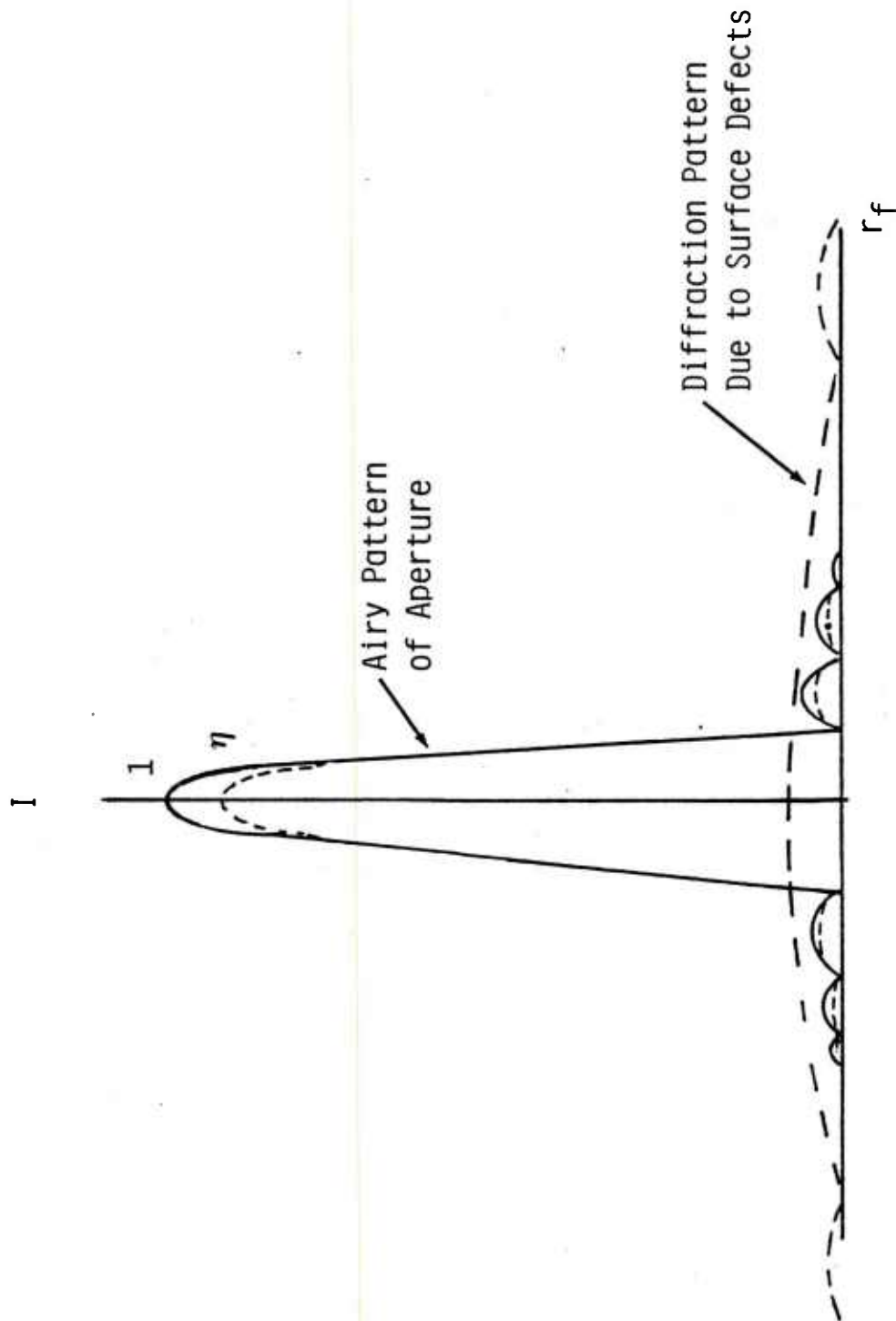
81

Fig. 4.1 Schematic of optical system.

Fig. 4.2 Schematic of point spread function for undamaged (solid line) and damaged (dashed line) optical system.

A standard method to characterize optical performance is to use bar charts where contrast and (angular) distance between bars are varied. The threshold contrast for the eye as a function of spatial frequency (inverse of angle subtended by a cycle of the bar chart) is shown in Fig. 4.3. The results shown in the figure were taken from Ref. (8) and corresponded to a sinusoidal modulation of intensity, I, in the bar chart. The ordinate of the curves is the percentage modulation defined as

$$M = 100 \; \frac{I_{max} - I_{min}}{I_{max} + I_{min}} \quad .$$

One sees from this figure that the threshold for recognition of the pattern is a minimum at spatial frequencies in the range 1 to 10 cycles/degree. If the eye is coupled to an optical system, as shown in Fig. 4.2, then the role of the ocular is to project the virtual image to infinity and to perform an angular magnification of F/f when F(f) is the focal distance of the objective (ocular). The contrast ratio as seen by the eye is essentially the same as that of the image plane of the objective. Therefore, to determine system performance of simple systems, we need only calculate contrast ratios in the image plane of the objective. (For more complicated optical systems, it may be desirable to propagate the beam completely through the system -- the analysis approach is the same as for simple optical systems but the calculations are more involved.) System performance is best in those scenarios where the threshold for recognition by the eye is the lowest (i.e., spatial frequency = 1 to 10 cycles/degree × (f/F). If the sensing element is a detector array or an image vidicon, one must couple, in a similar fashion, information on the thresholds for detection and recognition for these sensors with image degradation.

We derive in the following subsection (subsection 4.2) the general relations of optical transfer using methods of Fourier optics. These relations are then used (subsection 4.3) to calculate the response of an optical system to a point source when the cover plate has various types of physical damage. The effect on system performance is discussed in subsection 4.4.
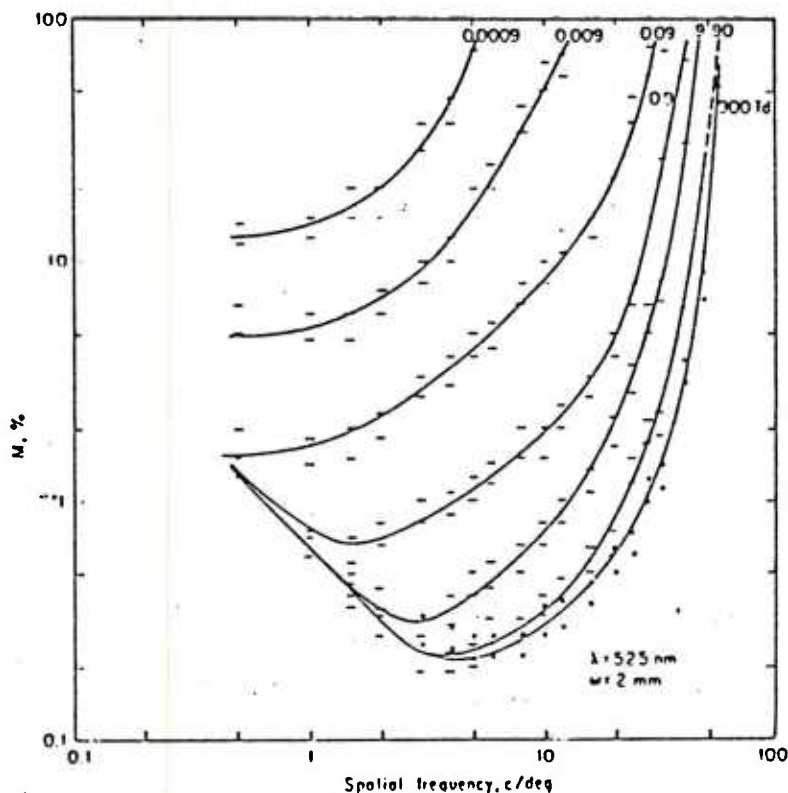
Fig. 4.3 Threshold-modulation transfer functions for green light (λ = 525 nm) at seven mean levels of retinal illuminance (2.0 mm diameter artificial pupil). The short horizontal lines denote the modulations in which the frequencies in question were perceived or not perceived. (These are the average results of three measurements.) For 900 Td they are replaced by dots. No difference was found between the modulation transfer function for 900 Td and that for 5,900 Td. Results of van Nes (1968).
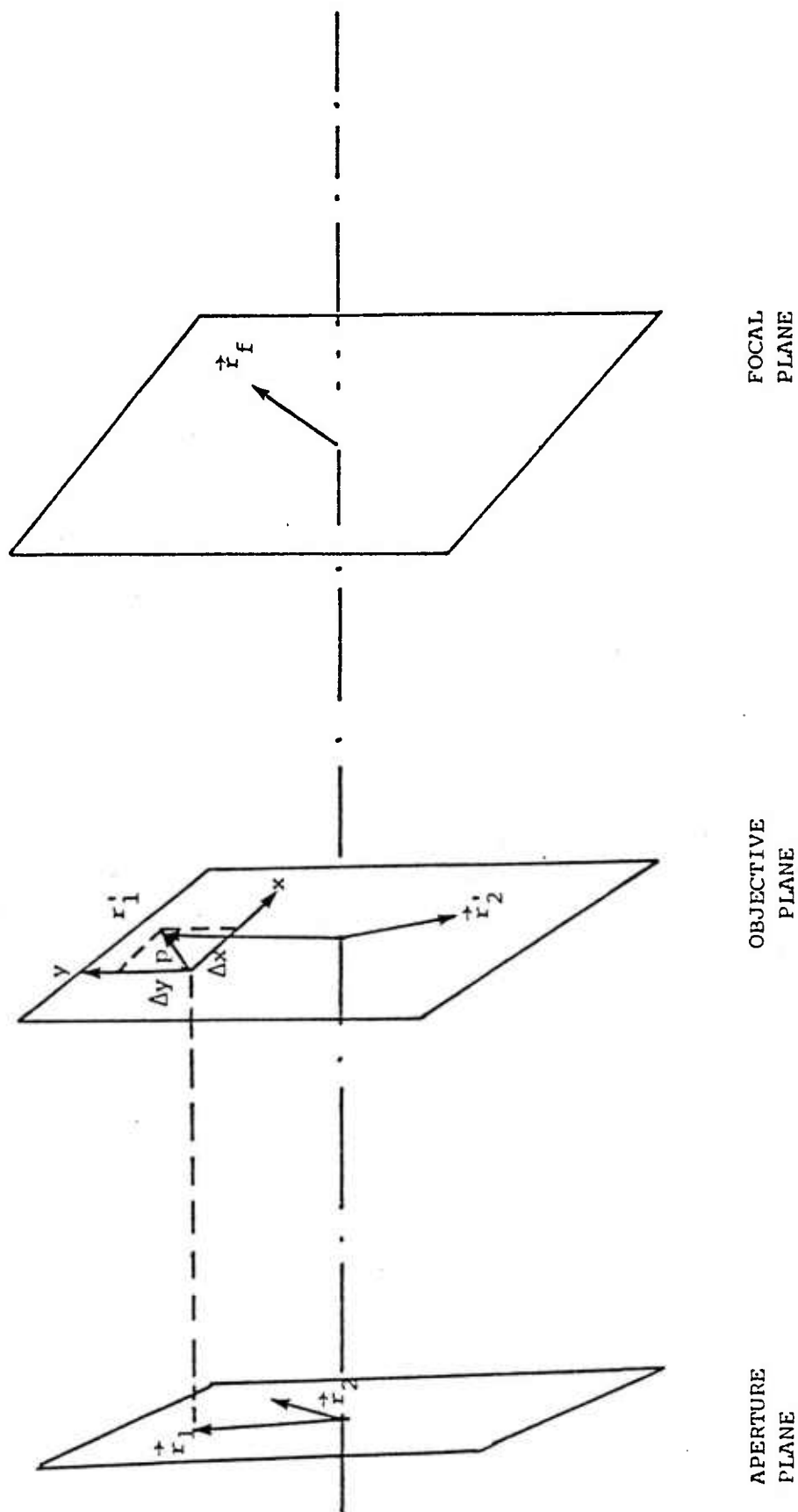
Fig. 4.4   Coordinates systems used in Eq. (4.4) to describe propagation from aperture plane to focal plane.

4.2. Derivation of the Optical Transfer Equations

We can find the field distribution in the image plane by successively using Fresnel's equation[9] to propagate the field through each optical element. If we know the field distribution along any closed surface Σ then from Fresnel's equation the field at $\vec{r}$ will be given by

$$u(\vec{r}) = \int_{\Sigma} G(\vec{r},\vec{r}') u(\vec{r}') d\vec{r}'. \tag{4.2}$$

In free space the propagator $G(\vec{r},\vec{r}')$ is given by[9,10]

$$G(\vec{r},\vec{r}') = \frac{1}{i\lambda} \frac{\exp ik\rho}{\rho} \cos(\theta), \tag{4.3}$$

where $\rho = |\vec{r}-\vec{r}'|$ and $\cos\theta \ (= \vec{n}\cdot(\vec{r}-\vec{r}))$ is the cosine of the vector $\vec{r}'-\vec{r}$ with the normal $(\vec{n})$ to the wave front at $\vec{r}'$. Equation (4.2) can be used successively through the optical system, the surfaces Σ being planes perpendicular to the optical axis and located at each optical element. Thus,

$$u(\vec{r}_f) = \int \cdots \int u(\vec{r}_s) G(\vec{r}_s, \vec{r}_1) G(\vec{r}_1, \vec{r}_2) \cdots G(\vec{r}_n, \vec{r}_f) d\vec{r}_s \, d\vec{r}_1 \cdots d\vec{r}_n, \tag{4.4}$$

where s(f) refer to source (focal) positions.

We consider, for the problem at hand, only 2 surfaces: one located at the cover plate and one at the objective lens, see Fig. 4.4. The effect of the cover plate can be easily described through the use of a transmission factor T relating the wave transmitted through the plate to the wave incident on the plate; that is,

$$u_p(\vec{r})(\text{transmitted}) = u_p(\vec{r})(\text{incident}) \times T(\vec{r}), \tag{4.5}$$

where $\vec{r}$ is a coordinate on the plate. For an undamaged antireflection coated plate and light incident normally to the plate we simply have $T(\vec{r}) = \exp(iknt_p)$, where n is the index refraction and t_p the thickness of the plate. Then

$T(\vec{r})$ is independent of $\vec{r}$. The transmission factor can then be factored out of the integrals in Eq. (4.4). Laser induced damage to the cover plate will have the effect of making $T(\vec{r})$ dependent on $\vec{r}$. Optical degradation will be related to the magnitude, phase and statistical properties of $T(\vec{r})$.

We consider, in order to simplify our calculations, a point source at infinity on the optical axis. The field at focus will be, using Eq (4.4),

$$u(\vec{r}_f) = u_o \iint T(\vec{r})G(\vec{r},\ \vec{r}')G(\vec{r}',\ \vec{r}_f)d\vec{r}\ d\vec{r}' \tag{4.6}$$

where the integral over $\vec{r}$ is taken over the cover plate and the integral over $\vec{r}'$ is over the objective lens plane. u_o is the constant field amplitude at the cover plate. The intensity (PSF) at focus is obtained by multiplying Eq. (4.6) by its complex conjugate (denoted by *),

$$
\begin{aligned}
I(\vec{r}_f) &= u(\vec{r}_f)u*(\vec{r}_f) \\
&= I_o \iiiint T(\vec{r}_1)T*(\vec{r}_2)G(\vec{r}_1,\vec{r}_1')G*(\vec{r}_2,\ \vec{r}_2')G(\vec{r}_1',\ \vec{r}_f)G*(\vec{r}_2',\ \vec{r}_f) \\
&\quad \times d\vec{r}\ d\vec{r}'\ d\vec{r}_2\ d\vec{r}_2'.
\end{aligned}
\tag{4.7}
$$

We evaluate the integrals using the following simplifying approximations:

a) the propagators from the plate to the lens are given by Eq (4.3) in which ρ in the denominator is replaced by the distance d between the plate and the lens, $\cos\theta$ is taken to be 1 and the exponent is approximated as follows (Fresnel approximation).

$$e^{ik\rho} = e^{ikd\sqrt{1 + \frac{\Delta x^2}{d^2} + \frac{\Delta y^2}{d^2}}} \approx e^{ikd}\ \exp\frac{ik}{2d}\ (\Delta x^2 + \Delta y^2). \tag{4.8}$$

The coordinate system is shown in Fig. 4.4.

b) the effect of the lens is to transform a plane wave into a spherical wave converging onto the focal plane. The propagator $G(r_1',\ \vec{r}_f)$ is thus approximated by[10]

$$G(\vec{r}_1',\ \vec{r}_f) = \frac{e^{ik\rho|\vec{r}_1' - \vec{r}_f|}}{i\lambda|\vec{r}_1' - \vec{r}_f|}\exp\left(-\frac{ik}{2f}\left[x_1'^2 + y_1'^2\right]^2\right)\exp(ikn\Delta_o), \tag{4.9}$$

where the last two factors represent the effect of the lens of focal length F, thickness on axis Δ_0 and index of refraction n.

    c) the Fresnel approximation, Eq. (4.8), is applied for propagation from the lens to the focal plane.

Using approximations a through c, we can write Eq. (4.6) explicitly as follows.

$$I(\vec{r}_f) = \frac{I_o}{\lambda^4 F^2 d^2}\left[\iiint_{plate} dx_1 dx_2 dy_1 dy_2 e^{\frac{-ik}{F}\left((x_1-x_2)x_f+(y_1-y_2)Y_F\right)} T(x_1,y_1)T^*(x_2,y_2)\right.$$

$$\left.\times \iiint_{lens} dx_1' dx_2' dy_1' dy_2' e^{\frac{ik}{2d}\left[(x_1'-x_1)^2+(y_1'-y_1)^2-(x_2'-x_2)^2-(y_2'-y_2)^2\right]}\right].$$

We perform the integral over the lens using the identity

$$\int_{-\infty}^{+\infty} e^{iu^2}\, du = -\sqrt{\pi}e^{i\pi/4}$$

and obtain

$$I(\vec{r}_F) = \frac{I_o}{\lambda^2 F^2}\iiint_{plate} dx_1 dx_2 dy_1 dy_2 T(x_1,y_1)T^*(x_2,\ y_2)e^{\frac{-ik}{F}\left[\left((x_1-x_2)x_F+(y_1-y_2)y_F\right)\right]}. \quad (4.10)$$

The integrals over coordinates $\vec{r}_1$ and $\vec{r}_2$ separate, and we obtain the well known result that the intensity at focus is proportional to the modulus square of the Fourier transform of the plate transmission factor T. If the plate is undamaged (i.e., a perfect transmitter), then we know from geometric optics that only that part of the plate whose shadow falls on the objective lens (or entrance pupil) can contribute to the intensity at focus. We should thus restrict the integrals over the plate to $|\vec{r}_{1,2}|<D/2$, or, equivalently, integrate over the whole plate, setting $T(\vec{r})=0$ if $|\vec{r}|>D/2$. One readily recovers the well known Airy pattern[9] at focus for a perfect optical system by setting T=1. Rewriting Eq. (4.10) in cylindrical coordinates, we find

$$I_{Airy}(r_f) = \frac{I_o}{\lambda^2 F^2} \left| \int_0^{2\pi} d\theta \int_0^{D/2} \rho d\rho e^{\frac{ik\rho}{F} r_f \cos\theta} \right|^2$$

$$I_{Airy}(r_f) = I_o \left(\frac{\pi D^2}{4\lambda F}\right)^2 \left(\frac{2J_1\left(\frac{kr_f D}{2F}\right)}{\frac{kr_f D}{2F}}\right)^2 . \qquad (4.11)$$

When the surface of the plate has been damaged, the defects that have been generated can scatter the incident radiation over large angles. Because of this scattering one should include contributions beyond the shadow that fall on the lens. The problem becomes much more complex since contributions from smaller defects have larger diffraction angles and contribute further out from the shadow. To circumvent the difficulties we will consider that the plate is very close to the objective lens (or entrance aperture). In calculations that will be performed in the next subsection for specific damage topologies of the surface, we find it always possible to separate $T(x,y)$ into a component T_o that is constant over the whole plate and a fluctuating component $t(x,y)$. The cross terms between T and t are shown to cancel for the types of damage considered, so we have

$$I(\vec{r}_f) = T_o^2 I_{Airy}(\vec{r}_f) + \frac{I_o}{\lambda^2 F^2} \int\int d\vec{r}_1 \, d\vec{r}_2 \, t(\vec{r}_1) \, t^*(\vec{r}_2) e^{-\left[\frac{ik}{F}(\vec{r}_1 - \vec{r}_2)\cdot\vec{r}_F\right]} \qquad (4.12)$$

For a given realization of damage sites we will have a given intensity distribution at focus. Due to the large number of (very small) defects we can only treat these in a statistical sense. We calculate then a most probable intensity pattern at focus by replacing $t(\vec{r}_1)t^*(\vec{r}_2)$ by its expectation value, which is only a function of $|\vec{r}_1 - \vec{r}_2|$. (Recall the discussion in Sec. 3)

$$\langle t(\vec{r}_1) t^*(\vec{r}_2) \rangle = f(|\vec{r}_1 - \vec{r}_2|) ,$$

where $f(r)$ is the correlation function (or Mutual Coherence Function) of the transmission factor for surface defects. The contribution of defects to the intensity at focus will therefore be, in a statistical sense, proportional to

90

the Fourier transform of the above correlation function. The response of the damaged optical system to a point source can then be written in the form of Eq. (4.1) where we identify η with T_0^2 and where $B(r)$ is proportional to the Fourier transform of $f(r)$, that is,

$$I(r) = \eta Ai(r) + (1 - \eta)B(r) \quad .$$

If we set I_0 equal to 1, then the right hand side of Eq. (4.1) is the response of a unit source on axis at infinity (the point spread function $P(r)$). If we have an extended <u>incoherent</u> source at infinity, the intensities are additive and the intensity at focus will be (Eq. (3.1))

$$I_F(\vec{r}) = \int I_0(\vec{r}') \ P(|\vec{r} - \vec{r}'|)d\vec{r}' \quad . \tag{4.13}$$

In the above equation, $\vec{r}'$ is the coordinate in the focal plane of the geometric image of a point on the source. One sees from Eq. (4.13) that P contains all the information necessary to calculate average optical performance and degradation for a given scenario.

4.3. Calculation of the Mutual Coherence Function (MCF) of Surface Defects and Point Spread Function for Different Damage Topologies

It has been experimentally and theoretically shown[1] that as the incident laser fluence on an AR coated optical glass element is increased the following damage mechanisms will successively occur:

a) removal of AR coating

b) formation of cracks normal to surface

c) flake formation (cracks parallel to surface)

d) bubble formation

e) vaporization of material leading to an uneven surface.

These mechanisms have been discussed in detail in Sec. 2. We study in this section the effects of mechanisms b, c and e on image degradation. Mechanism a, if complete, will simply result in an attenuation of the intensity at focus

by the ratio of reflectivity of a non-coated to reflectivity of an AR coated surface. Mechanism d is not believed to be important because few bubbles are formed; furthermore, the threshold for bubble formation by RP 10.6 μm lasers is very close to the threshold for vaporization, and vaporization dominates optical degradation.

4.3.1 Surface Cracks

As was shown previously,[1] surface cracks occur upon cooling of the surface, due to the presence of microscopic Griffith cracks that widen and deepen under thermomechanical stress. Microscopic examination of these cracks show a spacing that varies between 25 and 250 μm and a crack width in the 1 to 3 μm range. Cracks are not apparent in fused silica or 7900 series glass, whose coefficient of thermal expansion is small as compared to other glasses.

Let L be the (average) crack length, w the crack width, h the crack depth and N the number of cracks per unit area. Light incident on a crack will be refracted (scattered) to large angles and will not travel very far through the optical system before hitting a wall or an aperture plate. We therefore make $T(\vec{r})=0$ for all points M in a crack and set $T=T_0$ for all other points. Let C be the domain defined by the cracks. The probability that a point M does not lie on a crack, $P(M \notin C)$, is

$$P(M \notin C) = 1 - P(M \epsilon C) = 1 - NwL = 1 - a ,$$

where we defined $a = NwL$. The mutual coherence function due to cracks is

$$\langle T(M)T^*(M') \rangle = T_0^2 [1 - P(M \epsilon C) - P(M' \epsilon C)]$$
$$+ T_0^2 a P_2 (M' \epsilon C; M \epsilon C)$$

$$\langle T(M)T^*(M') \rangle = T_0^2 (1 - 2a) + T_0^2 a P_2(M' \epsilon C; M \epsilon C) , \qquad (4.14)$$

where P_2 is defined as the _conditional_ probability that if $M \epsilon C$, then also $M' \epsilon C$. Our major endeavor is to evalute P_2. If M and M' are on different cracks then P_2 is of order a and this will lead to a term of order a^2 in Eq. (4.14). Since a<<1 we need only consider the case where M and M' are on the _same_ crack.

Consider a Cartesian coordinate system XY on the surface with M on a vertical crack (length L along Y direction). We will later average over directions. Since MɛC, the center of the crack must lie within the rectangle of width w and length L centered on M as shown on Fig. 4.5, with constant probability. For M' to be on the same crack, the center of the crack must lie on a similar rectangle centered at M'. The conditional probability P_2 will be equal to the area of intersect of the two rectangles normalized by the area of the rectangle

$$P_2 = (w - |X - X'|)(L - |Y - Y'|)/(wL)$$

$$= \left(1 - \frac{|X - X'|}{w}\right)\left(1 - \frac{|Y - Y'|}{L}\right)$$

if $|X - X'| < w$ and $|Y - Y'| < L$. Otherwise $P_2 = 0$.

For arbitrary orientation, we define $r \cos \theta = |X - X'|$, $r \sin \theta = |Y - Y'|$ and average over θ. When $r < w$ we have

$$P_2(r) = \frac{2}{\pi} \frac{r^2}{wL} \int_0^{\pi/2} \left(\frac{w}{r} - \cos \theta\right)\left(\frac{L}{r} - \sin \theta\right) \qquad (4.15a)$$

$$= 1 - \frac{2}{\pi} \frac{r}{w} \left(1 + \frac{w + r}{L}\right) \approx 1 - \frac{2}{\pi} \frac{r}{w} \qquad r < w .$$

When $L > r > w$, we approximate the integral by neglecting $\sin \theta$ as compared to L/r and find ($\theta_1 = \cos^{-1} w/r$)

$$P_2(r) \approx \frac{2}{\pi} \frac{r}{w} \int_{\theta_1}^{\pi/2} \left(\frac{w}{r} - \cos \theta\right) d\theta \qquad (4.15b)$$

$$= 1 - \frac{2}{\pi} \cos^{-1} \frac{w}{r} - \frac{2}{\pi} \frac{r}{w}\left(1 - \sqrt{1 - \frac{w^2}{r^2}}\right) \qquad w < r < L$$

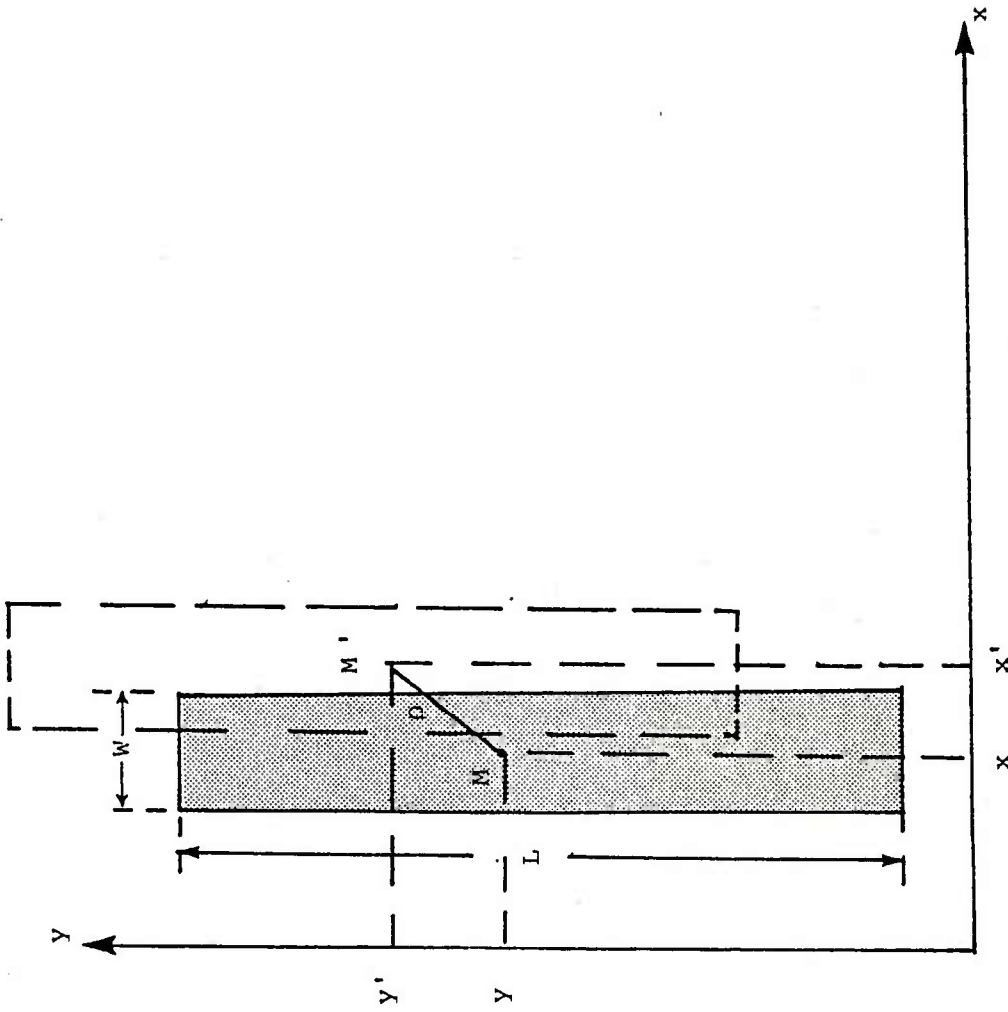and when $r > L$ we have $P_2 = 0$. The function P_2 is plotted in Fig. 4.6.
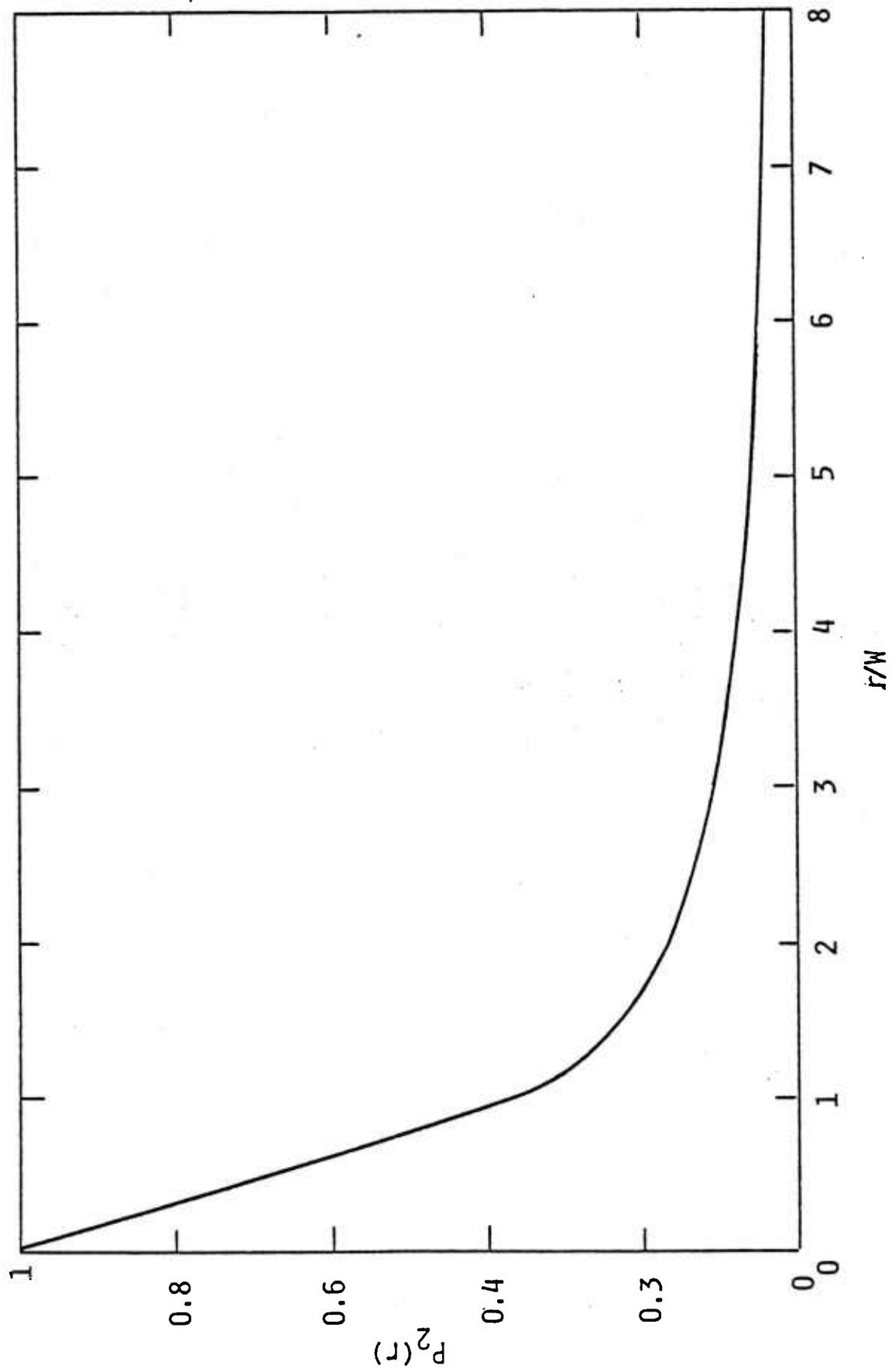
93

Fig. 4.5 Geometry for calculation of MCF of surface cracks.

94

Fig. 4.6 Conditional probability function P_2.

5439-10

The point spread function is given by Eq. (4.10), setting $I_0 = 1$ and replacing $\langle T(\vec{r})T^*(\vec{r}')\rangle$ by its average value given by Eq. (4.14). We find

$$P(r) = T_o^2\left[(1 - 2a)Ai(r) + \frac{\pi D^2}{4}\frac{a}{\lambda^2 F^2}\int_0^{2\pi}d\theta\int_0^{\infty}\rho d\rho P_2(\rho)e^{\frac{ik\rho r}{F}\cos\theta}\right] \qquad (4.16)$$

where we carried out two of the integrals by changing variables from (X_1, X_2, Y_1, Y_2) to $[u=(X_1+X_2)/2,\ v=(Y_1+Y_2)/2,\ \rho\cos\theta=(X_2-X_1),\ \rho\sin\theta=(Y_2-Y_1)]$ and used the fact that the integrand is independent of u and v, i.e.,

$$\iint dudv = \frac{\pi D^2}{4}\ .$$

The Airy function is defined as the ratio of $I_{Airy}(r)$ to I_0 in Eq. (4.11). The integral over θ in Eq. (4.16) leads to a Bessel function $J_o(k\rho r)$. We find

$$P(\rho) = T_o^2\left[(1 - 2a)Ai(\rho) + a\frac{\pi^2 D^2 w^2}{2\lambda^2 F^2}\int_0^{\infty}XdXJ_o\left(\frac{k\rho w}{F}X\right)f(X)\right]\ , \qquad (4.17a)$$

where

$$f(X) = 1 - \frac{2}{\pi}X \qquad X < 1$$

$$= 1 - \frac{2}{\pi}\left[\cos^{-1}\left(\frac{1}{X}\right) + X\left(1 - \sqrt{1 - \frac{1}{X^2}}\right)\right] \qquad X > 1$$

and

$$Ai(\rho) = \left(\frac{\pi D^2}{4\lambda F}\right)^2\left[\frac{2J_1\left(\frac{k\rho D}{2F}\right)}{\frac{k\rho D}{2F}}\right]^2 \qquad (4.17b)$$

Equation (4.17) shows the general feature of image degradation described in Sec. 3 and subsection 4.1, namely, a sharp Airy spot of width ($\Delta\rho\approx 2F/kD$) that has been attenuated by the factor (1 −2a) and a broad ($\Delta\rho\approx 2F/kw$) scattered contribution from the cracks. The ratio of intensities at peak from the two contributions is:

$$\frac{I_{max}(scattered)}{I_{max}(Airy)} \approx \frac{a}{1-2a} \frac{w^2}{D^2} \tag{4.18}$$

The integral in Eq. (4.17) is shown plotted in Fig. 4.7 for a specific choice of aperture diameter D, focal length F and crack width W.

It is interesting to note that the intensity of the main diffraction limited peak has been decreased by the factor (1-2a), though the surface coverage of cracks is only a (and not 2a). A contribution a has been absorbed from the beam (we set $T_O=0$ when light falls in a crack) and a contribution a has been diffracted out of the beam. This is the well known result of scattering theory for particles large as compared to the wave length where the extinction cross section is found to be double the geometric cross section.

4.3.2 Surface Flakes

Surface flakes are formed by thermomechanical stresses created upon cooling of the glass material near the surface. Their boundaries correspond to the location of Griffith cracks in the undamaged material. Typical flake dimensions are in the 100 μm range. Our model of a surface flake is shown in Fig. 4.8.

Flakes will affect propagation in the following ways.

a) Transmission loss due to reflection on surface (2) and (3) in Fig. 4.8.

b) Phase delay due to an increased (or decreased) path.

c) Interference effects in the air gap between surface (2) and (3) of Fig. 4.8.

d) Diffraction at the edges of the flake.

We include in our model effects a and b which we believe to be the dominant ones. Consider a typical glass of refractive index n=1.5. The amplitude reflection coefficient at surfaces (2) and (3) is calculated to be 0.19 so that transmission losses of intensity going through the flake are of the order of

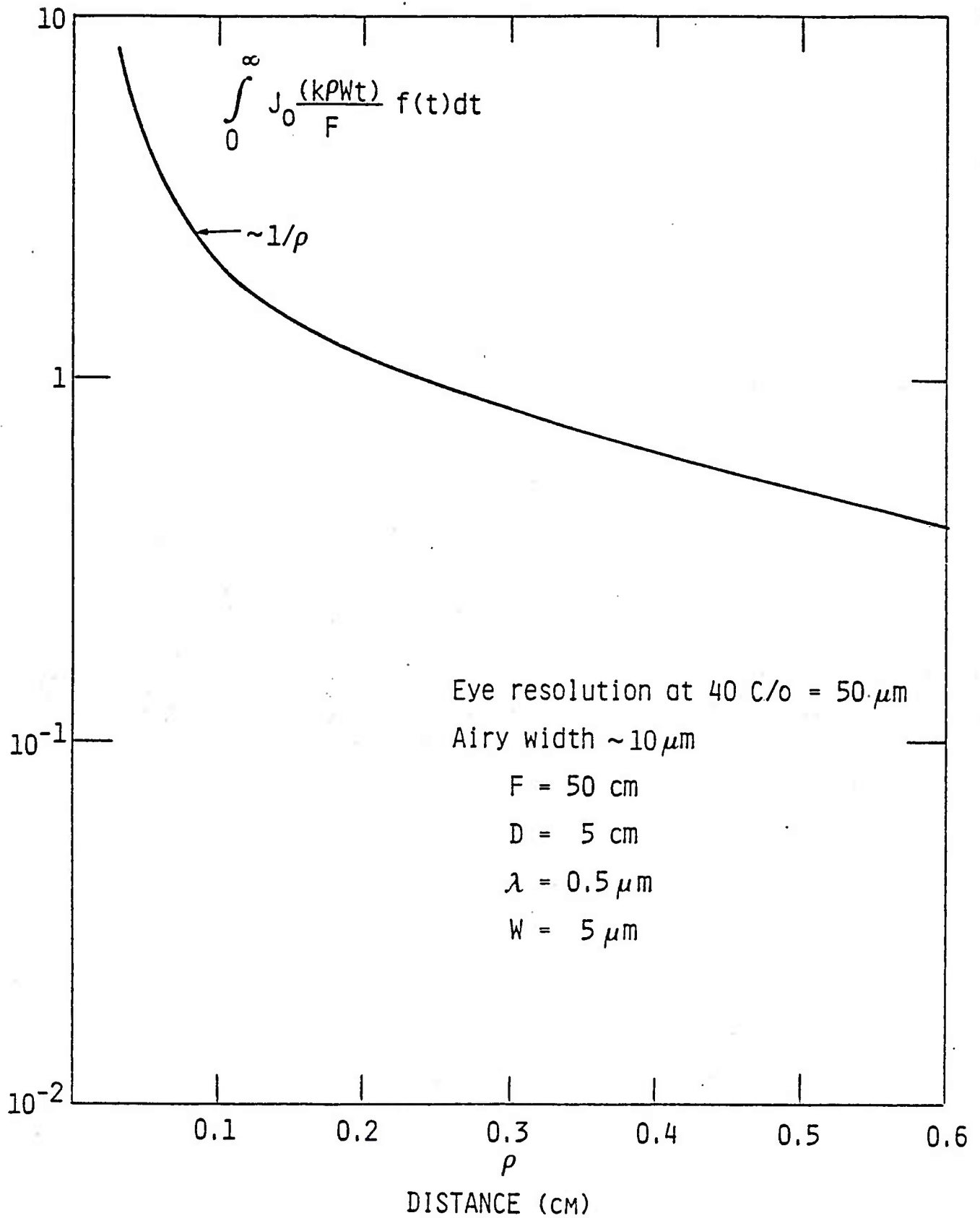$$\int_0^\infty J_0 \frac{(k\rho Wt)}{F} f(t)dt$$

~1/ρ

Eye resolution at 40 C/o = 50 μm
Airy width ~ 10 μm
F = 50 cm
D = 5 cm
λ = 0.5 μm
W = 5 μm

ρ

DISTANCE (CM)

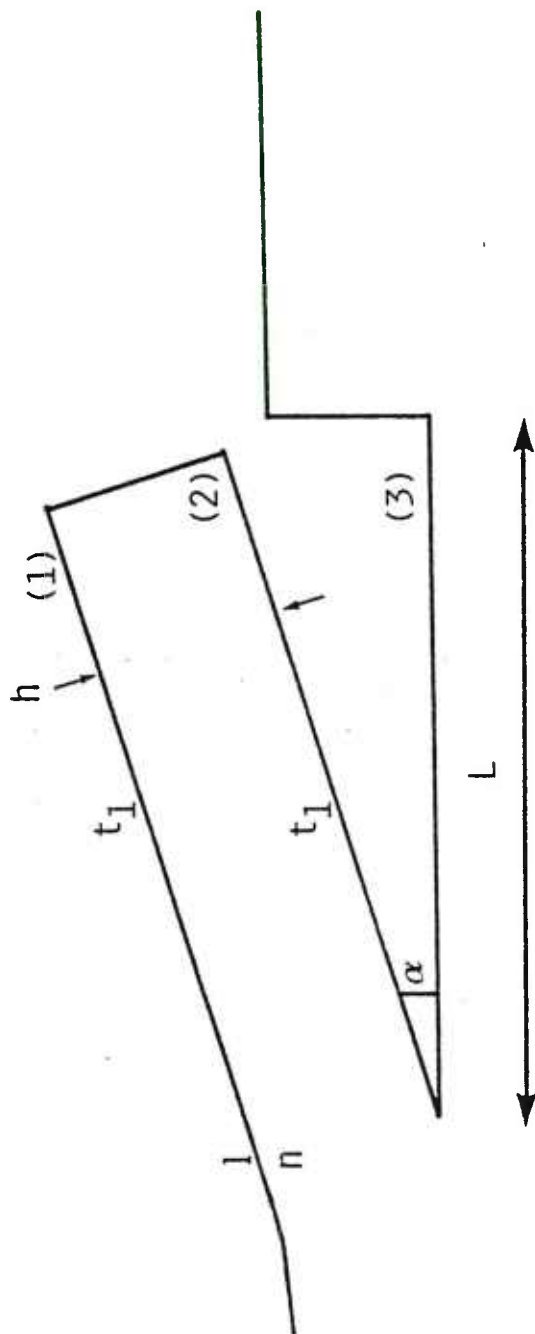Fig. 4.7 Point response function due to cracks.

98

Fig. 41 Schematic of flake.

$2 \times (0.19)^2 = 0.08$. If the flake is inclined by an angle α with respect to the undisturbed surface, then the optical path increase for rays normal to the surface is $nh(1/\cos \alpha - 1) \approx nh\alpha^2/2$, where h is the thickness of the flake. The extra phase delay is therefore

$$\delta\phi = \frac{\pi n \alpha^2 h}{\lambda} . \tag{4.19}$$

Typically $h = 10$ μm. Setting $\lambda = 0.5$ μm and $n = 1.5$ we calculate $\delta\phi = 0.03$ radian for $\alpha = 1°$, and $\delta\phi = 3$ for $\alpha = 10°$.

We treat transmission as follows. If a point is on a flake ($M \epsilon F$) then we set $T = t_1 e^{i\delta}$, where typically $t_1 = 0.96 \, t_o$ and δ depends on the thickness of the flake and on α. If $M \notin F$ then we see $T = t_o$. Let N be the number of flakes per unit area and L^2 the average flake area. We define the flake coverage ratio a through

$$a = NL^2 . \tag{4.20}$$

The contribution to $\langle T(M), T^*(M') \rangle$ comes from four types of terms:

A) M and M' are neither in a flake.

B) M and M' are both in the same flake.

C) M and M' are in different flakes.

D) M is in a flake and M' is not in a flake (or vice versa).

Define P(X) as the probability that event X(A, B, C or D) occurs. Then

$$\langle T(M)T^*(M') \rangle = t_o^2 \, P(A) + t_1^2 \, P(B) + t_1^2 \, \langle e^{(i\delta - i\delta')} \rangle P(C)$$

$$+ \, t_o t_1 (\langle e^{i\delta} \rangle P(D) + \langle e^{-i\delta} \rangle P(D)).$$

If all value of δ are equiprobable between $\delta = 0$ and $\delta = \delta_{max}$ with $\delta_{max} >> 2\pi$ then the averages $\langle e^{i\delta} \rangle$ are zero. We have considered this case for the calculations presented below.

We have

$$P(A) = (1 - a)P_2(M' \notin F; \, M \notin F).$$

It can be shown that for a random distribution of flakes of arbitrary orientation and having all the same size $L \times L$,

$$P_2(M' \notin F; \, M \notin F) = \begin{cases} 1 - \dfrac{4a}{\pi} \dfrac{r}{L} \left(1 - \dfrac{r}{4L}\right) & r < L \\[2ex] 1 - \dfrac{4}{\pi} a \left\{ \cos^{-1} \dfrac{L}{r} + \left(\dfrac{L}{2r} - \sqrt{1 - \dfrac{L^2}{r^2}} + \dfrac{r}{4L}\right) \dfrac{r}{L} \right\} & L < r < L\sqrt{2}, \\[2ex] 1 - a & r > L\sqrt{2} \end{cases} \tag{4.21}$$

where r is the distance between M and M'. Similarly, it can be shown that

$$P(B) = a \, P_2 \, (M' \epsilon F; \, M \epsilon F),$$

where

$$P_2(M' \epsilon F; \, M \epsilon F) = \begin{cases} 1 - \dfrac{4}{\pi} \dfrac{r}{L} \left(1 - \dfrac{r}{4L}\right) & r < L \\[2ex] 1 - \dfrac{4}{\pi} \left\{ \cos^{-1} \dfrac{L}{r} + \left(\dfrac{L}{2r} - \sqrt{1 - \dfrac{L^2}{r^2}} + \dfrac{r}{4L}\right) \dfrac{r}{L} \right\} & L < r < L\sqrt{2} \\[2ex] 0 & r > L\sqrt{2}. \end{cases} \tag{4.22}$$

We note that Eq. (4.22) is the same as Eq. (4.21) when a is set equal to 1. In order to simplify the notation we shall define $p_2(a, \, r/L)$ as the function given by Eq. (4.21). With this definition we have.

$$\langle T(o)T^*(\vec{r}) \rangle = t_o^2(1-a)p_2(a, \, r/L) + t_1^2 a \, p_2(1, \, r/L). \tag{4.23}$$

It is easy to verify that

$$p_2(a, \, x) - (1 - a) = a \, p_2(1, \, x). \tag{4.24}$$

Combining Eqs. (4.23) and (4.24), we obtain the more simple result

$$\langle T(o)T^*(r) \rangle = t_o^2(1 - a)^2 + p_2(1, \, r/L) \, a \left[(1 - a)t_o^2 + t_1^2\right] \tag{4.25}$$

When a→0 the MCF goes to the proper limit t_0^2 as it should, while when a→1 the MCF goes to the limit $t_1^2 P_2(1, r/L)$. A plot of the MCF of surface defects, $P_2(1, r/L)$, is shown in Fig. 4.9.

The point spread function is obtained by inserting the values of the MCF, from Eq. (4.25), into Eq. (4.10). We obtain

$$P(r_F) = (1-a)^2 t_0^2 \; Ai(r_f) + a\left[(1-a)t_0^2 + t_1^2\right]\frac{\pi^2 D^2 L^2}{2\lambda^2 F^2} \int_0^\infty x dx J_0\left(\frac{k r_f Lx}{F}\right)p_2(1,x) \quad (4.26)$$

The first term is the sharp Airy pattern defined in Eq. (4.17b) attenuated by the factor $(1-a)^2 t_0^2$ and the second term is the diffraction pattern due to the flakes, which has a width ≈ 2F/kL. The integral that gives the shape of the second diffraction pattern is plotted in Fig. 4.10 for a flake length of 100 μm, a focal length F of 50 cm and an aperture diameter of 5 cm. It has sharp minima; these minima would not have occurred if we had allowed for a variation in the size, L, of the flakes.

4.3.3 Surface Undulations After Vaporization

If one looks at a glass surface that had been heated up to the vaporization temperature by focusing a microscope slightly above or below the surface (see Fig. 4.11a) one observes light and dark patterns as shown schematically in Figs. 4.11b and c, when illumination of the sample is from below. This behavior is consistent with a surface that has ripples which create focusing and defocusing of the collimated light, the focal point being located alternatively above (real image) and below (virtual image) the surface of the glass (see Fig. 4.11d). The transverse distance between foci was found to be of the order 5 to 20 μm. The ripples may be due to uneven vaporization (glass is a composite material) or microcrystal formation. They may represent physical variations in the location of the surface or they may be just variations in the index of refraction near the surface.

We model their effect on transmission by assuming that the transmission has a sinusoidal phase variation in two dimensions.

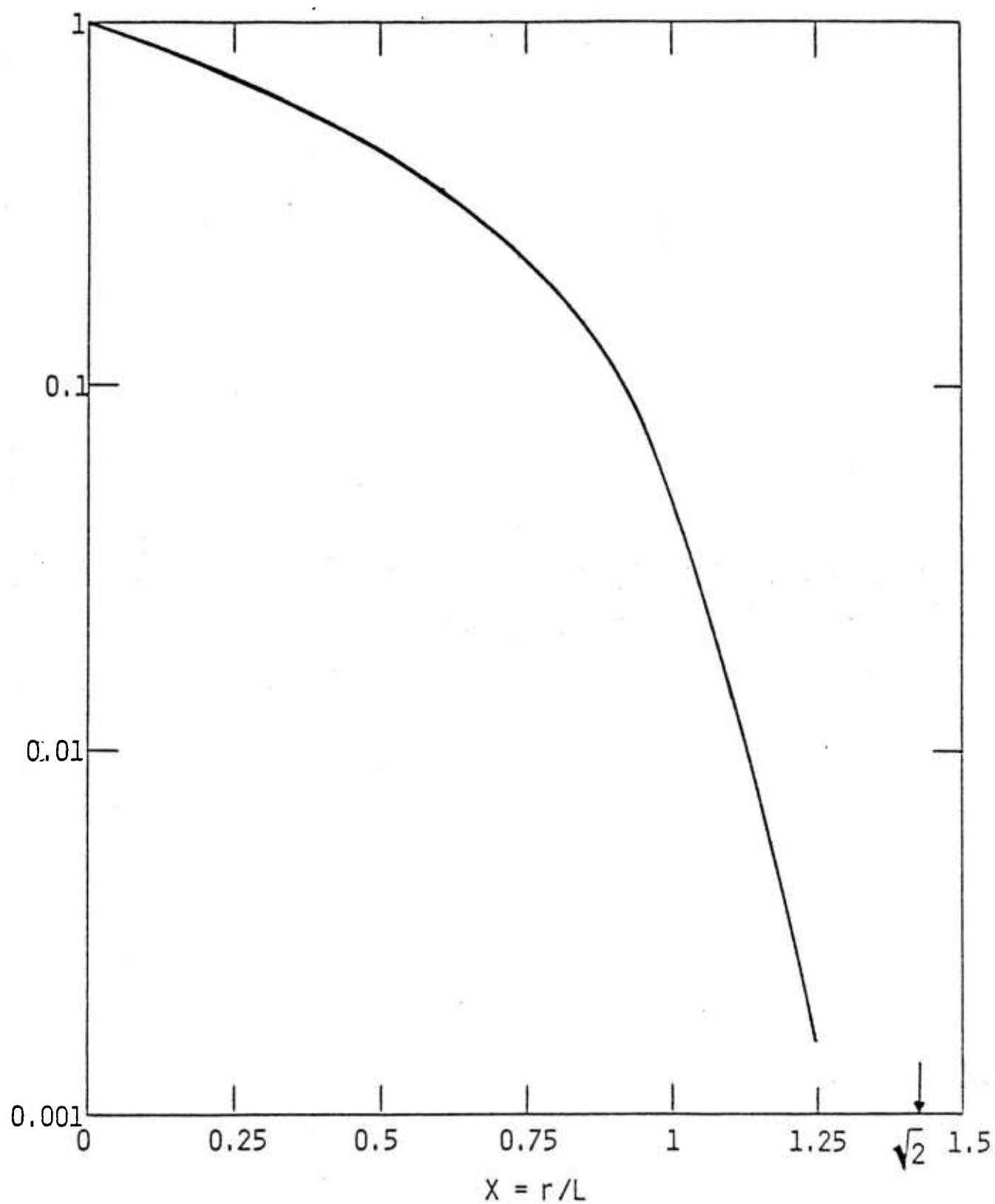$$T = t_0 e^{i\alpha \sin(kx) \sin(ky)}, \quad (4.27)$$

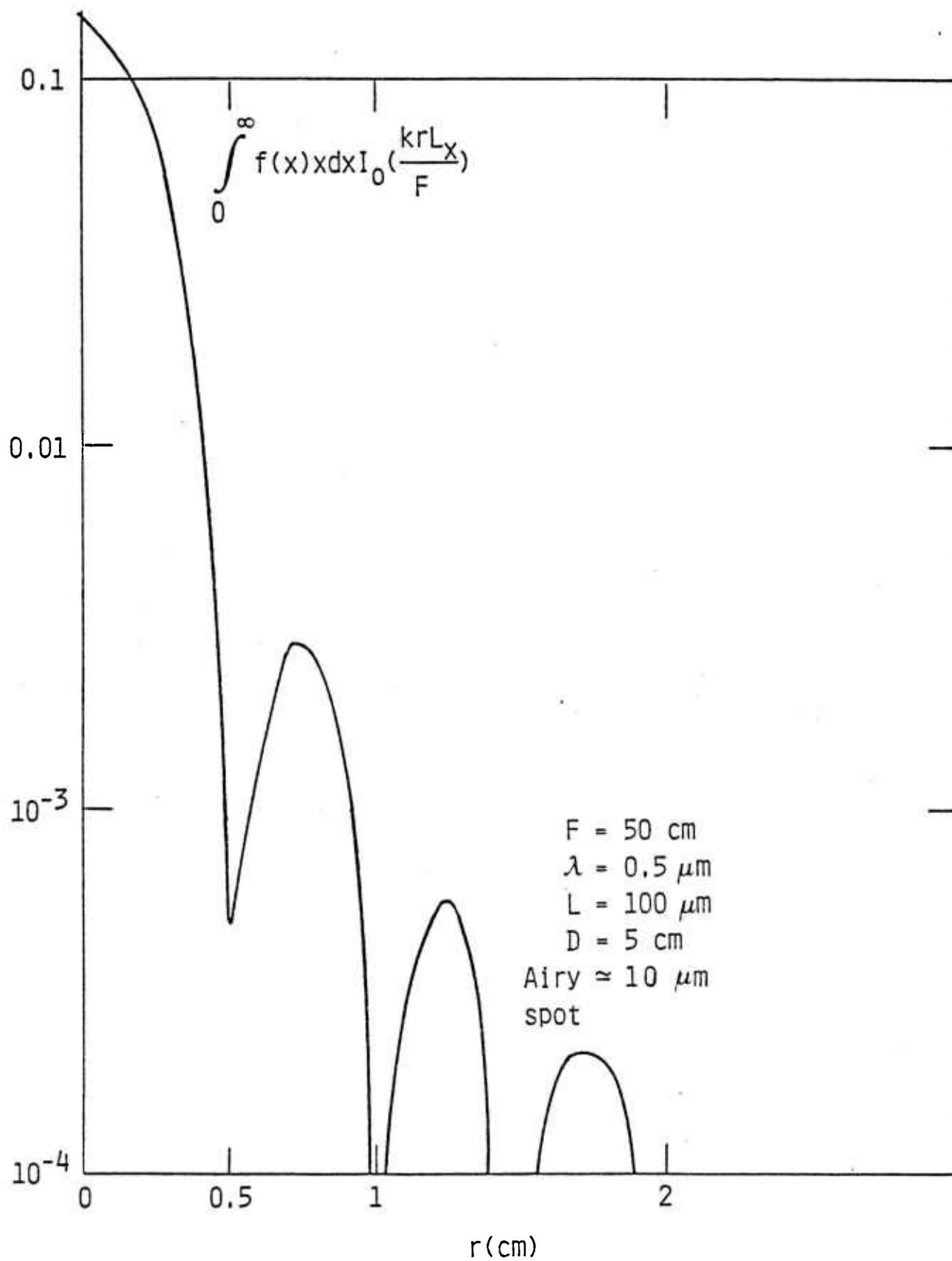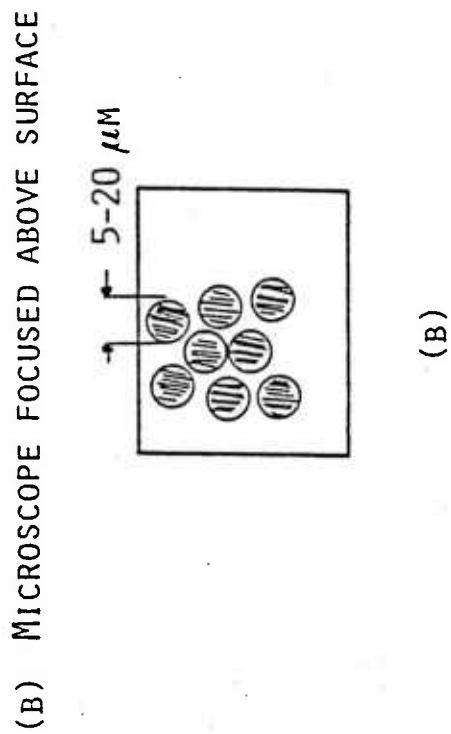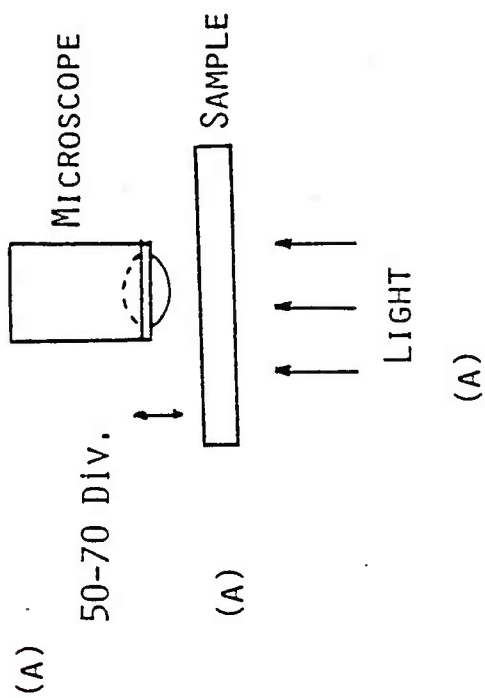Fig. 4.9   Mutual coherence function for flakes, $P_2(1,x)$.

$$\int_0^\infty f(x) x dx I_0 \left(\frac{krL_x}{F} \right)$$

F = 50 cm
λ = 0.5 μm
L = 100 μm
D = 5 cm
Airy $\simeq$ 10 μm
spot

r(cm)

Fig. 4.10 Point spread function for flakes.

(A)

MICROSCOPE

SAMPLE

LIGHT

50-70 DIV.

(A)

(A)

(B) MICROSCOPE FOCUSED ABOVE SURFACE

5-20 μM

(B)

MICROSCOPE FOCUSED BELOW SURFACE

(C)

EXPLANATION OF POSSIBLE CAUSE

5-20 μM
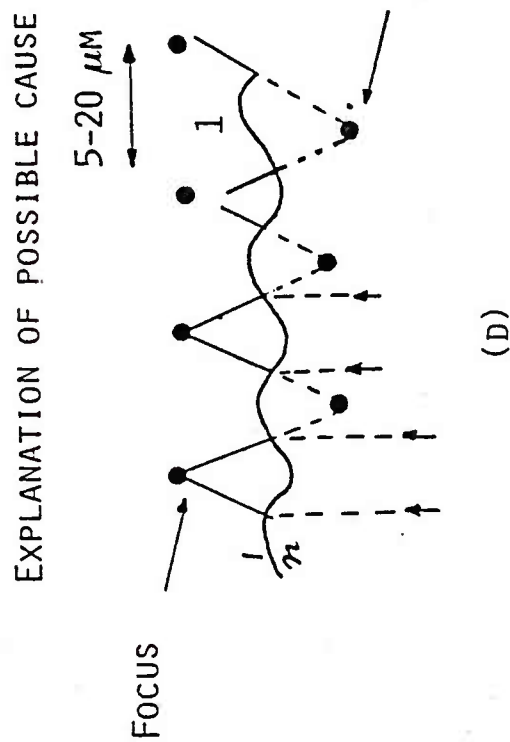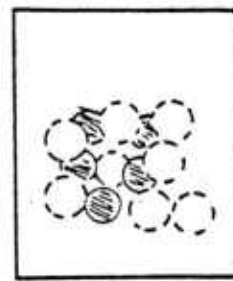
1

VIRTUAL FOCUS

FOCUS

n

(D)

Fig. 4.11 Analysis of surface after vaporization. a) optical set up, b) image with microscopic focused above surface, c) image with microscope focused below surface, d) focusing due to surface ripples.

105

where k is the wavenumber of the undulations and α the amplitude. Over some large distance of order L the undulations are uncorrelated, so that we must introduce a spread in k, $\Delta k = 2\pi/L$. We replace α sin kx sin ky by $\int \alpha(k)$ sin kx sin ky dk in Eq. (4.27). In order to be definite, let us model the spread by choosing $\alpha(k) = \alpha_o/\delta k$ if $k_o - \delta k/L < k < k_o + \delta k/L$ and $\alpha(k) = 0$ otherwise. Then $T(x, y)$ becomes

$$T(x,y) = e^{i\alpha_o \left[\sin(k_o x)\sin(k_o y) \frac{\sin\left(\frac{\delta k}{2}x\right)\sin\left(\frac{\delta k}{2}y\right)}{(\delta k/2)x\,(\delta k/2)y}\right]} \tag{4.28}$$

We evaluate the MCF of the surface undulations using Eq. (4.28) by averaging over one cycle of undulations in the x and in the y directions

$$\langle T(o)T(\vec{r})\rangle = \left(\frac{k_o}{2\pi}\right)^2 \int_{-\pi/k_o}^{\pi/k_o} dx \int_{-\pi/k_o}^{\pi/k_o} dy \; T(x,y)T^*(x+r,y) \quad .$$

We can readily perform one of the integrals and, after a change in variable, reduce the result to

$$\langle T(0)T^*(r)\rangle = f(r) = \int_0^1 du J_o \left\{ \frac{\alpha_o}{2\pi\beta}\left[\frac{\sin 2\pi u \,\sin 2\pi\beta u}{u} \right.\right. \tag{4.29}$$

$$\left.\left. - \frac{\sin(2\pi u + k_o r)\,\sin(2\pi\beta u + \beta k_o r)}{u + k_o r/2\pi}\right]\right\},$$

where $\beta = \delta k/k_o$ is a measure of the coherence of the undulations.

Approximations to Eq. (4.29) in several limiting cases can be obtained by expanding the Bessel function. For small arguments $J_o(x) \approx 1 - x^2/4$ and we have

$$\langle T(o)T^*(r) \rangle = 1 + \int_0^1 du(J_o - 1)$$

$$= 1 - \frac{\alpha_o^2}{16 \ \pi^2 \ \beta^2} \int_0^1 du \left[\frac{\sin 2\pi u \ \sin 2\pi \beta u}{u} - \frac{\sin(2\pi u + k_o r)\sin \ \beta(2\pi u + k_o r)}{u + k_o r/2\pi} \right]^2$$

$$+ \ \ldots \ldots$$

$$= 1 - \frac{\alpha_o^2}{2} \sin\left(\frac{k_o r}{2}\right) + O(\alpha_o^4). \tag{4.30}$$

The above expansion was obtained, assuming $\beta \ll 1$, by expanding the sin functions involving β; it is valid so long as $\beta k_o r \lessgtr 1$ and $\alpha_o^2 < 1$. When $k_o r \gg 2\pi$ we can neglect the second term in the bracket as compared to the first one and find

$$\langle T(o)T^*(r) \rangle = 1 - \frac{\alpha_o^2}{8} \left[1 + O\left(\frac{2\pi}{k_o r}\right) \right]. \tag{4.31}$$

The integral in Eq. (4.29) was numerically evaluated for $\beta = 0.1$ and various values of α_o varying from 0.01 to 1. When $(1 - MCF)/\alpha_o^2$ is plotted versus $k_o r$, one obtains the graph shown in Fig. 4.12. All the curves have collapsed onto one curve, which shows the validity of the expansions given by Eqs. (4.30) and (4.31) up to $\alpha_o = 1$. An evaluation of the integral with α_o set equal to 2π yields drastically different results with large and rapid fluctuations of the MCF as a function of r.

We have not calculated the point spread function for the case of surface undulations, but the qualitative features can be derived from Eqs. (4.30) and (4.31) and Fig. 4.12. The sharp Airy pattern of the lens is attenuated by the factor $(1 - \alpha_o^2/8)$ and the scattering pattern due the ripples has a width $\approx k_o F/k\pi$. As α_o increases from 1 to 2π the center Airy pattern substantially disappears and all of the radiation is scattered over large angles.

107

SINUSOIDAL PATTERN   T = EXP[I*A*(SIN(KX)*SIN(KY)]   5515-11

FREQUENCY SPREAD DELK/K = 0.1

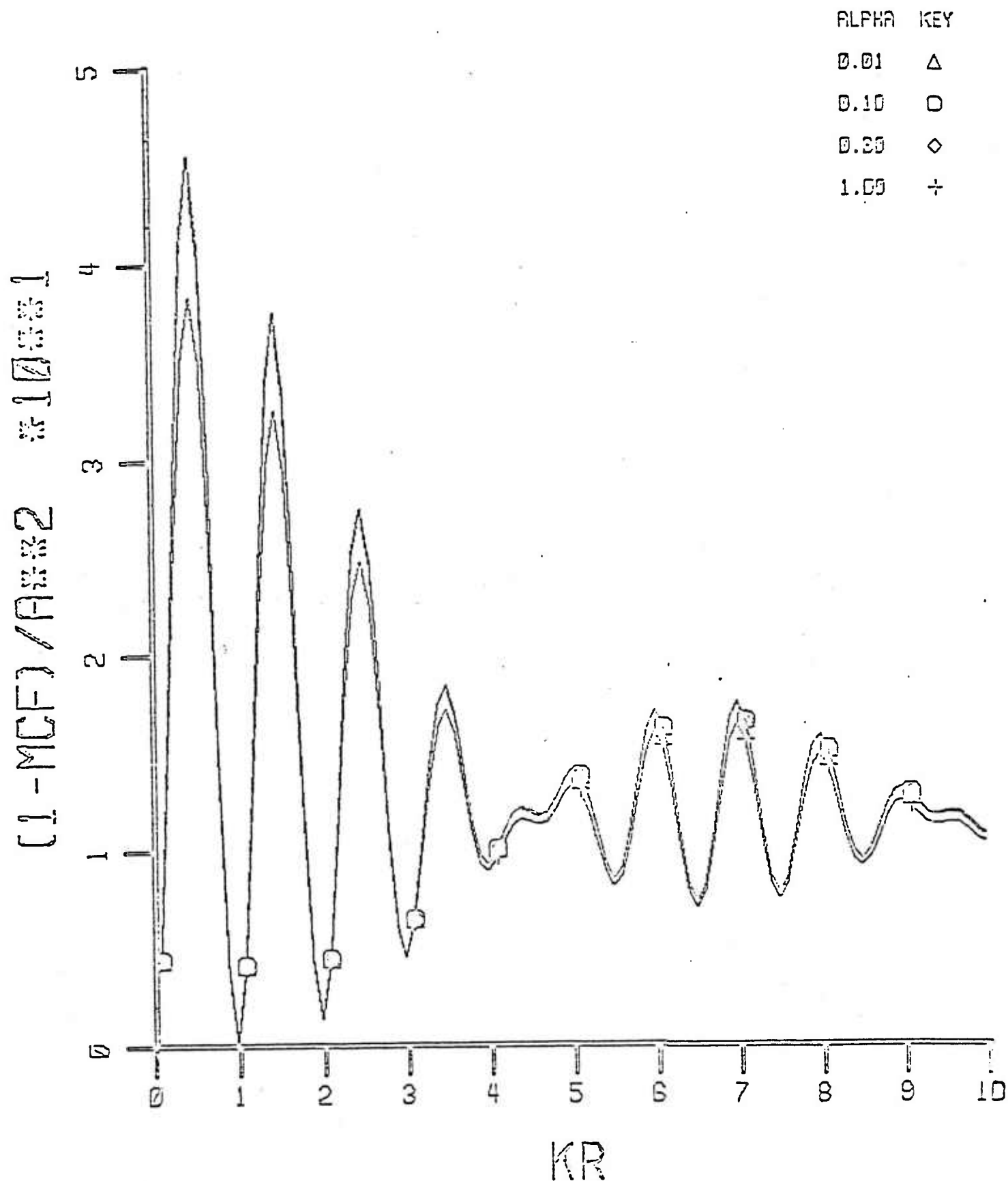| ALPHA	KEY
0.01	△
0.10	▢
0.35	◇
1.00	÷

Fig. 4.12 $(1-MCF)/\alpha_o^2$ versus kr for surface ripples on glass.

108

4.4.   Degradation of Optical Performance

As was stated in Sec. 4.2, the knowledge of the point response function of an optical system is all that is needed to determine image quality. Unfortunately optical performance of a system will depend also on the engagement scenario and unless a given scenario is specified, degradation of optical performance by laser induced defects cannot be estimated. As an example of how sensitive performance is to engagement scenario, consider an optical system operating on a moonlit night in the visible. If direct moonlight or radiation from a lamp hits the cover plate, even though the image of the moon (or lamp) is blocked by baffles or other types of spatial filters, the scattering of this light by defects may dominate the intensity field in the focal plant even for small defect concentrations. This system would, therefore, not be operational under such conditions, even though without illumination of the cover plate, good target recognition would be achieved for the same scene.

In order to <u>see</u> the target, the contrast of target must be above the threshold for the angle subtended by the target. Minimum thresholds for the eye as a function of spatial frequency are shown in Fig. 4.3. The criterion for target recognition is somewhat more stringent since at the threshold contrast ratio, recognition of the target requires that the target fill at least 3 resolution elements. We choose as an example a vehicle (a jeep) of length 2-1/2 meters that is 5 km away. An observer is searching the background with an optical system (binoculars) that is diffraction limited and is composed of a cover plate (filter), an objective of diameter $D = 5$ cm with a focal length F_{obj} of 50 cm, and an ocular having a focal $F_{OC} = 5$ cm. The angle subtended by the object is 2.5 m/5 km = 5×10^{-4} rad = 0.03°. As a result of the transverse magnification of the optical system, the angle subtended by the vertical image at infinity as seen by the eye is 0.03 x F_{obj}/F_{OC} = 0.29°. A resolution element for this object is one third of the above, i.e.; 0.1°, corresponding to a spatial frequency of 10/cycle degree. We see from Fig. 4.3 that the threshold contrast ratio for recognition of the target under such conditions is 1% (0.3%) at an average illumination of 9 Td(90 Td). If the object were at 20 km rather than 5 km, the threshold contrast ratio would be 3% (30%) at the

same illumination levels. The width of the Airy pattern due to the diffraction limited optics is one twentieth of the width of the image of the target in the focal plane so that in the absence of significant aberrations the quality of the optical system will not limit the recognition of the target if the contrast threshold criterion is exceeded.

Consider now the effects of optical degradation by cracks, flakes and surface ripples on the recognition capabilities of the system. The maximum crack coverage is $a = NLW = 3$ to 5% so that the attenuation of the Airy pattern due to scattering off cracks is 6 to 10%. The contrast ratio is decreased by the factors $(1-a)$, i.e., insignificantly and should not affect the visibility threshold in an appreciable way. Degradation due to surface flakes is expected to be important (i.e., an order of magnitude) when a phase change δ is of order 2π or more and surface coverage of flakes is almost complete. In this case the maximum of the Airy pattern is strongly attenuated and the contrast of target to background significantly modified. The same conclusion holds for surface undulations; coverage has to complete and the amplitude of the undulations, i.e., the parameter α_o in Eq. (4.28) exceed 2π.

For specific scenarios and optical systems, the optical imaging capability can be calculated on a case by case basis by using the point spread function and then explicitly integrating over the image plane to obtain the degraded image.

Although a detailed system performance analysis can not be performed without complete specification of the scenario, the detector, and the optical system, a sample calculation is extremely instructive for identifying important features. Consider the point spread function of flakes, which is shown in Fig. 4.10 for a given simple optical system. Two example calculations illustrate how sensitive the image contrast is to the object size (i.e., angle subtended) and structure. The first object consists of a black bar of angular width θ (full width), and the parameter that is calculated is the ratio of the contrast, as viewed through the damaged system to the contrast as viewed through the undamaged system. Since the calculation is being done to illustrate trends as various parameters are varied, the contrast is calculated by

convoluting the point spread function with a one-dimensional top hat intensity distribution. The integral over the transverse direction has not been performed -- although a two-dimensional convolution is required for accurate quantitative calculations with an azimuthally symmetric point spread function, the simpler one-dimensional calculation manifests the qualitative trends. The contrast ratio is plotted in Fig. 4.13 as a function of the angle subtended by the object. Results are shown for various combinations of the exfoliation point spread function and the diffraction-limited point spread function. The contrast ratio falls as the target size decreases, but the ratio never is less than the fraction of the power which resides in the diffraction-limited Airy pattern. Thus, to degrade the contrast an order of magnitude, no more than 10% of the power can remain in the residual diffraction peak, and a degradation of two order of magnitude requires that the residual diffraction peak contain less than 1% of the power. In addition, severe degradation requires that the object size be small compared to the width of the point spread function. The calculation presented above is useful for estimating the requirements for detecting an object. The requirements for recognizing an object are better illustrated by considering an alternating pattern of black and white stripes as being the object. The ratio of the contrast of the degraded and undergraded images is plotted in Fig. 4.14. The same one-dimensional convolution is used and calculations have been made for the same ratios of power in the diffraction-limited Airy pattern to power in the exfoliation diffraction pattern. The minimum contrast is still controlled by the fraction of intensity in the diffraction-limited spike, but the contrast is seen to approach the minimum values at much larger sizes of the stripes than in Fig. 4.13. Thus the reduction in contrast depends not only on the size of the elements of the object, but also on the proximity of other elements.

These calculations illustrate the qualitative trends expected for image degradation by damaged optical systems.
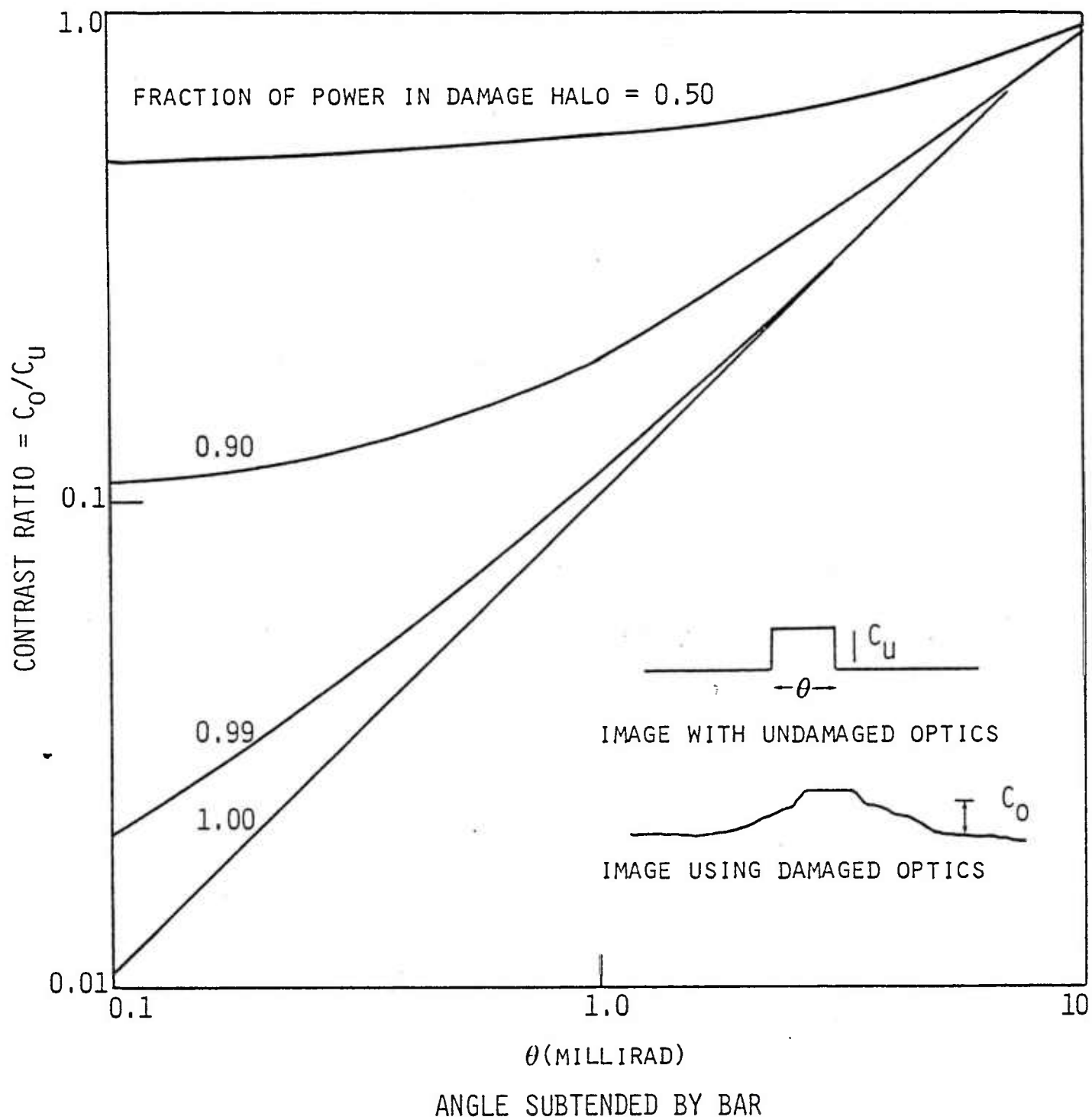
Fig. 4.13 Ratio of contrast of stripe observed with damaged optics to contrast ob-
served with undamaged optics for several values of the fraction of the
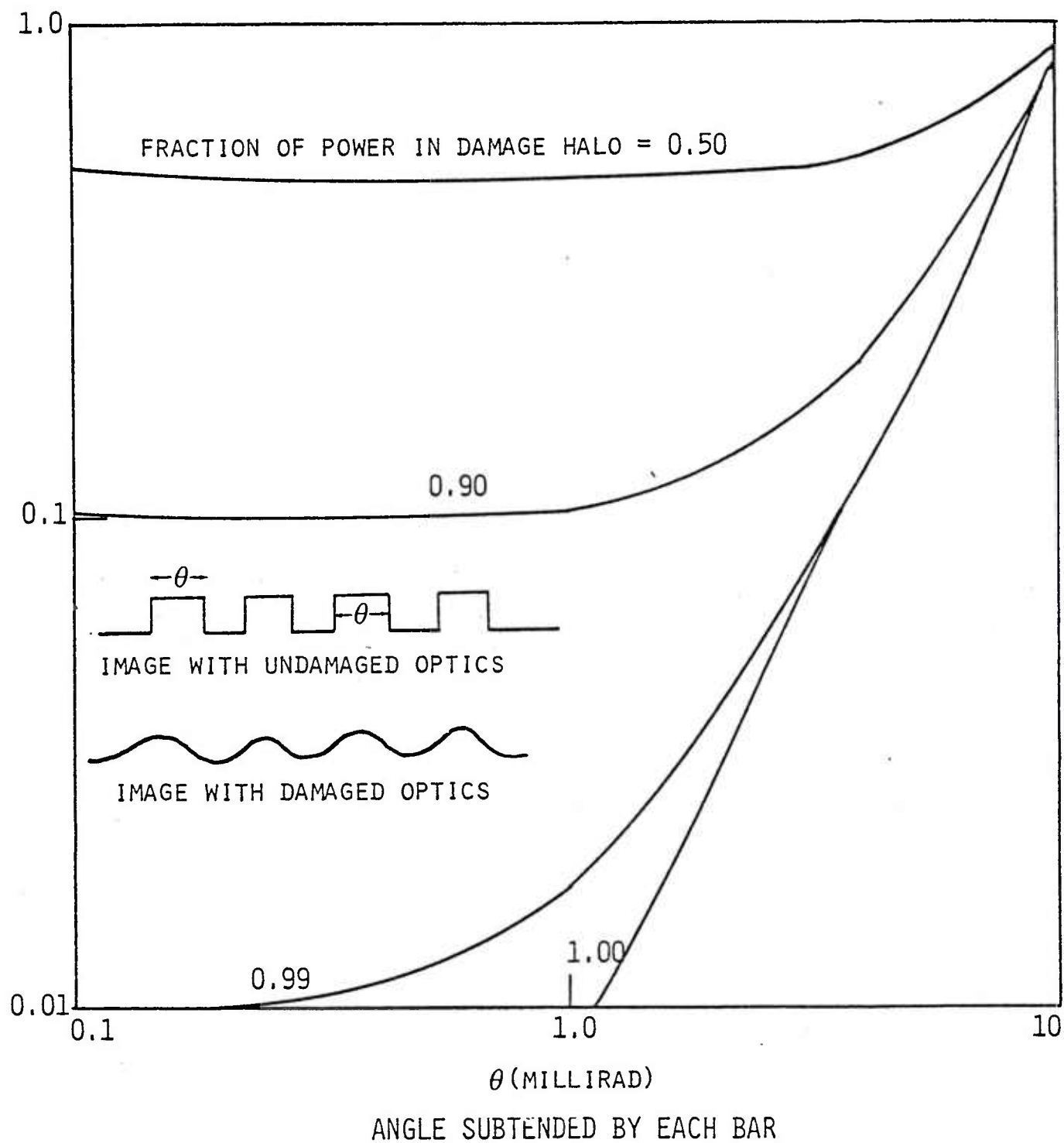area which is damaged by exfoliation.

Fig. 4.14 Contrast of image of alternate black and white stripes as observed through
optics which have a fraction of the area damaged by exfoliation.

4.5   Summary

In this section, models have been developed to implement the methodology described in Section 3. Potential optical aberrations caused by three types of physical damage have been quantified. The point spread functions for simple, damaged optical systems have been determined. It is impossible to evaluate the degradation of the optical performance in the field without specifying the scenario and the optical system; similarly, laboratory data cannot yield definitive tests of the models without details of the optical system and objects. Nevertheless, example calculations show that severe degradation results only if the complete surface of the optical element is damaged. Thus, surface cracks cannot cause severe damage, whereas melting, exfoliation and vaporization can.

The models presented in this section allow image degradation to be calculated for a given optical system and a given object; they must now be validated and applied.

5. SUMMARY

Laser irradiation of optical elements can degrade the performance of an optical system. In this report methodology has been established for predicting the system performance of an irradiated optical system. Models required to implement the methodology have been developed and improved; the models predict (1) the physical damage caused by laser irradiation, (2) the optical aberrations corresponding to the physical damage, and (3) the point spread function (or optical transfer function) for the optical system which includes the aberrations induced by laser irradiation.

The glass damage models have been upgraded to include improved material properties and to predict the fraction of the surface damaged by the various mechanisms. Simple models have been used to relate the damage to the reduction in contrast ratio. In general, the models predicted the trends in contrast ratio; however, for some types of damage, the expected reduction cannot be accurately quantified unless details of the optical system used in measurements are specified.

The optical aberrations caused by three types of physical damage have been modelled. The aberrations are represented as a local change in amplitude and phase of the light. Surface cracks effectively reduce the local transmission to zero. Exfoliation reduces the transmission slightly (≈ 0.08) but its main effect is to introduce a random phase difference between different flakes. Vaporization does not affect transmission, but it introduces potentially large phase differences over distances associated with variations in the vaporization dynamics.

The point spread function has been calculated for a simple optical system which has optical aberrations produced by laser irradiation. The main features of the point spread function are (1) a central spike whose width is determined by the overall aperture dimensions and whose height is proportional to the square of the area which is not damaged, and (2) a damage halo whose width is determined by the characteristic size of the individual damage elements and whose total height is proportional to the incoherent sum of the

square of the area of each damaged element. The description of the damage
halo given above assumes that the phase difference between any two damage ele-
ments is large (greater than 2π) and random. Severe optical degradation re-
quires that the central spike have only a small fraction of the total energy,
therefore the damage must completely cover the surface of the damaged optical
element and the phase difference between adjacent damage elements must be
large.

Specific results of the modeling are:

(1) Surface cracks can be adequately predicted for RP 10.6 μm
    interactions, but the cracks cover only a small fraction
    of the surface. They cannot cause extensive optical de-
    gradation.

(2) Exfoliation occurs over the whole surface. It relieves
    lateral stresses, thereby increasing the intercrack dis-
    tance. If the phase difference introduced by different
    flakes (exfoliations) is large and random, significant
    optical degradation may result.

(3) Melting in CW 3.8 μm interactions correlates well with
    stress relaxation when reasonable values of the laser
    absorption coefficient are used. Melting occurs over the
    entire surface; therefore it has the potential to cause
    significant optical damage when the melt depth is
    sufficient to produce large random phase changes.

(4) Vaporization results in a change in surface composition
    for glasses that are mixtures (i.e., all glasses but
    fused silica). Since vaporization takes place over the
    entire surface, it can produce severe degradation when
    the phase change is large.

(5) First fracture of BK7 and ZKN7 are well predicted for CW
    and RP interactions.

(6) The damage models have been extended to Vycor. It is
    predicted to respond much as fused silica does, but it
    will display more damage in the vaporization regime.

(7) The main damage feature of fused silica - namely, its
    resistance to severe optical degradation - can be
    understood on the basis of the damage models, but the
    details of the threshold behavior have not been well
    characterized. It is not known whether this represents
    an inadequacy in the damage mechanism models or merely
    reflects the uncertainty in the absorption coefficient.

116

In addition to these specific conclusions, there are two important implications of the discussions presented in this report. The first is that laser induced glass damage has an inherent statistical nature. Although the main features of the physical damage may be predictable - for example the size and distribution of damage elements - the details of the point spread function depend on the specific location of the damage features and on the phase relationships between different elements. Furthermore, for a specific realization of glass damage, the detailed structure of the point spread function will depend upon the optical system. It is important that the difference between ensemble averages and specific realizations be remembered both in the interpretation of laboratory data and in the prediction of overall system performance.

The second implication concerns the general relationship between optical damage features and system performance. System performance will not be degraded if the damage halo of the point spread function has a scale size much smaller than the scale of the features of the image produced by the undamaged system. If the system is operating near its performance limits so that small changes in image quality severely degrade system performance, the system performance model predictions will be sensitive to the details of the shape of the damage portion of the point spread function. Conversely, if the scenario and optical system are such that the undamaged system is performing orders of magnitude beyond the threshold limits, then severe damage is required -- the performance of the damaged system is most sensitive to the features near the center of the point spread function. Different approximations are usually appropriate for detailed modeling of the damage halo as compared to the center of the point spread function. Thus, although a simple representation is sufficient to identify regimes in which the damage is small from those which suffer orders of magnitude of degradation, precise predictions of the degradation for a specific optical system and scenario are sensitive to the detailed modeling of selected portions of the point spread function.

In conclusion, a methodology has been established for predicting optical degradation as a result of laser irradiation. Models which are necessary to implement the methodology have been developed; they can now be applied to specific systems and scenarios.

ACKNOWLEDGEMENT

REFERENCES

1. Root, R. G., Wu, P. K. S., Popper, L. A., Hastings, D. E., Clarke, A. S., and Pugh, E. R., "Repetitively Pulsed Laser Effects Studies," PSI TR-295, Physical Sciences Inc., Andover, MA.

2. Touloukian, Y. S., Ho, C. Y., Ed. Thermophysical Properties of Selected Aerospace Materials, Part I; Thermal Radiative Properties, Purdue University, Lafayette, IN, 1976.

3. Amimato, S. T. and Hofland, R., "Absorption by Selected Glasses at DF Wavelengths," Technical Memorandum to U. S. Army Missile Command from the Aerospace Corporation, El Segundo, CA.

4. Hynes, T. V., personal communication.

5. Gardon, R., "Some Heat Transfer Problems in Glass Technology," in Eighth International Congress of Glass, Society of Glass Technology, Sheffield, England, 1969.

6. Edwards, O. J., "Optical Absorption Coefficients of Fused Silica in the Wavelength Range 0.17 to 3.5 microns from Room Temperature to 480°C," NASA TN D-3257, Lewis Research Center, Cleveland, Ohio, 1966.

7. Morrissey, J., "Preliminary Test Report for Capistrano Test 30 August - 3 September," Letter Report DRDAR-BLV-R referred to with permission of R. Mitchell, U. S. Army Missile Command.

8. Van Ness, F., Experimental Studies in Spatio-temperal Contrast Transfer by the Human Eye, Thesis, University of Utrecht, Netherlands (1958).

9. Born, M. and Wolf, E., Principles of Optics, Pergamon Press, Third Edition, Chapter 8 (1965).

10. Goodman, J., Introduction to Fourier Optics, McGraw Hill (1968), p. 45.

11. Goodman, J., Introduction to Fourier Optics, McGraw Hill (1968). p. 80.

DISTRIBUTION LIST

DISTRIBUTION LIST

No. of Copies	Organization	No. of Copies	Organization
1	Commander US Army Missile Command ATTN: AMSMI-R Redstone Arsenal, AL 35898	3	Commander Naval Research Laboratory ATTN: Code 6630, R. Wenzel Code 6652, G. Muller Code 6652, J. DeRosa Washington, DC 20375
1	Commander US Army Missile Command ATTN: AMSMI-YDL Redstone Arsenal, AL 35898	1	Commander USAF School of Aerospace Medicine ATTN: SAM/RZL, MAJ D. Maier Brooks AFB, TX 78235
1	Commander US Army Missile Command Directed Energy Directorate ATTN: AMSMI-RH, COL A. Haddock Redstone Arsenal, AL 35898	1	AFWL/AREE LTC W. Golbitz Kirtland AFB, NM 87117
2	Commander US Army Missile Command Directed Energy Directorate ATTN: AMSMI-RHT, R. Mitchell Redstone Arsenal, AL 35898	1	AFWL/SUL Kirtland AFB, NM 87117
1	Commander US Army Tank Automotive Command ATTN: AMSTA-TSL Warren, MI 48090	1	Air Force Wright Aeronautical Laboratories AFWAL/FIES/CDIC Wright-Patterson AFB, OH 45433
1	Director US Army TRADOC Systems Analysis Activity ATTN: ATAA-SL White Sands Missile Range, NM 88002	1	AVCO-Everett Research Lab ATTN: P. Rostler 2385 Revere Beach Parkway Everett, MA 02149
1	Commander US Army Development & Employment Agency ATTN: MODE-TED-SAB Fort Lewis, WA 98433	1	Fairchild Republic Company ATTN: Central Document Control R.D. Miller Conklin Street Farmingdale, NY 11735
1	Commandant US Army Infantry School ATTN: ATSH-CD-CSO-OR Ft. Benning, GA 31905	1	W.J. Schafer Associates, Inc. ATTN: J. Reilly 10 Lakeside Office Park Wakefield, MA 01880
		1	Air Force Armament Laboratory ATTN: AFATL/DLODL Eglin AFB, FL 32542-5000

DISTRIBUTION LIST

No. of
Copies   Organization

Aberdeen Proving Ground

Dir, USAMSAA
ATTN: AMXSY-D
        AMXSY-MP, H. Cohen
        AMXSY-GS, F. Campbell
        AMXSY-CA, P. Beavers
Cdr, CRDC, AMCCOM
ATTN: SMCCR-RSP
        SMCCR-MU
        SMCCR-SPS-IL
Cdr, USATECOM
ATTN: AMSTE-TO-F

USER EVALUATION SHEET/CHANGE OF ADDRESS

This Laboratory undertakes a continuing effort to improve the quality of the reports it publishes. Your comments/answers to the items/questions below will aid us in our efforts.

1. BRL Report Number_____ Date of Report_____

2. Date Report Received_____

3. Does this report satisfy a need? (Comment on purpose, related project, or other area of interest for which the report will be used.)_____

_____

_____

4. How specifically, is the report being used? (Information source, design data, procedure, source of ideas, etc.)_____

_____

_____

5. Has the information in this report led to any quantitative savings as far as man-hours or dollars saved, operating costs avoided or efficiencies achieved, etc? If so, please elaborate._____

_____

_____

6. General Comments. What do you think should be changed to improve future reports? (Indicate changes to organization, technical content, format, etc.)

_____

_____

_____

	Name
	Organization
CURRENT ADDRESS	
	Address
	City, State, Zip

7. If indicating a Change of Address or Address Correction, please provide the New or Correct Address in Block 6 above and the Old or Incorrect address below.

	Name
	Organization
OLD ADDRESS	
	Address
	City, State, Zip

(Remove this sheet along the perforation, fold as indicated, staple or tape closed, and mail.)